Integrated analysis across cortical morphometric analyses in human brain development: a cross-sectional and longitudinal study

Hadis Kalantar-Hormozi

April 2022

Integrated Program in Neuroscience

McGill University, Montreal, Canada

A thesis submitted to McGill University in partial fulfillment of the requirements of the degree of Master of Science

Abbreviations

bPLS: behavioral Partial Least Squares

C: Component

CT: Cortical Thickness

CV: Cortical Volume

GI: Local Gyrification Index

GMV: Gray Matter volume

ICA: Independent Component Analysis

IQ: Intelligence Quotient

LC: Longitudinal Component

LV: Latent Variable

MC: Cortical Mean Curvature

NIMH: National Institute of Mental Health

NMF: Nonnegative Matrix Factorization

OPNMF: Orthogonal Nonnegative Matrix Factorization

PCA: Principal Component Analysis

PLS: Partial Least Squares

SA: Cortical Surface Area

SES: Childhood Socioeconomic Status

sMRI: Structural Magnetic resonance imaging

T: Tesla

Abstract

Characterizing patterns of development across measures of brain structure is critical to developing a "normative" characterization to better situate neuroanatomical variation in behavioral and, potentially, clinical contexts. Using data from the long-running National Institute of Mental Health (NIMH) longitudinal developmental cohort (ages 5-25), we sought to examine patterns across cortical morphometric features; namely: cortical thickness (CT), surface area (SA), local gyrification index (GI), and mean curvature (MC). We integrated cross-sectional and longitudinal morphometric metrics using nonnegative matrix factorization (NMF), a matrix decomposition technique that estimates a "parts-based" representation using orthogonal components. The cross-sectional analysis identified six components of variation across cortical morphometry features describing key neuroanatomical patterns such as higher CT and lower GI covariation in frontotemporal areas and lower CT and higher SA covariation in unimodal areas. The longitudinal analysis examined covariation in rates of change, and NMF identified another six components describing age-related coordinated change across cortical morphometry measures from childhood to early adulthood, demonstrating preserved SA in unimodal areas through brain development. We further examined the putative relationships of these components with key demographic and cognitive variables. Behavioral partial least squares (bPLS) identified one significant latent variable (LV; 96% covariance) where the older age, lower Intelligence Quotient (IQ), and lower socio-economical status (SES) were related to decreased covariance patterns of GI, CT, and SA throughout the cortex and local increase in MC in associative cortices sulcal depth. In the longitudinal analysis, bPLS identified three significant LVs (97% covariance altogether). The first LV was related to the female sex, higher SES, higher IQ, and older ages and followed a pattern of accelerated maturation of SA and CT covariance across significant portions

of the cortical sheet. This novel characterization of cortical morphometric features maturation provides an important understanding of the interdependencies between morphological measures, their coordinated development, and their relationship to critical factors impacting development.

Résumé

Caractériser les modèles de développement à travers les mesures de la structure cérébrale est essentiel pour développer une caractérisation «normative» afin de mieux situer la variation neuroanatomique dans les contextes comportementaux et, potentiellement, cliniques.
À l'aide des données de la cohorte longitudinale de développement longitudinale de l'Institut national de la santé mentale (NIH) (âgés de 5 à 25 ans), nous avons cherché à examiner les modèles à travers les caractéristiques morphométriques corticales; à savoir: l'épaisseur corticale (CT), la surface corticale (SA), l'indice de gyrification local (GI) et la courbure moyenne (MC). Nous avons intégré des mesures morphométriques transversales et longitudinales à l'aide de la factorisation matricielle non négative (NMF), une technique de décomposition matricielle qui estime une représentation «basée sur les parties» à l'aide de composantes orthogonales. L'analyse transversale a identifié six composantes de variation à travers les caractéristiques de la morphométrie corticale décrivant des modèles neuroanatomiques clés tels qu'une covariation de CT plus élevée et une covariation de GI inférieure dans les zones fronto temporales et une covariation de CT plus faible et une SA plus élevée dans les zones unimodales. L'analyse longitudinale a examiné la covariation des taux de changement et NMF a identifié six autres composantes décrivant le changement coordonné lié à l'âge à travers les mesures de morphométrie corticale de l'enfance au début de l'âge adulte, démontrant une SA préservée dans

les zones unimodales à travers le développement du cerveau. Nous avons ensuite examiné les relations putatives de ces composantes avec des variables démographiques et cognitives clés. L'analyse des moindres carrés partiels comportementaux (bPLS) a identifié une variable latente significative (LV; 96 % de covariance) où l'âge plus avancé, un quotient intellectuel inférieur (IQ) et un statut socio-économique inférieur (SES) étaient liés à une diminution des schémas de covariance de GI, CT et SA dans tout le cortex et augmentation locale de MC dans la profondeur sulcale des cortex associatifs. Dans l'analyse longitudinale, bPLS a identifié trois LV significatifs (97 % de covariance totale). La première LV étant liée au sexe féminin, à un SES plus élevé, à un IQ plus élevé et à un âge plus avancé et suivait un schéma de maturation accélérée de la covariance SA et CT sur des parties importantes de la feuille corticale. Cette nouvelle caractérisation de la maturation des caractéristiques morphométriques corticales, fournit une compréhension importante des interdépendances entre les mesures morphologiques, leur développement coordonné et leur relation avec les facteurs critiques ayant une incidence sur le développement.

Acknowledgments

First and foremost, I would like to thank my supervisor and mentor, Dr. Mallar Chakravarty, for giving me the honor and opportunity to join his research group and pursue my life-long passion under his supervision. Mallar, I could not have imagined having a more supportive, encouraging, considerate, and patient supervisor; joining CoBrA Lab has been a life-changing experience for me that allowed me to learn so much and grow far beyond my comfort zone for which I consider myself privileged and am forever grateful.

I would like to especially thank Dr. Raihaan Patel, without whom this work could not have been possible. Thank you, Rai, for helping me get this work started and mentoring me through many aspects of it, but also for being an incredible teacher. I would also like to thank Dr. Gabriel Devenyi for getting us set up to work as efficiently as possible from home; it would not have been easy to complete a Master's degree over two challenging years in a global pandemic if not for your efforts and support. Thank you, Justine Ziolkowski, for being my troubleshooting companion, your constant positive energy, and the Fridays' inspirational quotes. And to Vanessa Valiquette, for being a super supportive friend and my study buddy since day one, and not to forget, for helping me with the French translation of the abstract.

I would like to thank my esteemed committee members, Dr. Boris Bernhardt and Dr. Xiaoqian Chai, for their valuable feedback, insightful comments, and encouragement during my committee meetings. I am also grateful to the Healthy Brains for Healthy Lives Initiative, the Integrated Program in Neuroscience, and the Quebec Bioimaging Network for investing in my research and scientific development.

Lastly, a heartfelt thank you to my wonderful family: to my mom and dad, for being my most constant inspiration and unwaveringly encouraging and supporting me through every

journey I embarked on. To my grandparents, Mahboube and Manouchehr, who have always filled me with their pure love. And to Hessam, for being my home, miles away from home, and my happy place, no matter how hard the day is; thank you for keeping me grounded and always believing in me, even when I did not, and for being excited about my big and small wins, even more than I was. And finally, to my friends, for always being there for me, despite being oceans apart.

Preface

This thesis is an original, unpublished, independent work by the author, Hadis Kalantar. All processing and analysis, as well as writing this thesis, were performed by the author.

The data used in this thesis was generously contributed by Dr. Armin Raznahan, our collaborator at the National Institute of Mental Health (NIMH; Bethesda, Maryland, USA). Dr. Raihaan Patel developed the integrated analytic technique described and used in the analyses of this thesis. Dr. Gabriel Devenyi aided in troubleshooting and developed the iterative n4 bias field correction image processing technique used and described here. Alyssa Dai aided in performing the gradient analysis presented in this thesis. Quality control was performed by Hadis Kalantar. Dr. Mallar Chakravarty provided academic guidance and supervision, troubleshooting, and initial project design and conceptualization.

Preliminary results from this work have been presented at the Annual International Conferences of the Society for Neuroscience (SFN; 2021) and the Organization for Human Brain Mapping (OHBM; 2021).

Chapter 1. Introduction

Characterizing patterns of neurodevelopment across morphological measures is essential for understanding the dynamic processes underlying typical brain development. There has been a significant amount of effort devoted to mapping “normative” neuroanatomical trajectories as a means of characterizing neurodevelopmental disorders using single neuroanatomical features [1–16]. However, the anatomy of the cortical sheet is convoluted and complex and can only be properly defined through the integration of multiple morphometric measures, each having neuroanatomical and neurodevelopmental correlates. Moreover, each of these cortical properties undergoes significant remodeling at different developmental epochs: gyrification and curvature undergo remodeling at the earliest stages of postnatal development [14,17], followed by a significant expansion in brain volume until about five years old that results in increases in the surface area [15,18,19], and an apparent cortical thinning from childhood into early adulthood [18–22]. Accordingly, alterations in each of these features are expected to be imprinted with different spatio-temporal patterns as well.

Although complementary, each morphometric feature describes a unique facet of the underlying biology, in addition to being related to differing evolutionary [23], genetic [24–29], cellular properties [30], developmental trajectories [31–35], and sensitivity to different clinical conditions [36–38]. Given the dynamic biological relationships between these distinct morphometric properties, each carrying specific yet complementary neurobiological information, it is crucial to study their inter-relatedness in the context of typical cortical maturation. In this regard, multivariate approaches simultaneously assessing several features may provide an insight towards the morphometric inter-relatedness. Previous studies integrating these measures have

estimated subject-specific morphological brain networks derived from combining multiple gray and white matter morphometric/cortical features [39]. Other studies have used partial least squares correlation of multiple features of morphometry in order to investigate the patterns of regional correlation between cortical gray matter and white matter properties [40–42]. Recent studies proposed the Morphometric Similarity Networks (MSNs) [43] to elucidate the relationship between multiple dimensions of brain architecture using a graph-theoretical approach. Innovatively, this group demonstrated that network properties were related to transcriptomic and cell-specific architecture [44,45]. However, this analytical technique provides limited interpretability with respect to the distinct morphological measures that contribute to specific connectomic features (although sensitivity and specificity analysis are included in the original work) [39,44–46]. Therefore, establishing distinct sources of variation across morphometric patterns is crucial as a means of better understanding genetic, cellular, and environmental factors in the context of adaptive and maladaptive brain development and organization.

To address the limitations of previous studies, we propose a novel implementation of a multivariate variance detection technique, nonnegative matrix factorization [NMF] [47–51]. NMF is conceptually similar to other unsupervised matrix decomposition techniques [52–56], but with a nonnegativity constraint across all inputs and outputs. This technique has been proposed in the context of neuroimaging studies [49,50,57–59] and has been used to capture reproducible spatial patterns of cortical thickness variation in the brain development period [57]. More recently, this method has been further expanded upon by our group [51,60] to enable the integration of multiple structural metrics in the context of the human hippocampus [51] and striatum [60] that are related to inter-individual variation in demographic and cognitive features.

1.1. Research statement

Here, we leveraged Nonnegative matrix factorization to study cortical neurodevelopmental covariance, cross-sectionally and longitudinally, across multiple cortical morphological measures of cortical thickness, surface area, local gyrification index, and mean curvature in the context of developing brain anatomy. We further related these patterns to age and sex, socioeconomic background, and cognitive ability to better understand inter-individual differences in cortical patterning and maturation. Finally, we assessed how the identified morphometric covariance patterns situate along the maturational stages of the principal gradients of functional connectivity within the different periods of childhood, adolescence, and adulthood.

Chapter 2. Background

2.1. The basis of cortical neurodevelopment

Brain development is a protracted dynamic process that begins in utero a few weeks after conception [61,62] and continues through adolescence into adulthood [63] (Fig.2.1). During this prolonged period, “the brain develops from a tubular structure to a highly complicated yet organized organ with adult-like architecture” [64]. The foundations of microstructure and anatomy of the brain are established primarily during the prenatal period and early childhood [65]; however, the neural networks undergo substantial modifications and refinement over the course of the lifespan [66,67]. A prerequisite to better characterize normal brain structural changes through childhood and the maturation in adolescence and early adulthood is to understand early brain structural development and examine the origins of these developmental processes. In the following, these fundamental processes will be briefly described.

In the second week of gestation, the developing embryo organizes into a spherical, three-layered structure, in which an area of thickened cells forms the neural plate (Fig.2.1). Following that, by folding the neural plate, the neural tube forms (Fig.2.1), which starts to close from bottom to top. Subsequently, the neural tube becomes a three-vesicle anatomical structure (the forebrain, midbrain, and hindbrain) [68–71] (Fig.2.2A), in which each part starts to differentiate into a distinct brain structure. The most anterior vesicle will form two vesicles in which the most anterior one, Telencephalon (Fig.2.2B), will originate the cerebral hemispheres [72–74] through “a complex, dynamic, sequential, and yet temporally overlapping series of cellular events that are genetically determined, epigenetically directed, and environmentally influenced” [71] (Fig.2.2).

The innermost layer of neural tube cells (neural stem cells) begin proliferation to create neuroepithelial cells such that the number of initial cells repeatedly multiply at a logarithmic rate. Even though the apoptotic processes will modulate this accelerated proliferation, the number of brain cells at birth outnumbers adult neurons. Following the overproduction of neurons after reaching a sufficient population of neuroepithelial cells, the cells take a radial morphology along the radial direction [75] transforming into cell types known as radial glial cells (RGCs). Most RGCs, known as progenitor cells, undergo an asymmetric mitotic division. They will produce either intermediate neuronal precursors, neurons directly, or glial cells. Neurons and glial cells will then migrate through the neural tube's layers in a radial path along with radial glial cells (known as radial units), which guide the path of neurons to reach their final destination [71,72,76]. This migration occurs within a radial path in an inside-out manner (ventricular zone (VZ) → intermediate zone (IZ) → marginal zone (MZ)) such that the first migrating cells become the deepest layer of the six cortical layers (cortical plate (CP)) [77–79]. On the other hand, interneurons migrate in a tangential manner (i.e., parallel to the cortical layers). These processes of neuronal migration from their origin to their ultimate destination peak between 12-20 post-conception weeks and are almost complete before the 29th post-conception week [71–74,80,81] (Fig.1.3).

After the migration of the neuronal cells to their final destination, about half of the neurons will undergo apoptosis. Meanwhile, the remaining neurons mature and commence the development of neuronal processes that facilitate inter-neuronal communication, such as the outgrowth of dendrites and axons [74,82]. With the acceleration of the simultaneous neuronal production, migration, and differentiation, the sulcal and gyral pattern of the cortex begins to form around the third trimester [83,84]. Although not completely understood [85], the formation

of gyri is thought to result from the differential rates of tangential division and growth in the progenitor cells [86]. The emergence of gyral patterns allows for substantial cortical surface expansion within the restricted skull space [87]. Simultaneously, cortical thickening, which had started at 10 - 15 weeks post-conception [65], increases exponentially [87], partly due to dendritic arborization and axonal elongation [88,89]. Following the formation of axonal and dendritic branches, synapses start to form and develop starting from the 18th-week post-conception prenatally [71,90,91]. This process, referred to as synaptogenesis, reaches its peak in the first year of life on average and continues well into childhood. Since there is a gap between the timepoint that each part of the brain reaches its peak synapse production, the regions accounting for sensorimotor functions mature faster, while the regions accounting for higher cognitive function mature later. For example, while the production of synapses in the visual cortical areas reaches the peak about 4th-8th after birth, prefrontal cortical regions show the peak around 15th months postnatally [92,93].

Followed by the formation and rapid overproduction of synapses, the brain undergoes a process of synapse elimination through synaptic pruning; this process starts near the time of birth and continues well into adulthood [92,94]. Similar to the heterochronous temporal pattern of synaptogenesis, the pruning also shows a regional-specific developmental time frame. The sensorimotor cortical areas undergo synaptic pruning around the age of 5, and the pruning peaks in higher cognitive areas through adolescence as a hallmark of cortical reorganization [92,95–97].

Starting near birth [83], the synapses that have survived the refinements will be myelinated (by oligodendrocytes) to optimize the network of functionally important white matter fibers by improving the conduction velocity. This process is also experience- and

environment-dependent such that the neurons within synapses and circuits that have been activated the most will be myelinated to form the organized adult-like brain [65]. While the myelination of most pathways, such as specific sensorimotor areas, completes around early childhood, this process in prefrontal areas continues well through adolescence into the third decade of life [94,98–101] (Fig.2.3).

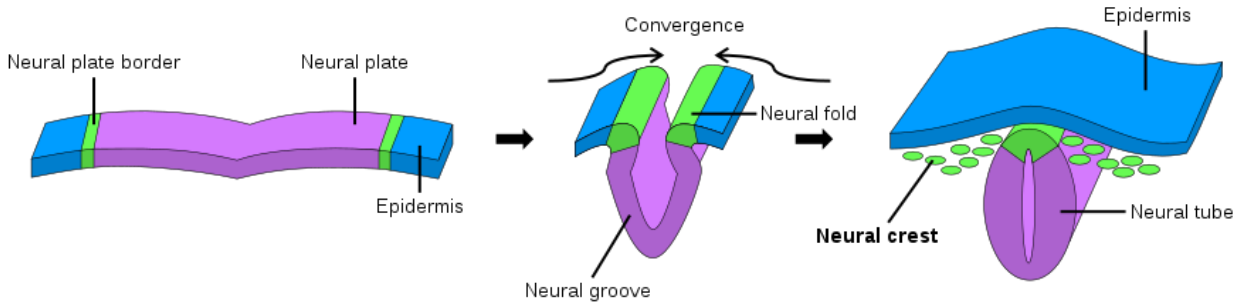

Fig.2.1. From Neural plate to Neural Tube. An area with thickened cells forms the neural plate in the embryo, which further undergoes a folding process, creating the neural tube. Schematic from [102]. (This file is licensed under the Creative Commons Attribution 4.0 International license.)

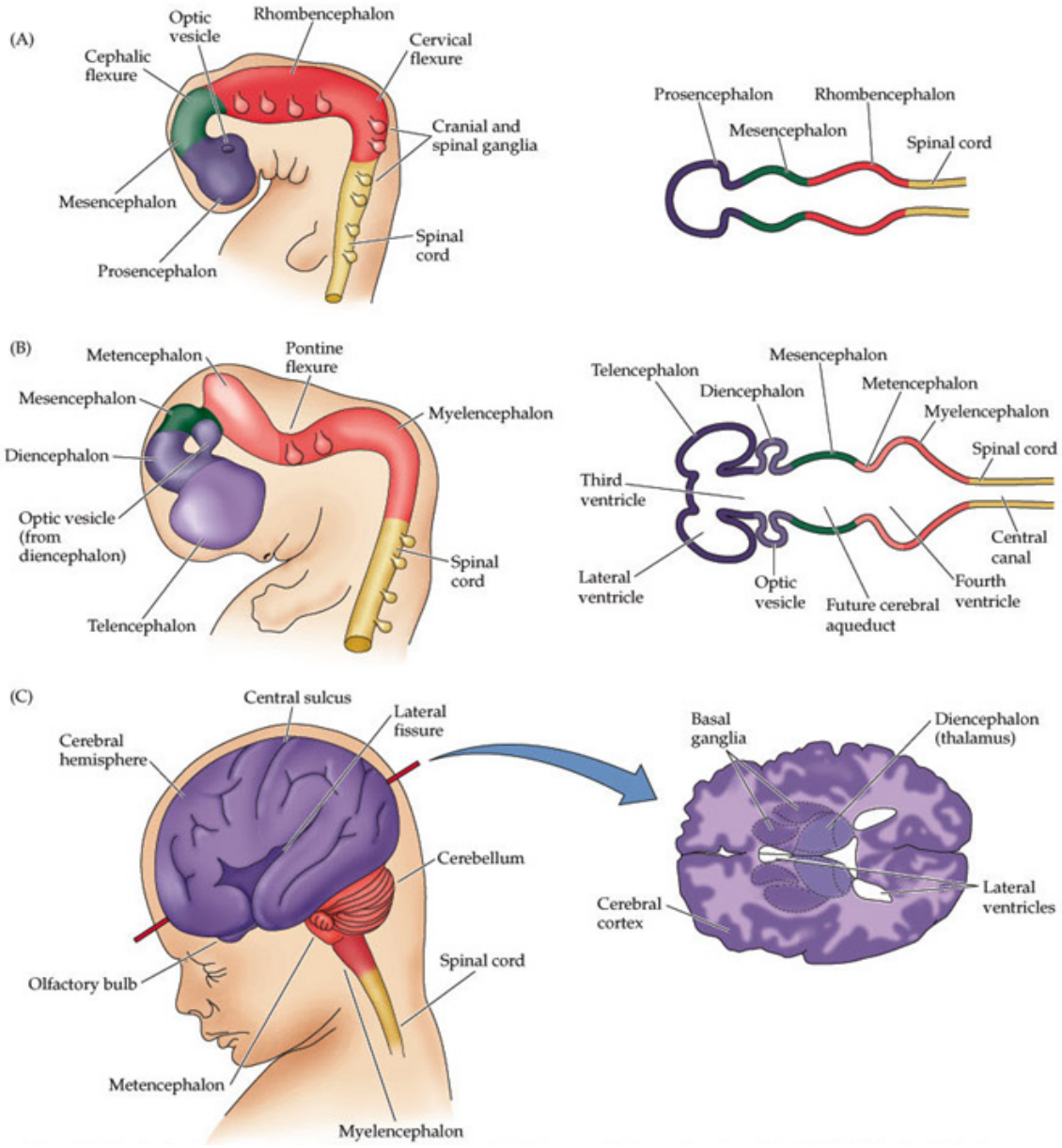

Fig.2.2. From the neural tube to cerebral hemispheres. The neural tube becomes a five-vesicle anatomical structure. Each part will further differentiate into a distinct brain structure; the anterior vesicle (Telencephalon) will form the forebrain, which further originates the cerebral hemispheres. Schematic from [91].

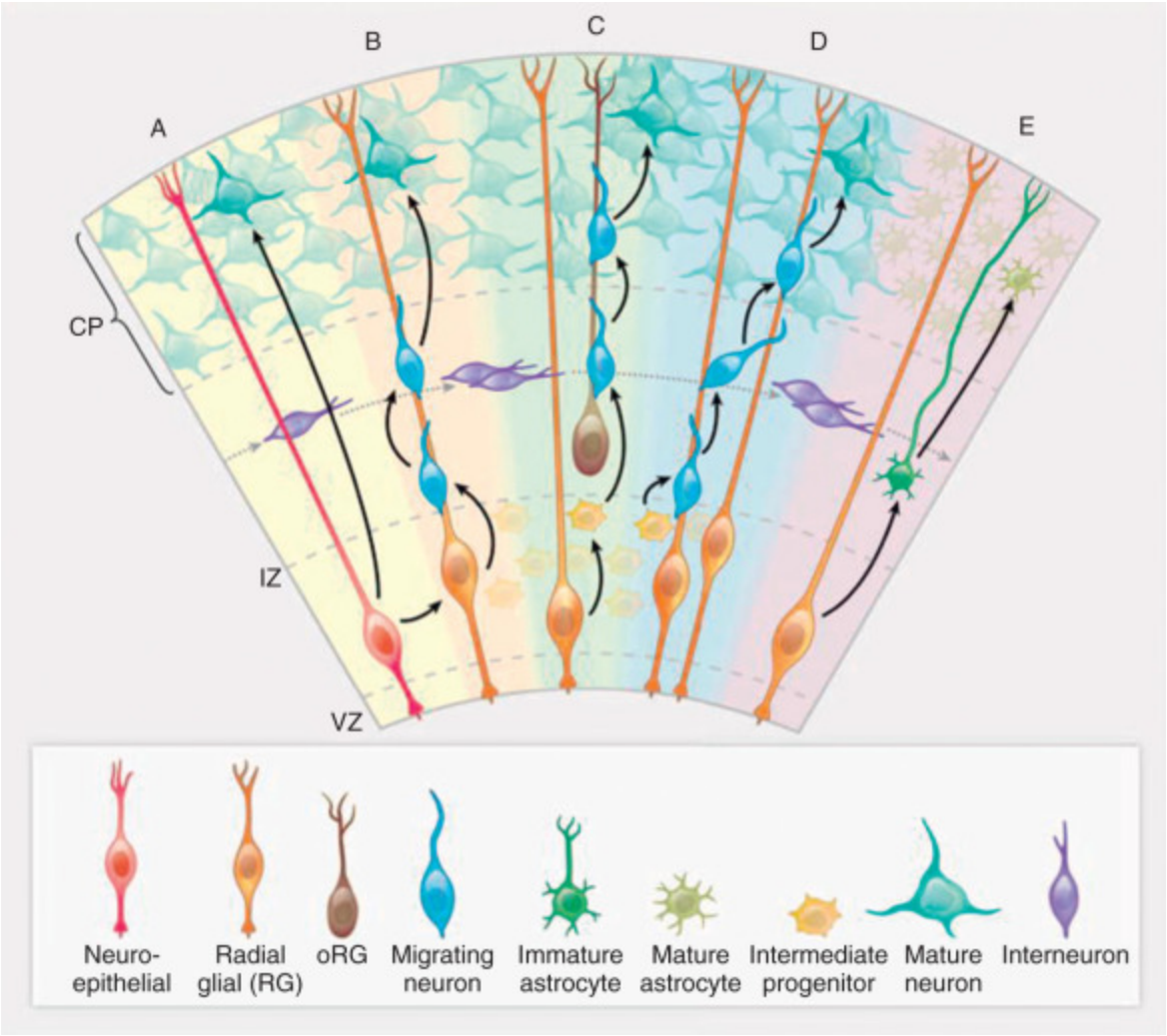

Fig.2.3. Schematic demonstration of cortical layers formation and development, highlighting the radial and tangential neuronal and glial cell migration.VZ, ventricular zone; *CP*, Cortical plate; *IZ*, intermediate zone; Schematic from [103,104].

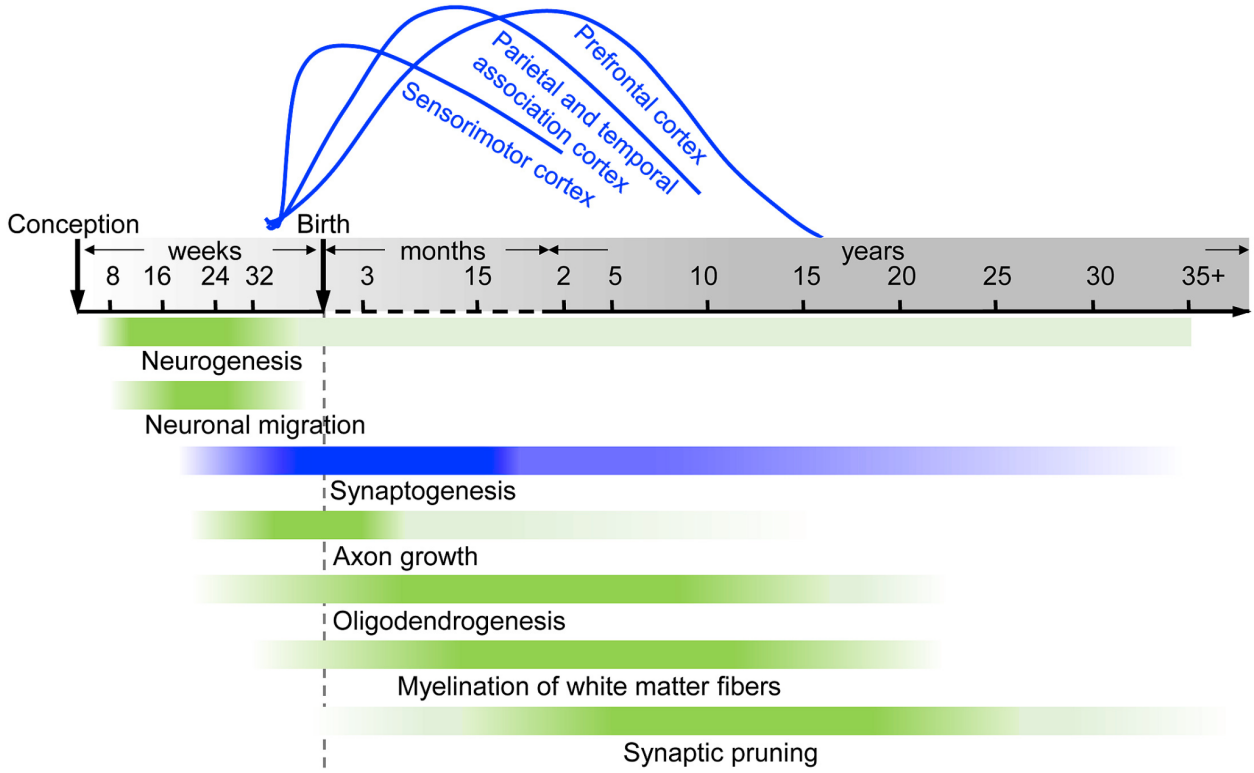

Fig.2.4. Timeline of cerebral maturational processes. The x-axis denotes the time, and the color intensity in each bar corresponding to developmental processes demonstrates their rate of change, with the hottest color corresponding to the mean peak of each process. The spatiotemporal pattern of the progression of the synaptogenesis process has been illustrated in blue, starting from the sensorimotor cortex and ending with the prefrontal cortex. Schematic from [64].

2.2. Brain development from childhood to early adulthood

As discussed above, the foundations of brain microstructure, function, and anatomy are established primarily during prenatal and early childhood [64,65,105]. After birth, as a result of continual neurogenesis, synaptogenesis, gliogenesis, axonal growth, and myelination, the brain

undergoes substantial changes: brain size increases most rapidly. It reaches approximately 80% of its adult brain size by the age of two [2,106], and 90% of its adult volume by the age of five, which reaches its peak in late childhood [3–7,15,16]. The myelination processes that had started during the fetal period continued throughout adolescence [3,4,6,15,16], concurrent with the peak of the synaptic pruning, which is considered the hallmark of brain transformations during adolescence. Synaptic pruning leads to substantial synaptic density reductions, such that the number of excitatory synapses reduces two to three times in adults compared to children [107–109]. These harmonious modifications and refinements lead to a massive cortical structural remodeling leading to an apparent gray matter volume decrease throughout adolescence that continues to adulthood [1,2,6,9–13,15,16,110–112] and stabilizes around the third decade of life [94].

This prolonged period of brain development and remodeling from childhood to adulthood predisposes the brain to vulnerability. It is likely that subtle alterations in the neurocircuitry refinements may result in aberrant formations [113]. Several studies have shown that the dynamic variation in neurobiological, neurochemical, and social maturation processes is concurrent with the peak vulnerability of several neuropsychiatric disorders [114–117]. More precisely, more than half (62.5%) of the psychiatric disorders emerge before the age of 25, with a mean peak age of onset at 14.5-18 [118]. This evidence has even led to the reconceptualization of many neuropsychiatric disorders resulting from maladaptive brain development [119]. As a result, there has been a significant amount of effort devoted to mapping the “normative” development [4,120–122] as a means of characterizing neurodevelopmental and neuropsychiatric disorders as deviations from this norm [13,114,115,123–126].

2.3. Cortical cytoarchitecture and morphometric features

Since we cannot directly measure the neural properties of cortex *in vivo*, structural magnetic resonance imaging (sMRI) has been a robust, reliable, and reproducible tool that provides the opportunity to study brain (discussed thoroughly in section 2.7) and its development through measures each having different neuroanatomical and neurodevelopmental correlates. According to the radial unit hypothesis [127], the cerebral cortex is organized into columnar units of neurons [128]. The morphology of the cerebral cortex is commonly described through measures of cortical thickness and cortical surface area, which topologically includes cortical gyrification and folding.

Cortical thickness (CT) is thought to reflect the radial (vertical) radial expansion of the cortex [127] and represents the cellular density within the radial units. Changes in the CT are thought to reflect the radial neuronal migration, synaptic pruning, axonal remodeling, dendritic arborization, and glial support and myelination in cortical columns [92,107,127,129–131] in earlier stages of development and with advancing age, cortical thinning may be more reflecting neuronal and dendritic shrinkage [92,107,129,130,132].

Cortical surface area (SA) reflects the tangential (horizontal) growth of the cortex [23,127,133] and is rather linked to the tangential expansion of the cortex. SA is, in part, determined by the number of cortical columns and is likely indicative of the rate of neural stem cell proliferation in the periventricular area and migration early in development [30] as well as synaptogenesis and cortical myelination [19,94,127,133–140].

Cortical local Gyrification Index (GI) represents the folding characteristics of the surface of the cerebral cortex. Cortical folding is thought to accommodate the increase of neurons and the number of columnar functional units and enables the expansion of cortical surface area

within the limited cranium volume [133,141]. Even though cellular mechanisms underlying the gyrification are not clearly understood yet [142], theories have been proposed based on topologically specific differential growth [143,144], cranial pressure and constraint [145], mechanical tension [145,146], stress-dependent folding [147,148], axonal tension [149], and the spatiotemporal patterns of neuronal birth and migration [142].

Cortical Mean Curvature (MC) is a local folding characteristic of the cortex that is determined by cortical surface's mechanical folding, provides spatial information on how the surface is embedded in the three-dimensional space [150], and is thought to be reflective of white and gray matter boundary changes [151,152]. Mean curvature follows the pattern of gyri and sulci [150,153] and represents the local topography of the brain.

Each of these cortical properties undergoes significant remodeling at different developmental time frames: gyrification and curvature undergoing remodeling at the earliest stages of postnatal development [14,17], followed by a significant expansion in brain volume until about five years old [90] that results in increases in the surface area [15,18,19]. The surface area will then undergo a general decrease during adolescence [15,18,19], concurrent with the apparent cortical thinning from childhood into early adulthood [18–22]. Accordingly, alterations in each of these features are expected to be imprinted with different spatio-temporal patterns.

Overall, these properties are related to different cellular and neurobiological neurodevelopmental properties[30] having differing evolutionary[23] and genetic[25–27,154] and demonstrate different developmental trajectories[15,20,31–35,155], and are differentially impacted in different clinical conditions [25,36,154,156,157]. Therefore, investigating these cortical features and knowledge about their relative contributions to cortical architecture can provide important, although indirect, insights into understanding the basic processes

underpinning cortical structure development [19].

2.4. Sex differences in developing brain

To define a normative morphometric mapping of brain development, it is also crucial to consider sex-specific brain development [15,21,158–160] as a means of improving our understanding of sex-based prevalence disparities in neurodevelopmental disorders, such as autism spectrum disorder (M/F:3/1) [161]. For example, males are more prone to developing autism in their early childhood, which is associated with a cortical volume overgrowth [162,163]. However, by decomposing Cortical Volume (CV) into its subcomponents and tracking their separate trajectories, studies have suggested that this volume overgrowth could potentially be due to a surface area overgrowth rather than CT [15]. As previously mentioned, many psychiatric disorders that emerge in youth, specifically during adolescence, demonstrate notable differences in their prevalence between sexes [119,164–169]; while females show mood and anxiety disorders almost twice as males [165,170], attention deficit hyperactivity disorder is twice in male than females [119,171]. The disparities in the prevalence of such neurodevelopmental and neuropsychiatric disorders have led to investigating sex differences in brain development to identify potential sources of sex-specific vulnerability or resilience for certain symptoms [119].

Over the course of the lifespan, brain size is larger in males than females [119]. Specifically, around an overall 9-12% larger brain size has been reported in males [172] across childhood [119,121,173–175], adolescence [119,121,173–176], and adulthood [119,174,175,177–179]. At the level of distinct morphometric features, cortical thickness [180,181], surface area, gyrification, and convex hull area have been reported to have sexually

dimorphic maturational patterns over the course of development [15,119]. Sex differences across global and regional variations in CT trajectories [174,180,181] and structural covariance networks of CT [57] have been reported. In covariance networks, it has been reported that while males show thicker parietal cortices around childhood, there is no such difference present in cortices by adulthood [57,119]. In another study, while males at younger age demonstrated greater CT in the insula, frontal and occipital lobes than females, adolescent females showed a greater CT in those regions [119,175]. Overall, studies have suggested that while there is evidence of CT differences across males and females, the direction might depend on age and the target region [119]. SA is greater in males than females, independent of brain volume differences [21,119,179]. The gyrification index has also been reported to be greater in males than females from ages 5 to 25 [182]. In adults, although gyrification has been reported to be greater in men in most cortical areas, after controlling for Gray Matter Volume (GMV), it has shown inconsistent findings [183].

Females have been reported to mature earlier than males [184,185]: in childhood, gray matter volume peaks earlier in females [2,186], and adolescent females undergo cortical remodeling earlier than males [15], such that females reach peak cortical SA earlier compared to males [15] while males show a slower overall SA loss (i.e., delayed maturation) compared to females. Females also demonstrate significantly higher rates of cortical changes [187], specifically higher rates of cortical thinning in the temporal, temporoparietal, and orbitofrontal cortices, which is interpreted as "a faster maturation of the social brain areas in females" [159]. While sex differences captured in most cortical regions were mainly reported to be driven by sex differences in SA and to a lesser extent CT maturation [15], GI has been reported to show only subtle sex differences with age in localized frontal regions, suggesting that the mechanisms

underlying of age-related changes are distinct [159]. In another study by Raznahan et al. [188], sexually dimorphic patterns of CT maturational coupling were reported within a frontopolar-centered prefrontal system corresponding to cortical areas involved in complex decision-making [188]. These differing spatiotemporal sex-related patterns are thought to be genetically determined [187] and could be explained by the different timing and rate of fundamental biological maturation moderated by hormonal processes and puberty [189,190].

2.5. Socio-environmental factors impacting brain development

Childhood socioeconomic status (SES) is an index estimated using the parental level of education and income, the two factors that are associated with children and adolescents' environments and can shape their experiences [191,192]. Parental education could be representative of the parent-child interactions experiences [193], and parental income may indirectly represent material resources available to children [193] that jointly may contribute to the individual's environment.

Brain development occurs within the context of individuals' pre-and postnatal environments. In the utero, the cerebral cortex undergoes substantial changes, during which fundamental aspects of cortical development are established [120,194,195] as described in section 2.1. After birth, the extensive synaptic pruning [196] in adolescence followed by white matter fiber myelination [197] are highly experience-dependent [65,198] and are therefore influenced by each individual's environment as well.

Such inter-individual environmental differences may therefore result in alterations in both structure and maturation of the cerebral cortex that could be detected through surface-based

measures driven by MRI [193]. A recent investigation by Rakesh et al. [199] has used SA and CT as a proxy of maturation and demonstrated that individual youth with neighborhood disadvantage exhibit an altered pattern of brain maturation, interpreted as a delayed maturation compared to their advantaged counterparts [199]. These findings were consistent with previous studies investigating the association of other types of disadvantage with delayed brain development [192,199–203] and altered CT, SA, and GI development.

Consistently, individuals with higher SES have been shown to demonstrate accelerated functional brain development, such as increased functional specialization [204] and resting-state connectivity [205–209] in children and adults. Specifically, SA maturation has shown to be vulnerable to the prenatal environmental differences [120] affecting maturation into late adolescence.

2.6. Cognitive ability and variability in substrates of cortical structure

Previous studies have suggested that the neural structure and function relationships are more complex than can be influenced by single cortical measures [210]; therefore, investigating the associations between the integration of multiple features of brain structure with the variations in cognitive ability could be more insightful. Such covariation has been shown in previous studies [211–214]: CT has been reported to be negatively correlated with intelligence maximally around the age of 10 when the relationship seems to be reversed later in adult life such that with the increase of age from childhood through adulthood [212]. As for SA, it has been observed that intelligence might be associated with the timing and magnitude of the change in SA, rather than the microstructure alone [212].

Cortical folding characteristics, specifically gyrification, have also been observed to have neuroanatomical correlates related to cognitive ability [212]. Recent studies investigating the regional association between GI and general cognitive ability have revealed a pattern of positive correlation between the two in mainly parietal and frontal cortical areas [215]. Overall, previous studies have reported a pattern of positive correlation between general cognitive ability as indexed by Intelligence Quotient (IQ) with cortical SA expansion [192,193,216] and thickness [192,212,217–219], and the gyrification that also exhibits a pattern of positive correlation to general cognitive ability [214,215]. Notably, the study by McDermott et al. [192] demonstrated a positive association with SES [192].

The pace of maturation has also been reported to be linked to variations in cognitive ability. Earlier thinning of CT has been reported to be positively linked to IQ in typically developing individuals in their late childhood, adolescence, and adulthood [212] which becomes more pronounced with increasing age: the higher the IQ, the faster the thinning of cortex over time [212]. Similarly, higher IQ has been linked to a faster maturational rate of decrease in SA [212].

2.7. Magnetic resonance imaging

Magnetic resonance imaging (MRI) is a non-invasive imaging technique that generates detailed images of the different organs and tissues of the body, such as the human nervous system, using magnetic fields and radio waves [220]. In the field of neuroimaging, MRI is widely used in different clinical and non-clinical contexts to capture the functional and structural properties of the brain [220]. MRI is a safe and non-invasive procedure that allows repeated

scans to be obtained at high spatial resolutions and has enabled the investigation of brain structural changes *in vivo*. Thus, the MRI technique has been an ideal tool that provides the opportunity to study brain developmental processes.

2.7.1. Principles of magnetic resonance imaging

MRI is based on the principles of nuclear magnetic resonance and the magnetization features of atomic nuclei. This technique is based on the magnetization of nuclei in the exposure of an external magnetic field produced in the MRI scanner. The MRI signal is mostly derived from hydrogen protons located in nuclei within the water molecules of the body tissues. Hydrogen is not only an omnipresent atom in the body tissues but is also highly sensitive to external magnetic fields; these properties make hydrogen the main target to absorb and release the electromagnetic energy and produce MRI signals.

Protons present in the human body rotate (spin) around their axis. This precession characteristic of protons in hydrogen nuclei leads to the generation of a local magnetic field specific to each nucleus [221,222]. In the presence of a strong external magnetic field, such as the powerful magnet of the MRI scanner (B0; measured in Tesla (T)), protons within the examined tissue will align in a parallel or antiparallel direction to the B0 axis (aligned with the z-axis) [223]. In this process, most of the protons will be aligned parallel to B0, as the process takes less energy than aligning against the B0. The portion of protons aligned with the magnetic field will create bulk magnetization (M0) and their current loop, parallel to B0, is known as longitudinal magnetization (M0 strength < B0 strength). The protons will then start to spin in the direction of the applied magnetic field, and the frequency in which they spin at (f0) is a function of the magnetic field strength and can be calculated using the Larmor equation:

$$f0 = \gamma B0 \qquad (1)$$

where γ represents a constant geometric ratio specific to nuclei.

To further derive an MRI signal, the radiofrequency (RF) coil in the MRI scanner provides an RF pulse tuned to the Larmor frequency and applied perpendicular to B0 (into the Bxy plane, at different flip angles, i.e., 90° based on the type of image being acquired.) [221,222]. This pulse leads to a perturbation in the initial magnetic field (B0) and an RF pulse B1. As a result of the change applied to the magnetic field, a portion of M0 will be tipped at a predetermined amount (often between 90° - 180°) from their steady-state position to start to process in the direction of the xy plane (Mxy).

With the elimination of the RF pulse, the protons return to their initial state alignment around the z-axis; as a result, the Mxy will decrease and the process is referred to as relaxation. The procession during relaxation generates a current in the receiver coil, which yields in the generation of the signals. These generated signals are recorded by the gradient coils in longitudinal (z) and transverse (x and y) axes and can be measurable via Faraday's Law of Induction [224]. The excited protons in different tissues return to their original energy state in different time frames, which varies depending on their structure [225]. The differential relaxation rates derive distinct signals with varied frequencies, which are spatially encoded in a matrix (k-space) in which each point (pixel) corresponds to specific spatial frequencies. This obtained frequency information from each location will be spatially encoded to specific intensity levels through a spatial gradient. Using the Fourier transformation [224,226], varying frequencies derived from different tissues at different positions can be reconstructed into an image matrix yielding an MR image.

2.7.2. T1-weighted imaging

Different types of MR images are obtained at different relaxation times and collect different RF pulse sequences. T1-weighted images are among the most common MRI sequences. There are two types of relaxation that occur in MR imaging. The first relaxation occurs in the longitudinal axis and is referred to as T1 or spin-lattice relaxation. This relaxation time (T1) is the time for protons to release their energy and realign to their original state along the longitudinal plane. Subsequently, the T1-weighted images are reconstructed according to time (T1) differences in different tissue types to reach the equilibrium state. Each tissue emits a different signal intensity, resulting in the contrast seen in MR images [221]. Specific characteristics of T1-weighted images are having a longer repetition time (TR). This refers to the time between two consecutive RF pulses and echo times (TE), which is the amount of time between the RF pulse and the echo signal peak, leading to acquiring the maximum signal difference from different tissues [221,222].

In T1-weighted images, tissues and regions containing higher water density show a slower rate of realignment (i.e., the ventricular zone containing cerebrospinal fluid), and the corresponding signal is encoded as dark shades of gray. On the other hand, tissues that are high in lipids show faster realignment (i.e., cerebral white matter) and are visualized in brighter grays. Any tissue with a combination of water-lipid density, such as cerebral gray matter and basal ganglia, will place in between.

2.8. Image pre-processing

In order to standardize the overall quality of T1-weighted images, several preprocessing steps are performed prior to extracting structural measurements from MRI images. Bias field correction and brain extraction are among the most crucial steps in preprocessing.

2.8.1. Bias field correction

The goal of bias field correction is to correct intensity inhomogeneity. This step is particularly crucial to processing an MRI image since tissue classification algorithms presume an intensity homogeneity within the classes of tissues. Bias fields are an imaging artifact in MRI that leads to inhomogeneity of the intensity in an image that may cause variability in the intensity within a single tissue. Several sources may cause this artifact, such as the spatial inhomogeneity in the magnetic field itself or the interaction between the human body and the magnetic field. The bias field is a function of the magnetic field strength such that the higher the magnetic field, such as scanners with 1.5 T or 3 T or above, the more the images are prone to be affected by the bias field, which may compromise the further MRI analysis [227].

Amongst the numerous bias field correction methods proposed in neuroimaging [228], the non-parametric non-uniform intensity normalization (N3) [229,230] and its improved version, N4ITK [231,232], are amongst the most commonly used algorithms. N3 is a fully automatic and iterative algorithm that exploits b-spline approximation to yield the “smooth multiplicative field that maximizes the high-frequency content of the distribution of tissue intensity” distribution [229,231], with no requirement of a priori knowledge. N4 algorithm performs a multiresolution iterative optimization framework, an improved form of the iteration optimization used in N3. N4 starts by initially fitting a low-resolution b-spline, and the resolution

is increased to reach the best fit of the bias field [231]. The iterative manner applied in N4 is such that the corrected image from each step will be input to the next, which allows for iterative, incremental updates of the bias field [231].

2.8.2. Brain extraction and masking

Brain extraction separates the brain from its non-brain surroundings, such as the neck, skull, and fat tissue. The goal is to improve the tissues of tissue classification by removing the non-brain tissues that have similar intensities with brain tissues that may interfere. This process includes classifying the head MRI voxels into brain or non-brain and generating a binary mask out of brain voxels [227]. The brain mask includes the cerebral gray matter and white matter tissues, cerebrospinal fluid, and non-brain tissue, including bones, muscles, eye, skin, dura mater, and fat tissue, separated and labeled non-brain. This generated brain mask can be further used to facilitate image processing steps (Fig.2.5).

A commonly used method for brain extraction is a recently developed tool, the Brain Extraction based on a nonlocal Segmentation Technique or BEaST [233]. This patched-based segmentation tool uses affine registration to the MNI space [234] to construct the brain mask and then, by transforming back to the native space, generates binary labeling of the brain. Notably, the BEaST algorithm has achieved significant accuracy compared to other existing brain extraction tools [233].

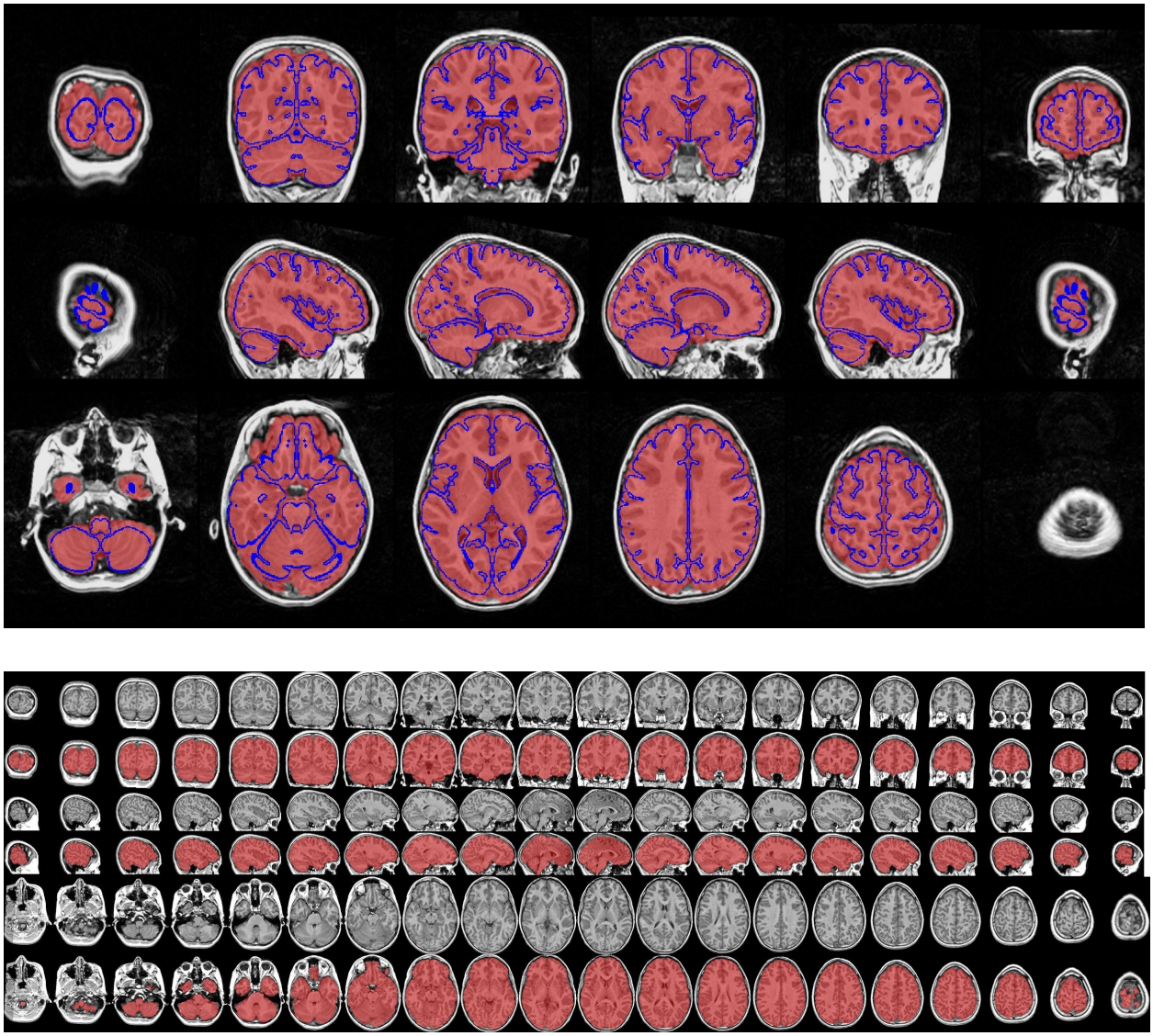

Fig.2.5) examples of T1-weighted image brain masking (red) using BEaST brain labeling.

2.9. Investigating morphometric measures from MRI

Over the last two decades, insight into human brain development has been fundamentally improved through structural magnetic resonance imaging (sMRI) [9,13,235]. Until recently, there was an assumption that substantial changes in the structure and function of the brain are limited to the prenatal period and early childhood [198,236]. However, this assumption was revisited due to large-scale and longitudinal neuroimaging studies [2], and it is now established that the brain also undergoes a massive remodeling and reorganization of cortical structure and functional circuits primarily during adolescence [2,6,188,198,211], which continues to some extent into early adulthood (discussed above sections 2.1 and 2.2), and later in life span [237].

Volumetric approaches provide automated quantitative analysis of the gray and white matter through voxel-based morphometry (VBM) approaches [238]; these methods have been used in many previous studies of neurodevelopment [7,110]. The work from Giedd and colleagues [2], one of the earlier works that provided insights into the cortical remodeling phase, showed this spatiotemporally heterogeneous/ heterochronous pattern of change in gray matter volume that occurs from childhood through adulthood. Volume-based methods, even though they provide the volumetric and gray matter density measures, are unable to distinguish the underlying geometrical changes. The measurements are hard to interpret since variations of gray matter volume/density could be driven by each of the thickness, surface area, or any potential combinations of these measures and could be influenced by regional folding characteristics of the cortex [239,240].

Surface-based morphometry computational techniques have provided the opportunity to overcome VBM limitations by decomposing the gray matter volume (GMV) measures into neurobiologically distinct morphometric features through vertex-based analysis. This involves

estimating cortical thickness and cortical surface area that jointly build the GMV, the folding properties of the cortex indexed by cortical gyrification, and cortical curvature. In fact, surface-based measures are required to parse the geometric complexity of the surface topology of the brain in a way that reflects its true complexity.

2.10. Extracting morphometric features: Image processing

Over the last two decades, advances in developing automated processing pipelines have enabled accurate, reproducible, and fine-grained estimations of cortical neuroanatomy [241–244]. CIVET [245] and FreeSurfer [242] are amongst the most widely used software for estimating cortical morphometric features. Recent investigations comparing the two have demonstrated CIVET to exhibit better reproducibility [246], lower variance, higher reliability [247], and higher stability and consistency in cortical thickness estimations [246,248].

The CIVET pipeline (Montreal Neurological Institute (MNI); http://www.bic.mni.mcgill.ca/ServicesSoftware/CIVET) [243,247,249] is a fully-automated pipeline for volumetric, corticometric, and morphometric analysis of human brain imaging data [250,251]. Images submitted to CIVET are linearly registered to MNI space using the MNI ICBM 152 average [252]. The brain tissue is then classified into white matter, gray matter, and cerebrospinal fluid [253] through the automated PVE algorithm that iteratively corrects the tissue class thresholds by "reseeding the tissue classification at the previous iteration to recompute the thresholds at the current iteration until convergence" [251]. The surfaces are extracted using the Constrained Laplacian Anatomical Segmentation using Proximities (CLASP) method [243,254]. Through the CLASP algorithm, the pial surface is expanded from the white matter surface to the

gray matter and cerebrospinal fluid boundary along a Laplacian field [255]. The Marching-cubes algorithm is applied during the extraction of the white surface for improved surface quality [251] (Fig. 2.7).

Following surface extraction, CT is estimated through an improved version of the tlaplace method that enables a more precise estimation of the cortical thickness at the sub-voxel level by intersecting radial lines with the cortical surfaces [251]. Cortical thickness is estimated as the minimum distance (in millimeters) between the corresponding vertices in gray matter and white matter surfaces at each vertex (transformed back to the native space of the original MR images) [245,256]. Surface Area is computed through the estimation of local variations (contraction and expansion) of the total area of all six polygons surrounding each vertex relative to the vertex distribution on the surface template on an intermediate tessellated surface mesh between pial and gray/white surfaces [257] (Fig.2.6A). Mean cortical curvature is calculated as the average of principal curvatures, derived from the inverse of the radius of the osculating circles at each vertex on the mid surface of the gray and white matter junction [150,152] (Fig.2.6B). The local Gyrification Index is calculated as the ratio between the pial surface contained in a sphere with a predefined area around each vertex and the area of a circle of equivalent center and radius on the cortical surface [258] (Fig.2.6C).

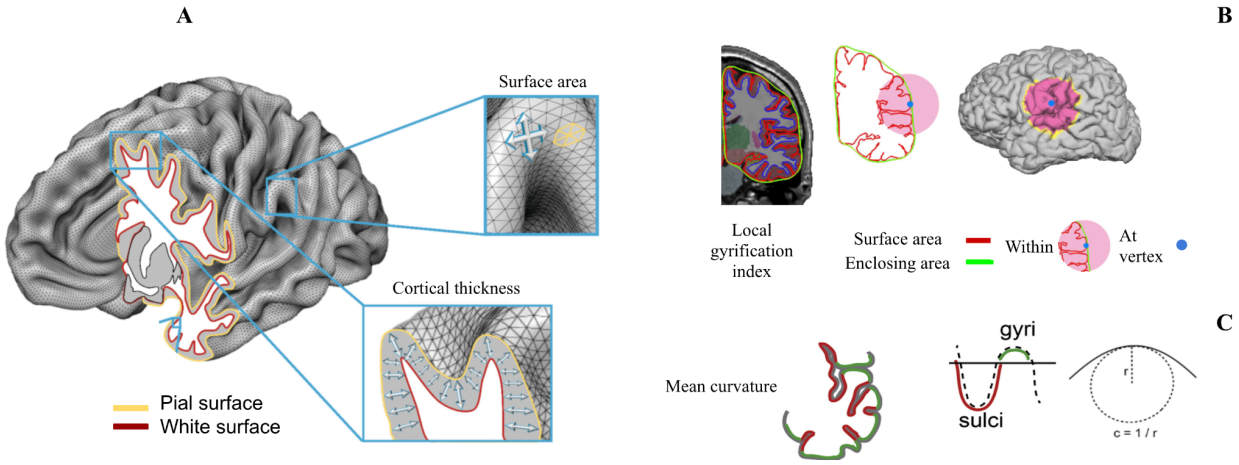

Fig.2.6. Schematic of cortical morphometric features estimation. A) Cortical thickness and surface area; adapted from [259] B) Local gyrification Index; adapted from [258,260] C) Cortical Mean curvature; adapted from [261].

2.11. Quality control

In neuroimaging studies, quality control, is of great importance, particularly to ensure the accuracy of further quantitative morphometric analyses. Quality control could be performed at several steps of pre and post-processing.

2.11.1. Motion quality control

MRI data are prone to be affected by in-scanner head motion, involuntary movements, or physiological sources of noise such as cardiac cycle and respiration, which subsequently may degrade the image quality and lead to general and regionally-specific biases and misinterpretation of the quantitative outputs derived from these images. Head motion has been

shown to compromise T1-derived gray matter volume and cortical thickness estimates [262–265], such that the seeming reductions have been reported to resemble cortical atrophy [264,265], even if the motion is not apparently detectable in the scan. Similarly, the subtle in-scanner motion has also been shown to confound measurements of MRI, such as mimicking decreases in cortical volume and thickness and increases in mean curvature with greater motion [265]. Given the inverse relationship between in-scanner motion and age [266], the issue is more critical in studies involving younger age populations and children, such as the present work.

2.12. Processing outputs quality control

In addition to the effects of motion on the quantitative estimations of neuroanatomical features, quality control of the processed images is also crucial as it could influence the output measurements. Ducharme et al. [18] have explicitly shown how different thresholds in quality control procedures could significantly impact the ultimate findings. In this study, which has investigated the effect of quality control in the context of characterization of cortical thickness developmental trajectories, it has been shown that while with no quality control, cortical thickness exhibited either a cubic or quadratic trajectory, with the inclusion of strictly screened scans the trajectories exhibited a linear pattern [18].

The CIVET pipeline automatically produces figures showing the gray and white matter classification and boundary delineations for quality control to be used for the purpose of quality control in order to prevent misleading quantitative results in further analyses [18,267] (https://github.com/CoBrALab/documentation/wiki/CIVET-Quality-Control-Guidelines) (Fig.2.7).

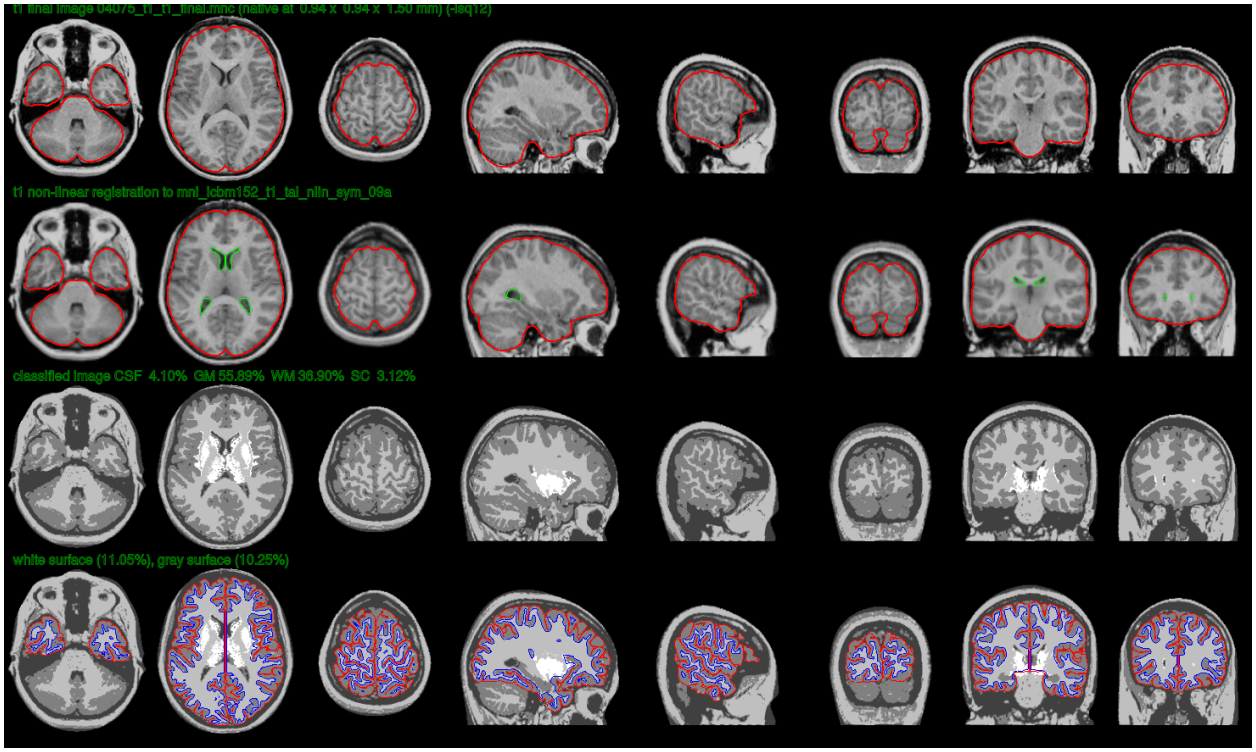

Fig.2.7. Examples of tissue classification (third row) and surface extraction (fourth row) by the CIVET pipeline.

2.13. Integrating Surface Morphology measures

Characterizing covariance across morphometric features during maturation and the relationship of the inter-individual variation related to those properties may provide important insight into their temporal patterning, sexual differentiation, environmental influence (such as socioeconomic status), and behavioral attributes related to cognition. To investigate multiple properties of cortical morphometry, several methods have been developed. Li et al. [39] have proposed a novel technique for constructing individual-based morphological brain networks using a combination of multiple morphometric features. In the proposed implementation, the interregional connections were computed as the Pearson correlation of feature vectors

comprising nine complementary morphometric features [39]. Other studies have utilized partial least squares correlation with multiple features of morphometry in order to investigate the patterns of regional correlation between cortical gray matter and white matter properties [40], or have proposed structural covariance networks using a mutually built vector based on two features of gray matter, namely SA and CT [41].

Innovatively, recent studies proposed the Morphometric Similarity Networks [MSNs], introduced by Seidlitz and colleagues [43] as a means to elucidate the relationship between multiple dimensions of brain architecture using a graph-theoretical approach. While being a critical innovation that has been shown to provide a critical relationship to transcriptomic and cell-specific architecture [44,45], this analytical technique provides limited interpretability with respect to the distinct morphological measures that contribute to specific connectomic features (although sensitivity and specificity analysis are included in the original work) [39,44–46].

2.14. Non-negative Matrix Factorization (NMF)

NMF is a data-driven matrix decomposition technique that can be used to identify dominant patterns of covariance across a dataset with a nonnegativity constraint. NMF is conceptually similar to unsupervised matrix decomposition techniques such as independent component analysis (ICA) and principal component analysis (PCA) [52–56] but requires both input and output matrices to be nonnegative. The standard decomposition methods such as PCA and ICA, commonly used to reduce the high dimensionality of a given dataset, decompose the original input matrix into a combination of positive and negative outputs [268]. Subsequently, due to the cancellation of the oppositely signed values, these techniques cannot optimally

reconstruct the input data in spatially localized and interpretably meaningful results through which the input matrix could be described [269]. NMF, alternatively, decomposes the input into purely positive outputs due to its nonnegativity constraint. This unique feature of NMF provides an additive reconstruction and representation of the data [48]. NMF is ideal for working with neuroimaging data as the elements of the input matrix are constrained to be nonnegative, it reduces the dimensionality of the high-rank neuroimaging data by providing spatially localized outputs which further facilitates the intuitive interpretation of the factorization and allows for a more straightforward interpretation of results.

Recently a variant of NMF, known as orthogonal projective nonnegative matrix factorization (OPNMF), has been explored in the context of neuroimaging data [49] which prioritizes sparsity in the solution and enforces minimally overlapping components resulting in a purely additive, part-based decomposition. More specifically, the OPNMF solution ensures that each part of the input data contributes to the reconstruction of the original input in a non-overlapping decomposition. This, in turn, provides a more biologically plausible interpretation of neuroimaging data compared to other methods of variance components that contain both positive and negative valued component weightings [49,269,270]. Moreover, despite being an unsupervised approach, the method has been shown to generate bilaterally symmetric spatial components [57] which in turn, matches well with the nature of biological data.

NMF has been investigated and used in the context of high-resolution structural neuroimaging data and has demonstrated distinguishing characteristics such as higher specificity and reproducibility compared to other multivariate approaches [49,57]. This technique has been implemented to identify structural covariance networks in neurodevelopment [50,57,89,271],

neuropsychiatric disorders [58,59,272–274], and structure-function brain networks relation [275–277] using voxel-based [50,59,269] and vertex-based [57,274,277] high-dimensional neuroimaging data. Notably, in work by Sotiras et al. [57], NMF has been used to capture reproducible spatial patterns of cortical thickness variation in brain development period [57], reflecting functional specialization and evolutionary expansion hierarchy of the cortex [57].

In the present work, we implement an orthogonal variant of NMF, orthogonal projective NMF (OPNMF) [49,278], which prioritizes sparsity in the solution and provides a part-based decomposition. The goal is to provide minimally overlapping components where each vertex is assigned to a specific component to ensure an additive parts-based representation. Thus, compared to graph theory approaches as in MSN, OPNMF identifies spatial patterns but better enables comparisons between neuroanatomical features and individual subjects.

More recently, this method has been further developed and extended by our group [51] to enable the integration of multiple structural metrics in the context of human hippocampal [51] and striatum [279] parcellation (Fig.2.8). In this implementation, briefly, a columnar stacking fashion would be applied to the vertex-wise indices of multiple structural features in order to build a single input matrix (data sample: vectorized map of multiple features). NMF would then be applied to decompose this matrix into two output matrices that their multiplication would reconstruct the input matrix with a minimum reconstruction error and high stability [51]. The results demonstrate that the output neuroanatomical definitions identify multi-modal patterns of spatial covariance with respect to multiple structural features and further can be related to inter-individual variation in demographic and cognitive features.

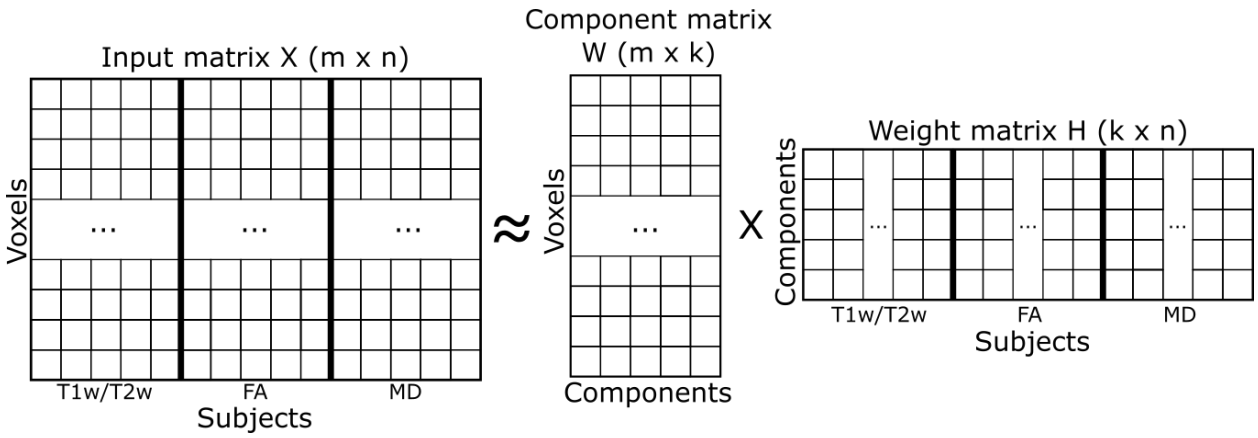

Fig.2.8. Integrated OPNMF implementation. OPNMF has been adapted to enable the integration of multiple structural metrics. Schematic adapted from [279].

2.14.1. OPNMF background

OPNMF decomposes a given input matrix V of dimensions [m x n] into a component matrix W [m x k] and a weight matrix H [k x n] in which k is the pre-defined number of components output from the decomposition. Decomposition of the input matrix is such that the multiplication of the component and weight matrices reconstructs the original input as accurately as possible with the minimum error of the reconstruction original input reconstruction [W*H]. The product of W and H matrices describes the input, and they can be used to describe patterns of covariance across both axes of the input matrix. [51,280]

Estimation of the components and weights is done through solving the nonnegative matrix factorization minimization problem formulated as follows:

$$|| X - WW^{T}X ||_2 \quad subject\ to\ W^{T}W = I;\ W > 0 \qquad (2)$$

The solution is obtained through non-negative double singular value decomposition choice of initialization [51,57,281] followed by the iterative multiplicative update rule [282] to construct W. the H matrix will then be constructed by projecting the original input X onto the W

matrix.

In the formulated solution of the nonnegative matrix factorization minimization problem, *I* represent the identity matrix, enforcing a columnar orthonormality in the W matrix. Moreover, the initialization choice enforces sparsity in the W matrix. Along with the nonnegativity constraint, these OPNMF key features result in non-overlapping and sparse columns in the output spatial components, leading to a more straightforward interpretation of the output data.

Chapter 3. Methods

3.1. Workflow Overview

We included a subset of the large-scale longitudinal T1-weighted magnetic resonance imaging (sMRI) data from the National Institute of Mental Health cohort (NIMH; Bethesda, MD, USA) [11–13,15,186,192]. Using measures of Cortical Thickness (CT), cortical Surface Area (SA), Mean Curvature (MC), and local Gyrification Index (GI) extracted from preprocessed sMRIs (Fig.3.1.A) we examined cross-sectional and longitudinal patterns of morphometric covariance using NMF (Fig.3.1.B). In the cross-sectional analysis, we used subjects' cortical measures to investigate cortical patterning, while in the longitudinal analysis, we extracted age-related slopes as a proxy of change in the cortical measures over time to investigate the pattern of coordinated maturation of the cortical features. Finally, we examined how these covariance patterns in morphometry relate to age, sex, intelligence quotient (IQ), and socioeconomic status (SES) using univariate measures to capture group-level trends and multivariate methods (PLS) to examine the relationship across demographic variables (Fig.3.1.C).

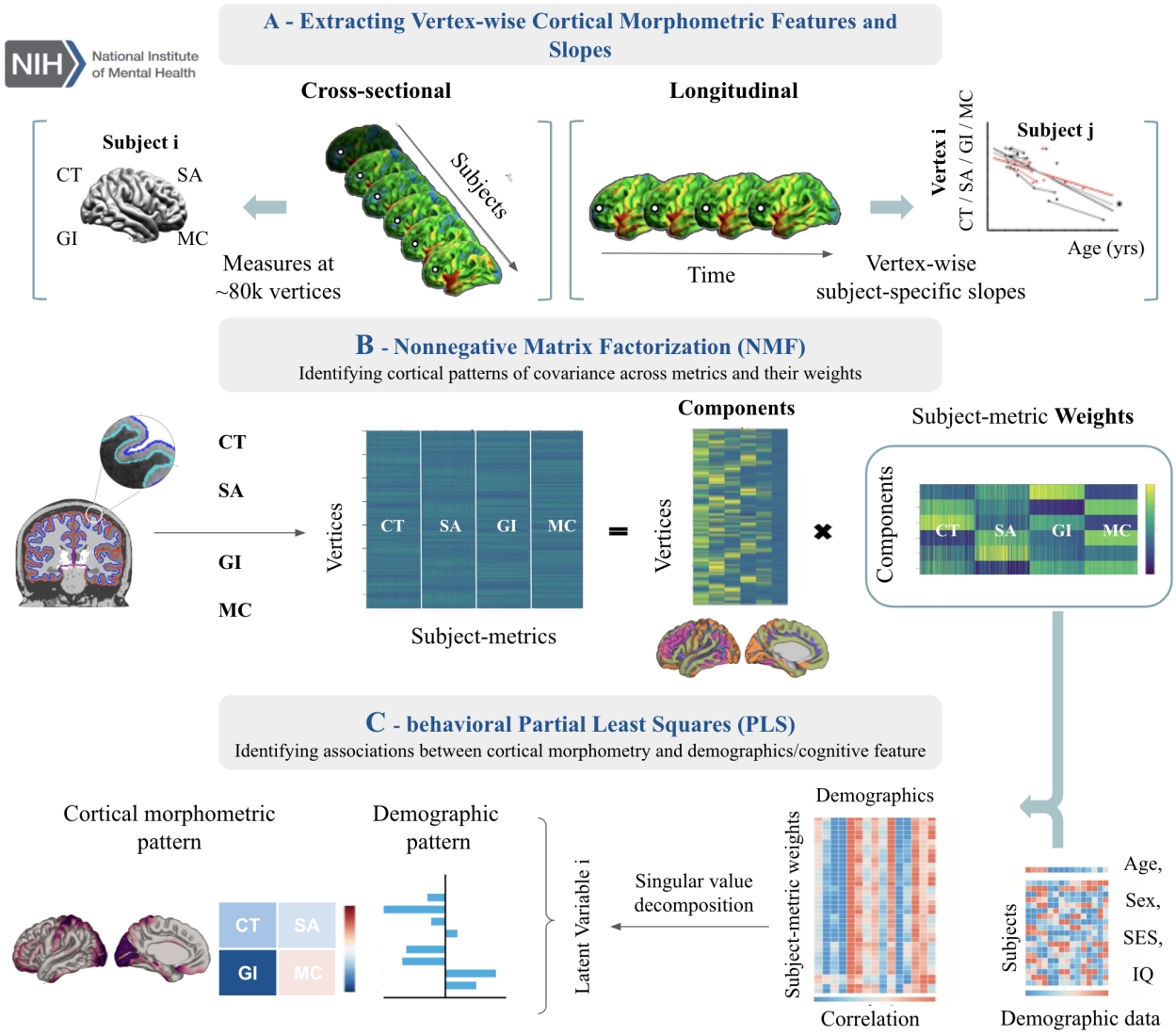

Fig. 3.1. Workflow. **A)** Four cortical metrics (CT, SA, GI, MC) were extracted, and cortical vertices of all subjects were concatenated in columns to build an input morphometry matrix. For longitudinal analysis, age-related slopes were extracted using linear mixed effect modeling. **B)** NMF decomposes the input matrix into a components matrix, representing spatially distinct components of covariance of morphometry across subjects, and a weights matrix, representing the extent to which each vertex loads onto the identified components. The optimal number of components was selected by balancing the accuracy and spatial stability of decomposition by

performing a stability analysis (see section 3.5). **C)** bPLS analysis was performed to identify patterns of covariance across components and their specific morphometric weights with demographic data (Age, Sex, SES) and cognitive ability (as indexed by IQ).

3.2. Dataset

This study includes structural magnetic resonance imaging (sMRI) data sample collected at the National Institute of Mental Health (NIMH; Bethesda, MD, USA). Participants were recruited based on their mental and physical health history for a study of brain development conducted at the National Institute of Mental Health between the years 1990 and 2014 [11,13,15,192]. Inclusions were based on the absence of a history of head trauma, neurological disease, and the diagnosis of psychiatric disorders. The NIMH cohort includes 2836 sMRI acquired from participants aged 3 to 30 years, with a similar proportion of males and females across the entire age range. All participants have 1 to 7 brain scans, acquired at intervals of approximately two and a half years. This dataset is well-characterized and has been extensively described in previous works [11–13,15,186,192].

3.2.1. Sample

We included two subsets of the NIMH dataset:

1) a cross-sectional sample, consisting of a total of 776 participants' scans at their baseline age sMRIs brain scans acquired from typically developing individuals (357 F, 46%) from age 5 to 25 (mean age:12.4, SD:3.49) for cross-sectional analysis.

2) A longitudinal sample consisting of 549 scans acquired from 183 participants, each being

scanned at three timepoints with approximately 2.8 yrs intervals, was selected. This sample was specifically ideal for capturing maturational changes in this period (see section 4.1 for participants' characteristics).

Other demographic and cognitive variables:

1) Full-scale Intelligence Quotient [IQ] estimation, using an age-appropriate Wechsler scale. 94% of participants have been assessed with the Wechsler Abbreviated Scale of Intelligence (WASI) [283], and the rest include WAIS-R, WISC-R, WISC-III, WPPSI, and WPPSI-III. Notably, since most individuals with repeated scans had fewer IQ estimated measures, we used each participant's most recent IQ estimation for the longitudinal sample analysis [192].

2) Childhood socioeconomic status (SES) score quantified by the Amherst modification of the Hollingshead two-factor index [191,284]. This variable is based on parental education and occupation, which was used to obtain a single SES score for analyses. Notably, the conventional directionality suggests that a lower Hollingshead score indicates a higher socioeconomic status such that the lowest Hollingshead score (i.e., 20) corresponds to individuals from the most advantaged families, while those from the least advantaged families have the highest Hollingshead score (i.e., 140) [192]. Accordingly, the Hollingshead score that has been used in the statistical analyses and figures has an opposite direction with socioeconomic status. For ease of interpretation, the directionality of socioeconomic status (rather than the Hollingshead score) will be discussed in the rest of the present work. [demographic and cognitive characteristics of the NIMH dataset have been extensively described in [192]]

3.3. Neuroimaging

3.3.1. Image acquisition

All scans used were T1-weighted sMRI images, collected on the same 1.5 T General Electric SIGNA scanner (Milwaukee, WI), with contiguous 1.5 mm axial slices and 2.0 mm coronal slices using a three dimensional (3D) spoiled gradient recalled-echo sequence. Image acquisition parameters are as follows: echo time: 5 ms, repetition time: 24 ms, flip angle: 45°; acquisition matrix: 256×192, number of excitations: 1, field of view: 24 cm, resulting in a voxel resolution of 0.9375×0.9375.0×1.5 mm. (for more details, see [11–13,15,186,192].)

3.3.2. Raw scan motion quality control

MRI data are prone to be affected by in-scanner head motion, involuntary movements, or physiological sources of noise such as cardiac cycle and respiration, which subsequently may degrade the image quality and lead to general and regionally-specific biases and misinterpretation of the quantitative outputs derived from these images. Due to the inverse relationship reported between in-scanner motion and age of the participants [266], the issue is more critical in studies involving younger aged populations and children, such as the present work. In the present work, all raw images were visually assessed and quality controlled for motion artifacts, such as ghosting and blurring, using the QC procedure previously developed in our group and described in [248,267] (for details, see: https://github.com/CoBrALab/documentation/wiki/Motion-Quality-Control-Manual).

3.3.3. Image Pre-processing

In order to standardize T1-weighted images quality, preprocessing was performed using the minc-bpipe-library pipeline (https://github.com/CobraLab/minc-bpipe-library). This pipeline by default performs the integrated steps of N4 bias field correction to correct for inhomogeneities in intensity [231], image registration to Montreal Neurological Institute (MNI) space (ICBM 2009c Nonlinear Symmetric) using bestlinreg [252,285], cropping the neck, field-of-view standardization using an inverse-affine transformation of an MNI space head mask, brain extraction and generating a brain mask using Brain Extraction based on nonlocal Segmentation Technique (BEaST) [233] as previously described in [286]. Following the preprocessing steps, the extracted brain bias field corrected T1 in native space with a specific brain mask for each subject was submitted to the CIVET processing pipeline.

3.3.4. Surface-based morphometry feature estimation

To estimate quantitative neuroanatomical features, we used the CIVET pipeline (Version 2.1.0; Montreal Neurological Institute; http://www.bic.mni.mcgill.ca/ServicesSoftware/CIVET; [243,249,287]. Preprocessed T1-weighted sMRI scans with matched masks, generated in minc-bpipe-library, were submitted to the CIVET for automated surface-based estimation of four cortical features of CT, SA, GI, and MC at 81,924 vertices across the cortex. T1-weighted images were linearly registered to the Montreal Neurological Institute (MNI) ICBM 152 average [288], brain tissue was classified into white matter, gray matter, and cerebrospinal fluid [253], and the surface was extracted using the Constrained Laplacian Anatomical Segmentation using Proximities (CLASP) method [243,254].

3.3.5. Extracting morphometric features

Followed by surface extraction, neuroanatomical metrics were estimated as follows:

SA: Surface Area was computed through estimation of local variations (i.e., contraction and expansion) of the total area of all six polygons surrounding each vertex relative to the vertex distribution on the surface template on an intermediate tessellated surface mesh between pial and gray/white surfaces [257]. The SA maps were blurred using a 40-mm geodesic surface kernel [243].

CT: Cortical thickness was defined and estimated as the minimum distance between the gray matter and white matter surfaces at each vertex [245,256]. CT maps were blurred using a 30-mm full-width at half-maximum (FWHM) surface-based diffusion smoothing kernel [243]. In CIVET 2.1, CT estimation has been specifically improved by intersecting radial lines with the cortical surfaces at the sub-voxel level.

GI: Local Gyrification Index was calculated for the local estimation of cortical folding at each vertex as the ratio between the pial surface contained in a small sphere around the vertex and the area of a circle of equivalent center and radius [152,258]. GI measures were estimated at a 20 mm radius.

MC: Mean cortical curvature was calculated as the average of principal curvatures, derived from the inverse of the radius of the osculating circles at each vertex on the mid surface of the gray and white matter junction [150,152].

Notably, the non-cortical midlines were masked out for analyses (4802 vertices), and we proceeded with the morphometric data of 77,122 vertices for each subject.

3.3.6. Output quality control

CIVET automatically produces figures showing the gray and white matter classification and boundary delineations for quality control. To prevent misleading quantitative results in further analyses [18], all CIVET outputs were controlled for white and gray matter classification accuracy and surface delineation by visual inspection following the QC procedure previously developed in our group [267]. Only scans that passed through the CIVET quality control will be used to extract morphometric features to be included in our analyses.

3.4. Nonnegative matrix factorization (NMF)

NMF is a data-driven matrix decomposition technique that models dominant patterns of covariance across a given dataset. The unique feature of this technique is the nonnegativity constraint which requires both input and output matrices to be non-negative. This feature of NMF is not only ideal for working with neuroimaging data as the elements of the input matrix are constrained to be nonnegative, but also provides an additive and parts-based reconstruction and representation of the data, which further facilitates the intuitive interpretation of the factorization and allows for a more straightforward and biologically plausible interpretation of neuroimaging data compared to other methods of variance components that contain both positive and negative component weightings [49,51,270].

In the current work, we employed the orthogonal version of NMF, orthogonal projective NMF (OPNMF) [49,278], which prioritizes sparsity in the solution and provides a part-based decomposition. The goal is to provide minimally overlapping components where orthogonality ensures each vertex is assigned to a specific component to reach an additive parts-based

representation and improves the specificity, and the projective features ensure that all components participate in the reconstruction of the input data sample, which improves sparsity. Compared to graph theory approaches, OPNMF identifies spatial patterns but better enables comparisons between neuroanatomical features and individual subjects.

3.4.1. Implementation

The input matrix was created such that for each subject, each of the four cortical metrics vertex-wise measures were stacked across hemispheres to create a single column of vertex-wise data for a given subject-metric. Given the inclusion of 776 subjects and the columnar stacking fashion of the four morphometric features of CT, SA, GI, and MC, the input matrix was built having 776* 4 columns such that the first 776 rows correspond to subjects' CT values, second 776 rows correspond to subjects' SA values, etc. Finally, a within-subject z-scoring normalization was performed to have different metrics with varying magnitudes on the same scale and shifted by the minimum z-scored value to eliminate negative values. This multivariate morphometry matrix would then be submitted to OPNMF.

3.4.2. Longitudinal Implementation

To better capture the dynamic relationship between cortical features, in order to investigate the coordinated pattern of cortical change across multiple measures, and how coordinated changes at different cortical regions are driven by changes at each cortical feature, we also leveraged a longitudinal implementation of NMF. To do so, we included 183 participants with three scans (a total of 549 total scans) acquired at three different time points with an average of 2.8 years intervals to extract vertex-wise and subject-specific age-related slopes. To do so, linear mixed-effects regression models with random intercept and slope for each subject were

performed. We next extracted subject-specific vertex-wise age-related coefficients, as a proxy of change over time, for each of the four morphometric features as the input for OPNMF.

To extract subject-specific cortical slopes, for each metric, a vertex-wise linear mixed-effects model was performed with age as the fixed effect and a random intercept and slope of age for each subject. Models were implemented in R (Version 3.6.3; www.r-project.com).

The coefficients for *i*th subject's *j*th vertex's metric n at *k*th time-point were calculated based on the regression model as follows:

$$Y_{subjectj\_vertexi\_metricn} = \beta 0 + dij + \beta 1\ (Age) + \beta j\ (1+Age|Subject) + eij \quad (3)$$

Where Y corresponds to subjects' metric measures at each vertex, β_0 corresponds to equation intercept, β_1 corresponds to fixed-effect coefficient, and β_j corresponds to subjects' random B-value. From each model, subject-specific age-related slopes (i.e. coefficient) were extracted using the R coef() function. Coefficients are the summations of the general fixed effect of age (β_1) and subject-specific random effects (β_j) [289], representing the impact of age on each cortical measure. Finally, to capture patterns of 'coordinated change' across cortical features, the input matrix was reconstructed similar to cross-sectional methods (see section 3.4.1) with columns containing vertex-wise calculated age coefficients in three consecutive timepoints for each subject-metric pair.

3.4.3. Running OPNMF

Following the construction of the input matrix, the OPNMF run was performed using the publicly available code by [49,278,290,291] at (https://github.com/asotiras/brainparts) using Matlab R2016a. The algorithm was initialized with a nonnegative, double singular value

decomposition (SVD) and followed a maximum iteration of 100000 and tolerance = 0.00001, as previously described in [51].

3.4.4. Interpreting OPNMF outputs

The implemented OPNMF outputs results are components matrix (W) and weights matrix (H), which together reconstruct the input matrix:

1) Component matrix (W) of dimensions [cortical vertices (m) x number of components (k)]: indicates the spatial location of the components indicating the extent to which each vertex in the brain loads onto each component. Due to the orthogonality feature of OPNMF, each vertex is assigned to the cluster of vertices for which it has the highest component score. Mapping back these identified clusters of vertices to the population average brain enables visualization of a parts-based representation of spatial cortical components that share the same patterns of covariance across four morphometric features.

2) Weight matrix H of dimensions [number of components (k) x subject-metric pairs (n)] represents each subject-metric pair contribution and loading onto each of the identified components. Accordingly, a higher subject-metric loading onto a given component's vertex would indicate a greater magnitude of that metric within a subject's covariance pattern. The components and weight matrix are then jointly used to describe the spatial location of identified components (W matrix) and the pattern of covariance across multiple morphometric features of the cortex (H matrix).

3.4.5. Interpreting longitudinal OPNMF outputs

Similar to outputs described in section 3.4.4, longitudinal OPNMF outputs a component and a weights matrix that jointly describe the extent to which each identified cortical component

is derived by a specific pattern of coordinated changes across morphometric features. In the weight matrix, higher weights indicate a relatively higher magnitude of slopes which implies a steeper decline, preservation, or decrease in the specific metric. Lower weights are indicative of a lower magnitude of slopes which implies relatively sharper decline and loss in the specific morphometric feature.

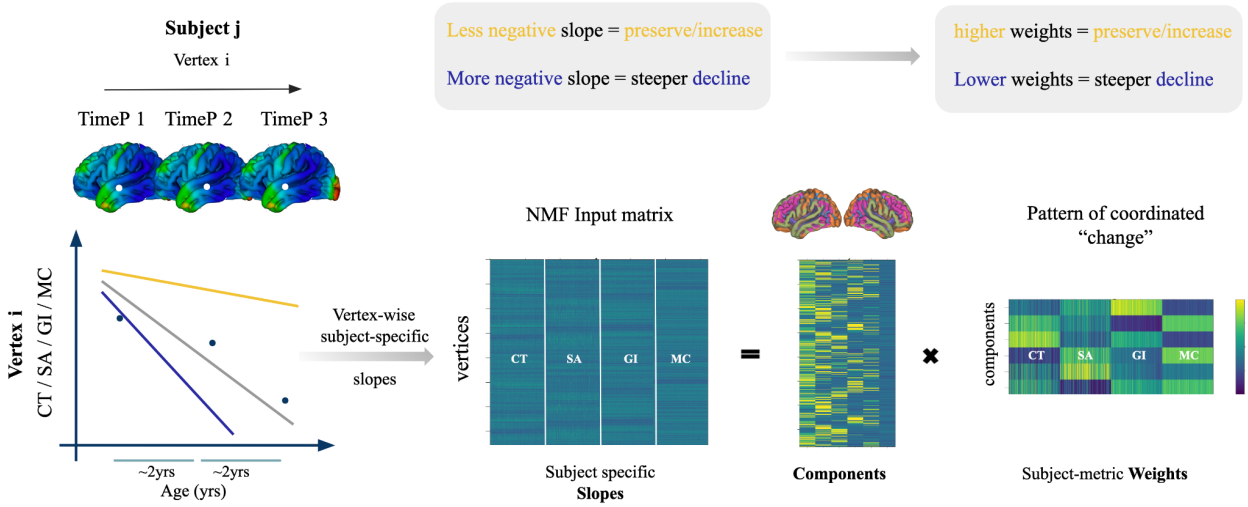

Fig.3.2. A schematic representation of longitudinal nmf implication and interpretation. While higher NMF weights indicate relative preservation of a metric, a lower weight indicates a steeper decline over time.

3.5. Stability analysis

To select the optimal number of components (k) for OPNMF decomposition, stability analysis was performed. In order to balance the high spatial stability of various decompositions while capturing major changes in the reconstruction accuracy, a split-half stability coefficient and the change in reconstruction errors were calculated for a range of 2-20 component decompositions [51]. To assess the stability, we measured the spatial similarity between the

component's output of OPNMF runs across varying random splits of the input data at each granularity of 2 - 20. Accuracy was calculated as the gradient in reconstruction error, based on the change in the reconstruction error from one granularity to the next (k to k + 1) [51]. The procedure was done by splitting the participants (i.e.,: n=776) into two groups of (n_a = 388) and b (n_b = 388) ten times. For each of the half-splits, a separate four-metric input matrix was built (Va and Vb), and we performed OPNMF on each of the half-splits independently. Each run outputs a weight and a component matrix, Wa and Wb matrices, of dimensions [#vertices * k].

To calculate the stability, a similarity matrix for each of Wa and Wb matrices (c_Wa, and c_Wb) was computed using cosine similarity for rows of W matrices such that in each similarity matrix, the cosine similarity of component scores between a specific vertex and all other vertices is represented in each row. The higher the cosine similarity for each vertex with other vertices, the more likeliness of those vertices to be clustered together. Next, the correlation coefficient between corresponding rows of the similarity matrices of each split (c_Wa, and c_Wb) was computed. The mean correlation across all rows (vertices) was taken as an indicator for stability at that specifically tested granularity such that a mean correlation coefficient of 1 represents the highest stability, while −1 represents the lowest stability [51]. To assess the accuracy of reconstruction of the original input matrix, we computed the subtraction of the reconstruction error matrix at each granularity (k) from the reconstruction error matrix at granularity at the following granularity (k+1) and averaged the differences across all splits to report the gradient reconstruction error at each granularity. These procedures were repeated for ten random splits of the data and at each even granularity of k = 2 - 20 [51].

3.6. Post NMF analysis

3.6.1. Multiple Linear regression models

To assess associations between metric-wise NMF components weigh on one hand and age, sex, IQ, and SES on the other hand, we performed multiple linear regression analyses to determine the statistical significance of the regression model.

To this end, we ran a metric paired components-wise regression model, in which for *i*th components' *j*th metric was modeled as follows:

$$Y_{Component\ (i)\_metric\ (j)} = \beta_0 + \beta_1(Age) + \beta_2(Sex) + \beta_3(IQ) + \beta_4(SES) \quad (4)$$

$$Y_{Component\ (i)\_metric\ (j)} = \beta_0 + \beta_1(Age \times Sex) + \beta_2(IQ) + \beta_3(SES) \quad (5)$$

Where Y corresponds to metric-wise OPNMF components weights, β_0 corresponds to equation intercept, and β_i corresponds to fixed-effect coefficient. We looked at all regression beta coefficients, with particular emphasis on age effects grouped by sex, and age and sex interactions. We looked for associations between component weights and each demographic variable, corrected for multiple comparisons across components, and thresholded at a false discovery rate (FDR; [292]) of $q < 0.05$.

3.6.2. Behavioral Partial Least Square Analysis (bPLS)

To investigate possible relationships across identified individual variation patterns of morphometry and demographics data, we performed behavioral partial least square analysis (bPLS). bPLS is a multivariate technique used to capture major covariance patterns between the two sets of data via singular value decomposition (SVD) of a mutually constructed correlation

matrix, which outputs uncorrelated sets of latent variables (LV). Each LV describes the linear combinations of the two datasets that are maximally covariant and can be interpreted as a pattern of association between the two sets of data [51,293–296]. For each LV, a singular value is computed describing the percentage of the data explained by that LV. Within each LV, both sets of variable parameters will be attributed to scores, reflecting the extent to which each parameter contributes to the identified covariance patterns represented by LVs [51,293–296]. In the context of neuroimaging analysis, this method has been originally and conventionally used to relate a set of neuroimaging data (i.e., voxel- or vertex-wise data) to a set of behavioral data [293–295]. This method has been further developed in our previous works to enable relating integrative structural and morphometric patterns derived from NMF, to inter-individual differences [51,60]. Here, we performed behavioral PLS to assess patterns of correlation across two sets of 1) brain data, the H matrix output from OPNMF containing components' subject-metric pair weights, and 2) demographics and cognitive data, including subjects' age, biological sex, SES, and IQ scores. the brain matrix of dimensions (776 subjects × 4 metrics × 6 components) and a demographic matrix of dimensions (776 subjects × 4 demographic variables) was used as the input matrices of PLS (Sex coded as 0 = Female, 1= Male, Age measured in years, SES measured in Hollingshead two-factor index, and IQ measured in Wechsler). PLS analysis outputs LVs representing patterns of covariance across component-wise morphometric brain data and demographic data. To assess the statistical significance of output LVs, we performed 10000 permutations testing such that rows of the brain data matrix were permuted 10000 times to obtain a null distribution of singular values under the assumption of permutations eliminating existing brain-demographics correlations, which yields to the computation of a non-parametric P-value for each LV in the primary data (non-permuted) [51]. We then applied a $P<0.05$ threshold for consideration of LVs

significance, indicating a chance of a 95% confidence that the singular value of the primary LV exceeds that of a singular value of the permuted LV [51]. To assess the contribution of each brain variable (component-wise morphometric brain data) to each identified LV, we employed bootstrap resampling. We randomly sampled 10000 sets of each brain and demographics matrices and replaced the rows to create a distribution of the singular vector weight of each brain variable in each LV. Next, to examine the contribution and reliability of a given brain variable, the bootstrap ratio (BSR) was calculated as the ratio of generated singular vector weight over the standard error of the weight from the bootstrap distribution. We then applied a threshold of $P<0.01$ (99% confidence) for consideration of brain variables' contribution significance, corresponding to a $BSR<2.58$ [51,293–296].

3.7. Situating Morphometric components along the gradients of brain function

Previous studies have shown that morphological networks can be used to investigate the hierarchy of cortical macroscale organization [39,282,297]. Importantly, in a recent study, Dong et al. [298] have demonstrated age-dependent patterns of gradual maturation in the macroscale of a cortical organization that may be key to understanding the processes through which cognitive capabilities and behavioral traits are shaped and refined [298]. In children (under 12 years old), the organizational gradient peaks within the unimodal cortices, between somatosensory/motor and visual cortices which in adolescence (12 years old and over), transitions into an adult-like spatial framework, with the default network at the opposite end of a spectrum from primary

sensory and motor regions [298].

Accordingly, we aimed to assess how the identified morphometric covariance patterns situate along the stages of the principal gradients' gradual maturation within the different periods of childhood, adolescence, and adulthood. To do so, gradient value distributions of vertices within each component's spatial boundaries were extracted from the maps of the second gradient of functional connectivity for children (6-12 years old) and the map of the first gradient map from adolescents (12-18 years old) and adults (22-35 years old). The child and adolescent maps were obtained from Dong et al. [298], and the adult map was obtained from Margulies et al. [299]. All gradient maps were transformed into CIVET space (MNI ICBM152 surface) using the neuromaps toolbox [300] (https://github.com/rmarkello/neuromaps) to further assess NMF components' position along the maps.

Chapter 4. Results

4.1. Final sample

From the initial 3097 scans of the NIMH dataset, 2658 scans were included based on the age range of this study and health profile. Of which, 811 were excluded at the level of motion QC (at both pre-and post- preprocessing steps; based on criteria described at [267]), and 159 were excluded at the level of software failure and post-processing quality control.

For cross-sectional analysis, 776 participants (357 F; mean age:12.4, Standard Deviation [SD]:3.49) (Fig.4.2), and for the longitudinal analysis, 183 participants (77 F; three repeated scans per subject; approximate interval 2.8 years; mean age: 11.2, SD: 2.7) were included (Fig.4.2). Full-scale Intelligence Quotient (IQ) and childhood socioeconomic status (SES) scores were included as demographics for further analyses (see Table 4.1 for both cross-sectional and longitudinal data samples participants' demographics data characteristics.)

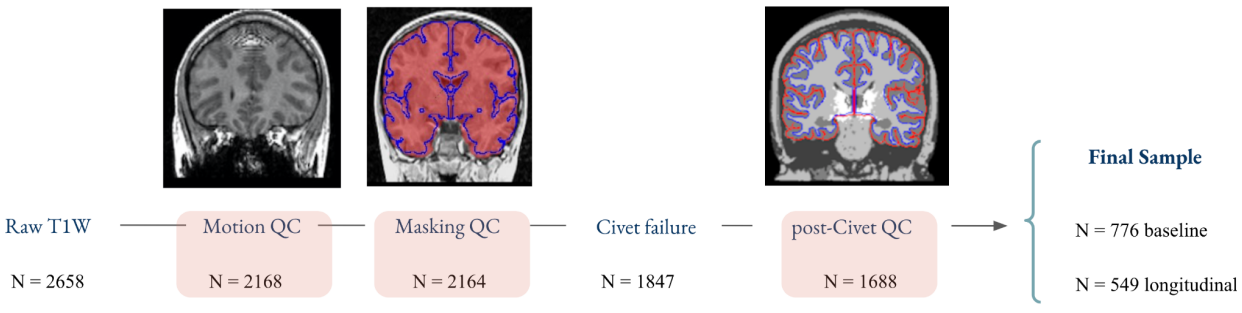

Fig.4.1. Quality control and scan exclusion procedure.

Table 4.1. Cross-sectional and longitudinal data samples participants' demographic data characteristics.

Characteristic \ Data sample	Cross-sectional sample	Longitudinal sample
Number of scans	776	549
Number of individuals	776	183
Age, years		
Mean (SD)	12.4 (3.49)	11.2 (2.7)
Range	5 - 25	5 - 24.2
Sex, n		
Female (%)	357 (46%)	77 (42)
Male	419	106
IQ		
Mean (SD)	110 (13.1)	114 (12.4)
Range	50 - 150	80 - 140
SES		
Mean (SD)	44 (18.3)	40 (19.7)
Range	20 - 94	20 - 90
Intervals between scans, years		
Mean (SD)	NA	2.8 (0.5)
Range	NA	1- 6

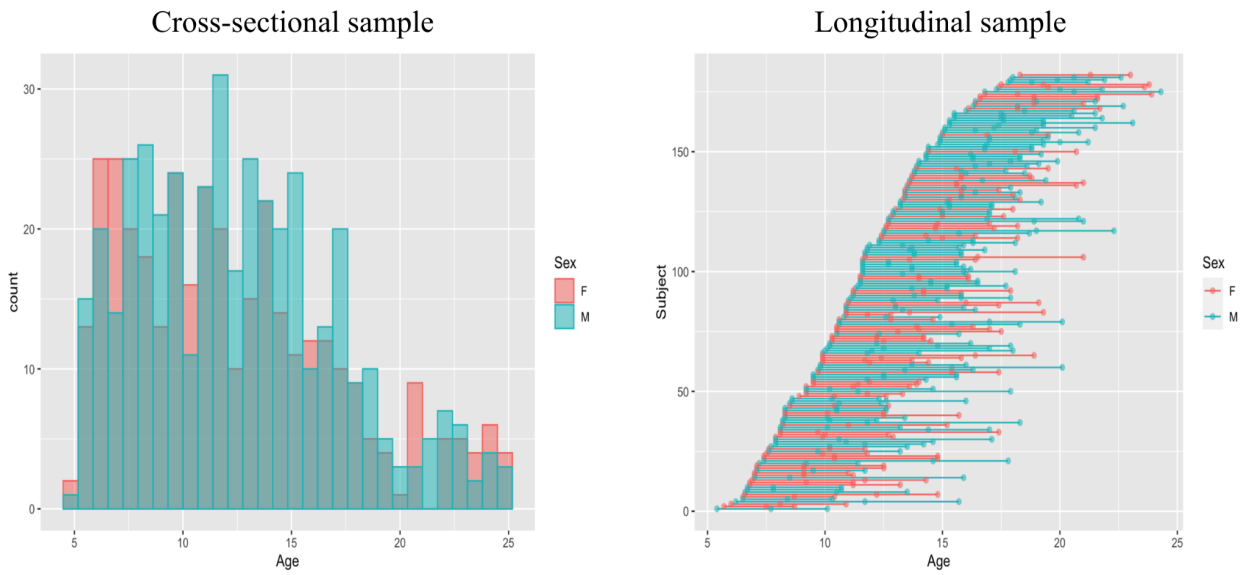

Fig.4.2. NIMH subsamples characteristics. left) Histogram showing the distribution of scans on the sample by subjects' age and sex (females in red). right) Dot and line plot showing the distribution of scans per subject by age and sex where each line indicates a subject with repeated scans identified by dots.

4.2. Stability analysis results

The stability analysis results for both cross-sectional and longitudinal analyses are shown in Fig.4.3: the stability coefficient (red) and the gradient of the reconstruction error (blue) of OPNMF decompositions are shown for every other granularity of 2 - 20. In Fig 4.3, the inverse relationship between the number of components and stability is shown. At $k > 6$, the stability coefficient is above 0.95, which sharply drops moving from $k = 6$ to $k = 8$. As a result, we chose $k = 6$ as a decision point for choosing parsimonious but stable spatial patterns. This choice also prioritizes stability while capturing complex spatial patterns.

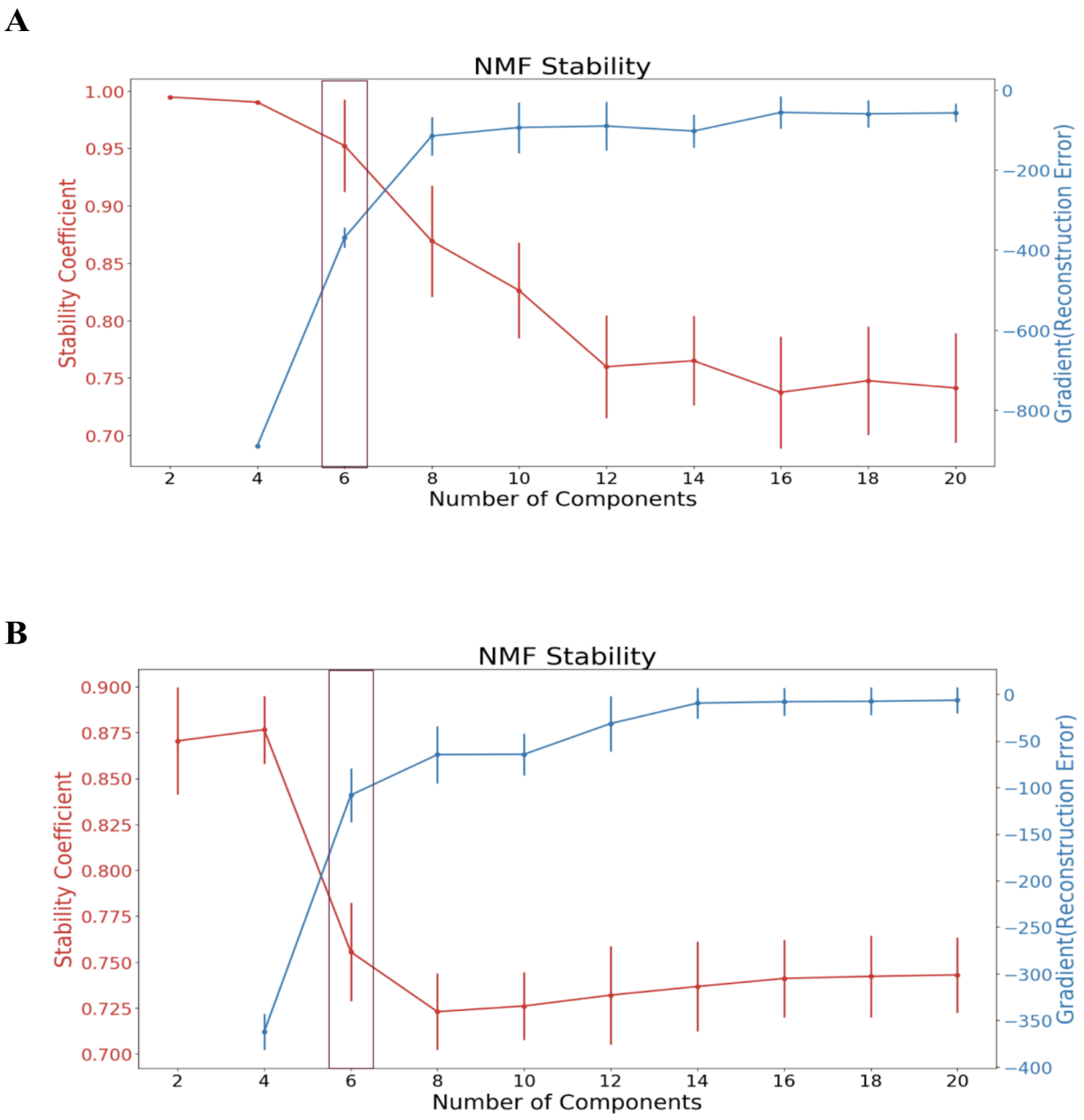

Fig.4.3. A) cross-sectional and B) longitudinal split stability analysis plots: Stability coefficients and gradient of the reconstruction error for granularities from 2 to 20. The k = 6 decomposition solution was chosen as a suitable balance of stability, and reconstruction accuracy for both decompositions as stability (red line) drops at k > 6, and the gradient in reconstruction error (blue line) from k = 6 to k = 8 is considerably less than from k = 4 to k = 6.

4.3. Morphometric Covariance Results

4.3.1. Cross-sectional morphometric covariance

Components identified in Section 4.2 reflect morphological covariance patterns across the four input metrics (Fig.4.4A), and the weights matrix describes the extent to which each subject-metric pair loads onto a specific component (Fig.4.4B; z-scored to facilitate visualization) [51,60].

The spatial extents of each component are described by their anatomical location, and the specific patterning of morphometric features is described in the weight matrix. Notably, even though there were no topological constraints in our analysis, there is significant topological specificity and bilateral representation for each component:

1. Component [C] 1 is characterized by higher values of GI and variation in SA, primarily in the sulcal depth of temporal, occipital, and parietal association cortices.
2. C 2 is characterized by higher values of CT and MC, moderate variation in SA, and lower values of GI in limbic and heteromodal regions along the medial surface, extending along the temporoparietal junction, Broca’s and Wernicke's area to the orbitofrontal cortex, and the superior gyrus.
3. C 3 is characterized by high GI and moderate SA weighting across the insular cortices and cingulate sulcus.
4. C 4 is characterized by higher MC and SA weight values along the fusiform and orbitofrontal gyri and unimodal regions along the lateral and medial occipital lobe and postcentral gyri.

5. C 5 is characterized by primarily higher SA weights in primary heteromodal regions of the inferior temporal, inferior parietal, and dorsolateral medial prefrontal cortex.
6. C 6 is characterized by low SA, moderate CT and GI, and high MC. This component includes cortical regions of pre and postcentral gyri (primary sensory and motor cortex) and precuneus.

4.3.2. Longitudinal morphometric covariance

Longitudinal analysis using NMF also identified six stable spatial cortical components representing a selection of vertices sharing a coordinated morphological pattern of change across the four metrics (Fig.4.4C). Here, the weights matrix describes the extent to which each subject-metric change (i.e., age-related slope) loads onto the identified spatial pattern (i.e., components) (Fig.4.4D).

Fig.4.4 shows the subject weight matrix, describing morphometric patterns associated with each component.

1. Longitudinal Component [LC] 1 describes relative preservation of GI, dominant decline of CT, and a moderate decline of MC and SA across much of the cortex, in keeping with the known literature on brain morphology changes during development.
2. LC 2 describes relative preservation of CT, a sharp decline of GI, and a decline of SA and MC in bilateral occipital and temporal poles and the right precentral gyrus/ primary somatosensory areas.
3. LC 3 describes the preservation of MC and a decline of CT, SA, and GI, respectively in the sulcal depths and precuneus.

4. LC 4 describes relative preservation of SA and steeper GI decline in GI and moderate CT and MC decline in unimodal areas such as primary somatosensory areas, cuneus, and lingual gyrus.
5. LC 5 describes a steep SA decline and moderate CT decline in the left temporoparietal junction.
6. LC 6 describes a steep decline in CT and a moderate decline of MC in the posterior cingulate gyrus.

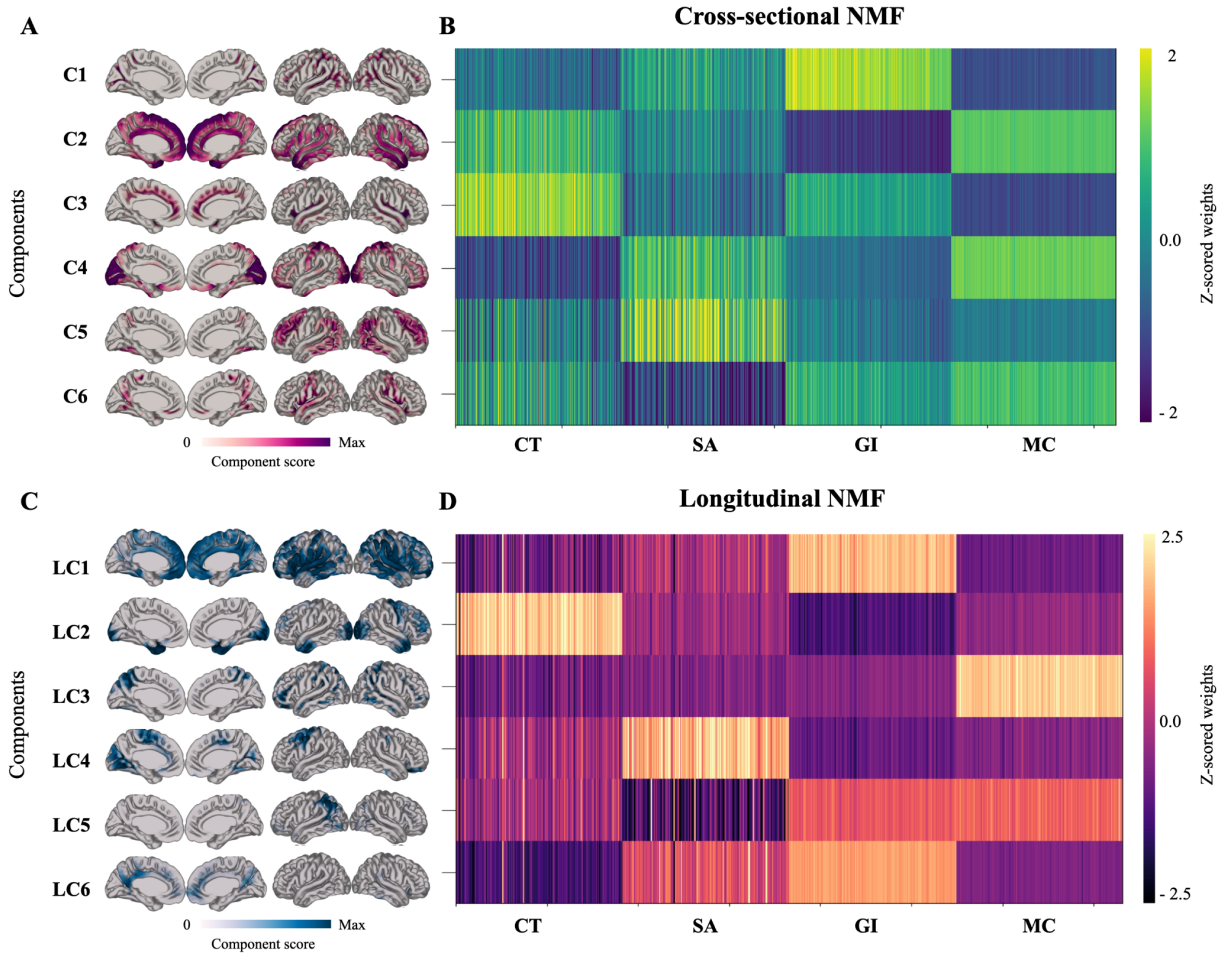

Fig.4.4) A & C. Spatial cortical components of a 6 component decomposition solution. Identified components are projected onto an average template brain. Lateral and medial views of both

hemispheres are shown. Warmer blues correspond to higher component scores. **A)** vertices that are grouped together in components share the same pattern of morphometry, while in **C)** vertices that cluster together share a coordinated pattern of maturation across four metrics. **B & D.** The weight matrix shows a comparative morphometric pattern of each component. **B)** brighter colors represent higher values (measurements) **D)** brighter colors represent higher slopes and preservation. Please note that the weight matrix is normalized by z-scoring within each row for the purpose of visualization to better capture the comparative morphometric features of each component.

4.4. Post-NMF analyses results

4.4.1. Multiple Linear regression models

To investigate the specific sex and age by sex associations with regional patterns of morphometric variation, we also performed multiple linear regression analyses to determine the statistical significance of the regression model. Fig 4.5 displays multiple linear regression models of OPNMF individuals' weightings, corrected for multiple comparisons across components (q-value = p-value <0.008), plotted against age for males and females.

All components' weights significantly decreased with age, except for MC weights being significantly increasing in C1 and decreasing in C2 and in the components of 3, 4, 5, and 6, which were not associated with age. Weightings of most components were significantly greater in males than females across morphometric measures; SA weights across all components, CT across components 4 and 6, GI across components 2, 5, and 6. Conversely, in MC weights, females' weights were significantly higher across all components (marked with green Astros in Fig.4.5). Significant age and sex interactions were observed across SA weightings in components

1, 4, 5, 6 such that males show a slower SA loss relative to females. Significant age and sex interactions were observed across CT weightings in component 4 such that males show a slower CT thinning loss relative to females (highlighted in light blue in Fig.4.5). SES analysis revealed associations exclusively with GI weights across components 1, 2, and 5 (highlighted in yellow in Fig.4.5). However, IQ scores weren't associated with cortical weights.

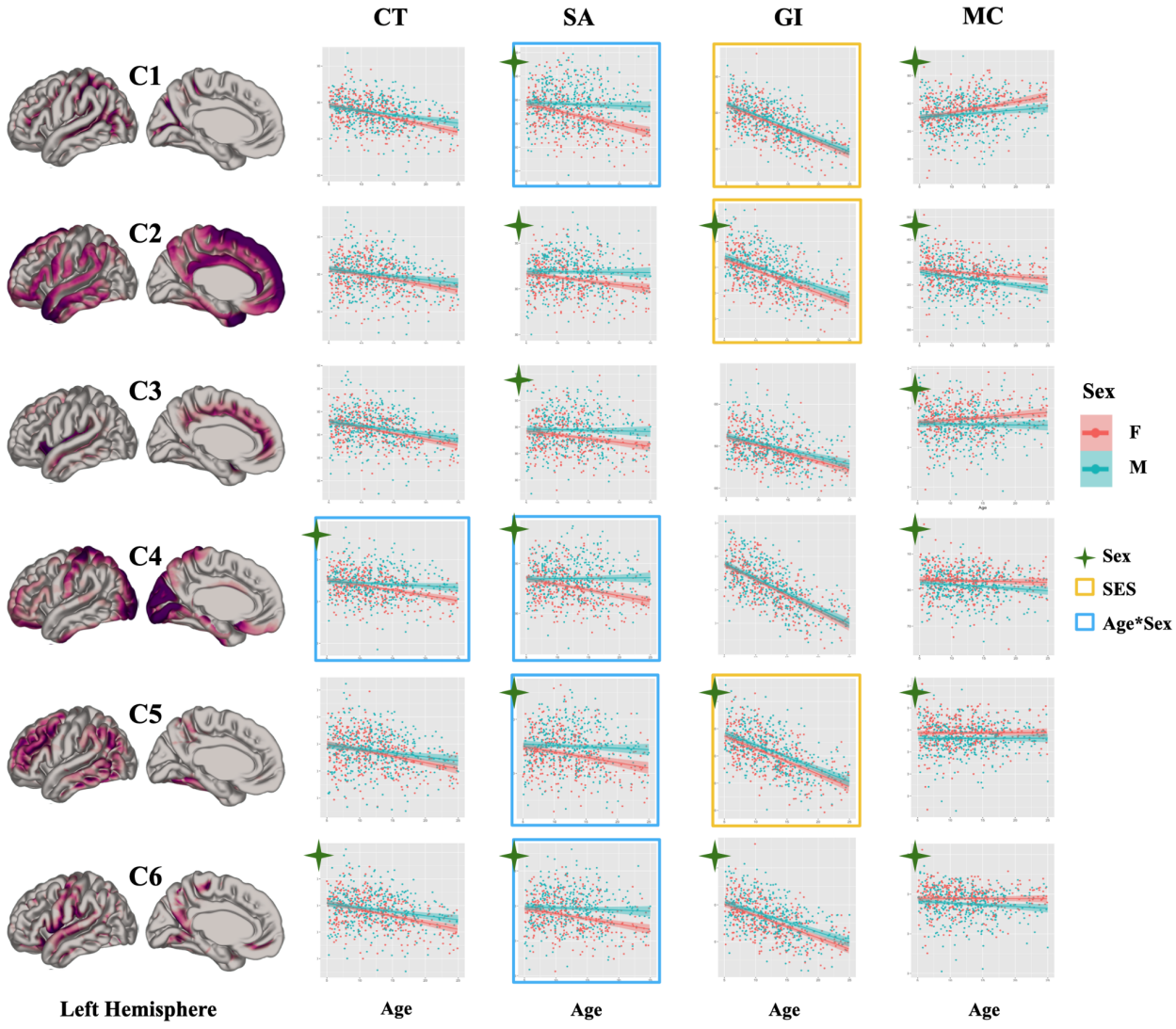

Fig.4.5) Multiple linear regression models of individuals' weightings plotted against age for males and females association with respect to age and sex. Component weights with significant

age-by-sex interactions are highlighted in blue, component weights significantly associated with SES are highlighted in yellow, and component weights significantly associated with sex are marked by green Astros.

Table 4.2. Summary of all linear model results. T-values (t) and p-values (p) (uncorrected) are bolded if they survive Bonferroni correction (q-value=p<0.008).

metric	CT					SA				
factor	**Age**	**SexM**	**SES**	**IQ**	**Age*Sex**	**Age**	**SexM**	**SES**	**IQ**	**Age*Sex**
C1	**t=-10.30 p=<2e-16**	t= 2.086 p=0.037	t= 0.659 p=0.5098	t=0.161 p=0.8718	t= 2.515 p=0.012	**t=-5.422 p=7.89e-08**	**t= 7.197 p=1.46e-12**	t=-1.252 p=0.211	t= 0.614 p= 0.539	**t= 4.125 p=4.11e-05**
C2	**t= -6.842 p=1.59e-11**	t= 2.238 p=0.025	t= 1.368 p=0.1717	t=0.433 p=0.6651	t= 1.359 p= 0.175	**t= -2.854 p=0.0044**	**t= 5.777 p=1.1e-08**	t=-0.823 p=0.410	t= 1.382 p= 0.167	t= 2.630 p= 0.00870
C3	**t= -8.769 p=<2e-16**	t= 2.080 p=0.037	t=0.0686 p=0.644	t=0.0842 p=0.141	t=1.406 p=0.160	**t= -3.005 p=0.0027**	**t=5.000 p=7.11e-07**	t= -1.118 p=0.263	t= 1.478 p=0.1397	t= 2.453 p= 0.01439
C4	**t= -6.101 p=1.67e-09**	**t= 3.655 p=0.0002**	t= 1.223 p=0.2217	t=0.293 p=0.7699	**t=3.307 p=0.000**	**t= -3.833 p=0.0001**	**t= 6.489 p=1.55e-10**	t= 0.051 p=0.959	t= 0.240 p=0.8107	**t= 4.432 p=1.07e-05**
C5	**t= -7.188 p=1.56e-12**	t= 1.591 p=0.112	**t= 1.392 p= 0.164**	t=0.617 p=0.538	t= 1.762 p=0.078	**t= -4.122 p=4.16e-05**	**t= 5.674 p=1.98e-08**	t=-1.076 p=0.282	t= 1.796 p=0.0729	**t= 2.649 p= 0.00824**
C6	**t= -8.545 p=2e-16**	**t= 2.664 p=0.007**	t= 0.924 p=0.3555	t=0.249 p=0.8036	**t=2.046 p=0.041**	**t=-4.428 p=1.09e-05**	**t= 6.159 p=1.18e-09**	t=-1.205 p=0.228	t= 1.865 p=0.0626	**t= 3.034 p= 0.0025**

Metric	GI					MC				
factor	**Age**	**SexM**	**SES**	**IQ**	**Age*Sex**	**Age**	**SexM**	**SES**	**IQ**	**Age*Sex**
C1	**t=-22.186 p=< 2e-16**	t= 2.297 p=0.0218	**t= -2.898 p=0.003**	t=-0.575 p=0.5653	t= 0.176 p=0.860	**t= 6.107 p=1.61e-09**	**t= -3.170 p=0.001**	t=0.725 p=0.46	t= -0.264 p=0.7918	t= -2.424 p= 0.0156
C2	**t=-16.589 p=<2e-16**	t= 3.861 p=0.0001	**t= -3.065 p=0.002**	t=0.597 p=0.5504	t=0.621 p=0.534	**t=-5.880 p=6.11e-09**	**t= -5.141 p=3.48e-07**	t=-0.36 p=0.71	t= -0.982 p=0.326	t= -1.629 p= 0.10379
C3	**t=-12.323 p=<2e-16**	t= 2.533 p=0.0115	t= -2.543 p=0.0112	t=0.360 p=0.7187	t=0.877 p=0.380	t= 1.548 p=0.122	**t=-4.342 p=1.6e-05**	t=0.957 p=0.33	t= -0.181 p=0.856	t=-2.141 p=0.03263
C4	**t=-24.249 p=<2e-16**	t= 1.652 p=0.0988	t= -2.632 p=0.0086	t= -0.320 p=0.7487	t=0.293 p=0.769	t= -2.537 p=0.0114	**t=-4.629 p=4.3e-06**	t= 0.02 p=0.32	t= -0.979 p=0.1476	t=-1.394 p=0.164
C5	**t=-19.030 p=< 2e-16**	t= 3.358 p=0.0008	**t= -2.978 p= 0.002**	t= 0.011 p=0.9913	t=0.306 p=0.759	t= 0.056 p=0.955	**t=-4.951 p=9.07e-07**	t=-0.10 p=0.91	t= -1.377 p=0.169	t= -0.122 p=0.9032
C6	**t= -17.391 p=< 2e-16**	t= 3.404 p=0.0006	t= -2.104 p=0.0357	t= 0.312 p=0.7554	t=0.981 p=0.327	t= -1.756 p=0.0795	**t=-5.101 p=4.25e-07**	t=0.074 p=0.94	t= -0.208 p=0.8352	t= -1.515 p= 0.130

4.4.2. Cross-sectional NMF analysis results are mostly associated with age

PLS identified a single significant LV ($p<0.05$), explaining 94.6% of the covariance across cortical and demographic data (Fig.4.6). The largest contribution to the demographic covariance patterns is clearly age, and in the morphometry pattern, we see a somewhat unexpected dominant contribution of GI across all components and the somewhat unexpected contribution of CT, and to a lesser extent of SA. However, we do also observe the subtle impact of lower SES and IQ scores on these patterns, suggesting patterns of brain maturation, distributed decreases in GI, CT, and SA through the cortex, and also local increase in the sulcal depth in MC, to be associated with lower IQ and SES.

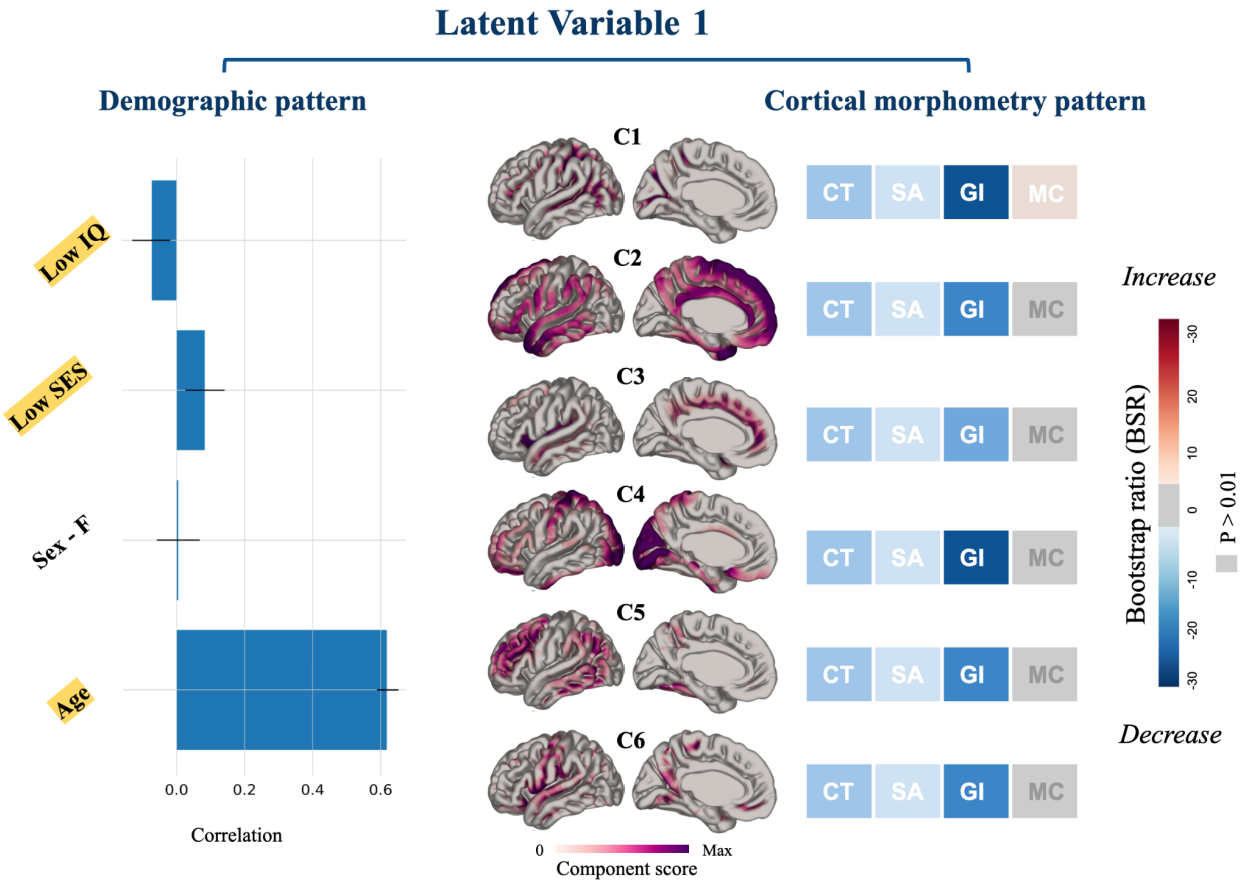

Fig.4.6) The single significant cross-sectional NMF and individual's characteristics LV. Cortical components of morphometric features (left) and demographic data (right) contributing to the LV are shown. Right) The brain maps are summarized with their morphometric profiles, each with a set of four metrics corresponding to a single spatial component; for each significant morphometric feature contributing to the LV, the bootstrap ratios are displayed on the components' morphometry profile, In which a decrease in a metric is color-coded in blue whereas increases, in red. Left) The Bar plot describes the contribution of demographic variables to the identified LV. The x-axis demonstrates the correlation of each demographic variable in the LV. Error bars indicate the 95% confidence interval; variables with a BSR> 0.196 ($p < 0.05$) are described as contributing to the LV [51] (color-coded in yellow). Please note the opposite directionality of the Hollingshead score used in the analysis and figure, and the SES.

4.4.3. Longitudinal NMF analysis results demonstrate increased specificity to demographics

bPLS identified three significant ($p<0.05$) LVs, altogether explaining 97.6% of the covariance across cortical and demographic data. In Fig.4, cortical morphometry and demographic patterns contributing to the LVs and their corresponding bootstrap ratios (BSR) are displayed.

LV1 ($p= 0.0001$), explaining 47% of covariance across the brain and demographic data, describes a sexually differentiated pattern of change in the cortical morphometry slopes which five of the cortical components (LC1 - 4 and C6). The results suggest that more socioeconomically advantaged and high IQ females accelerate through the neurodevelopmental processes. These are mostly related to their association with SA (LC1, LC3, LC4, LC6) and CT

(LC1, LC2) changes in specific components, almost uniquely in regions that are related to heteromodal processes. MC changes in LC6 exclusively, show a more stable or increasing rate of change in females and lower SES demographic groups as they mature (Fig.4.7A).

LV2 ($p = 0.005$), explaining 26% of covariance, describes a more component-specific pattern, loading predominantly onto LC1 and LC2. This LV reveals a pattern in which male sex and higher IQ are associated with changes in MC and CT in two of the cortical components (LC1, LC2). The relationship is such that male individuals with higher IQ show relative preservation of MC (in LC1, LC2) and CT (in LC4) compared to females and the lower IQ participants as they mature through adulthood. (Fig. 4.7B).

LV3 ($p = 0.02$), explaining 24% of covariance across the data (p-value= 0.005) describes a specifically age-related pattern in which changes of GI in two cortical components of LC2 and LC4, such that GI slopes show a milder decline in older ages (the slopes of GI change become less negative in older ages) (Fig. 4.7C). These LVs together (explaining 97% of the covariance) uncover patterns of co-ordinated anatomical change that are sexually differentiated and that are

influenced by environmental factors such as SES and related to different cognitive abilities.

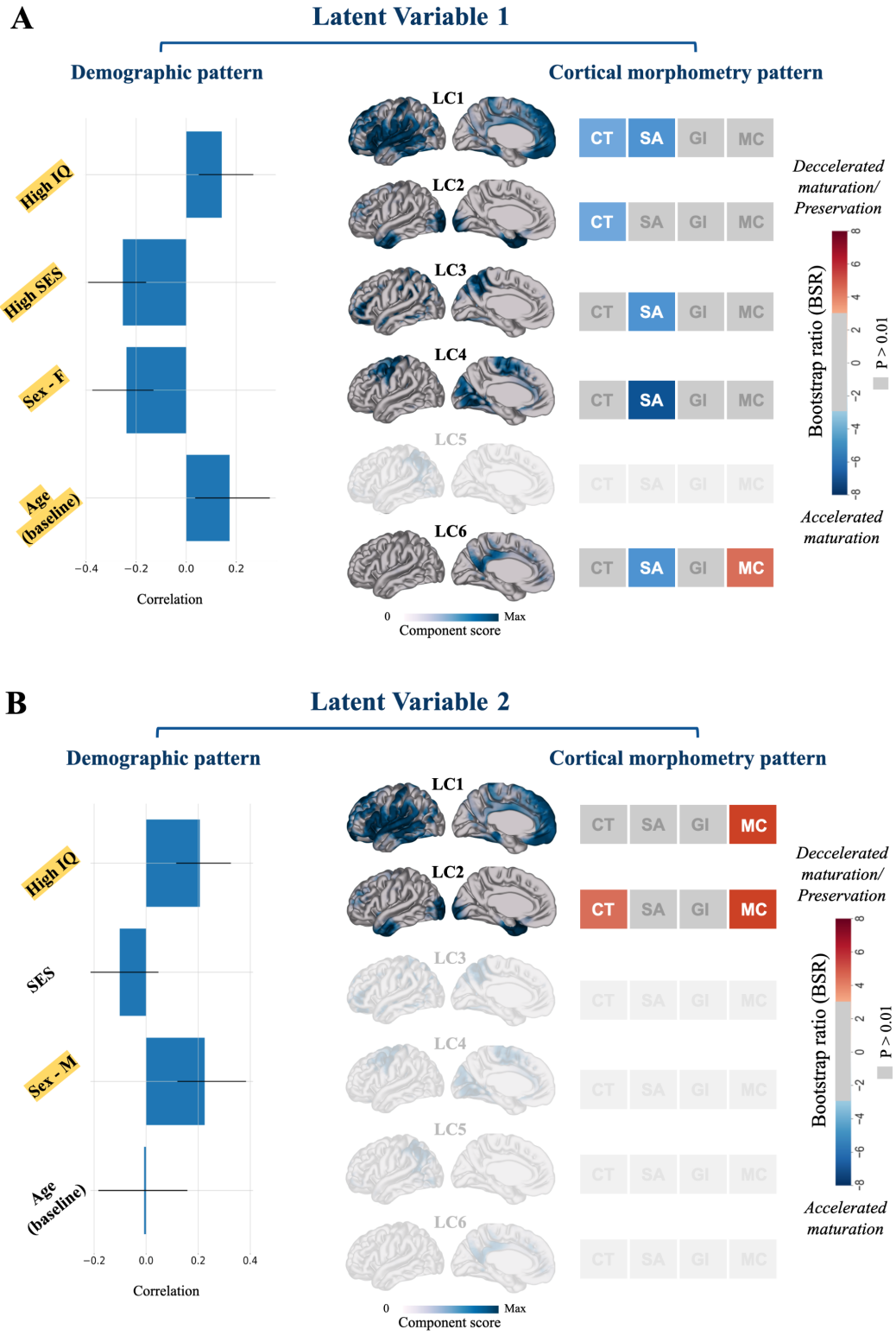

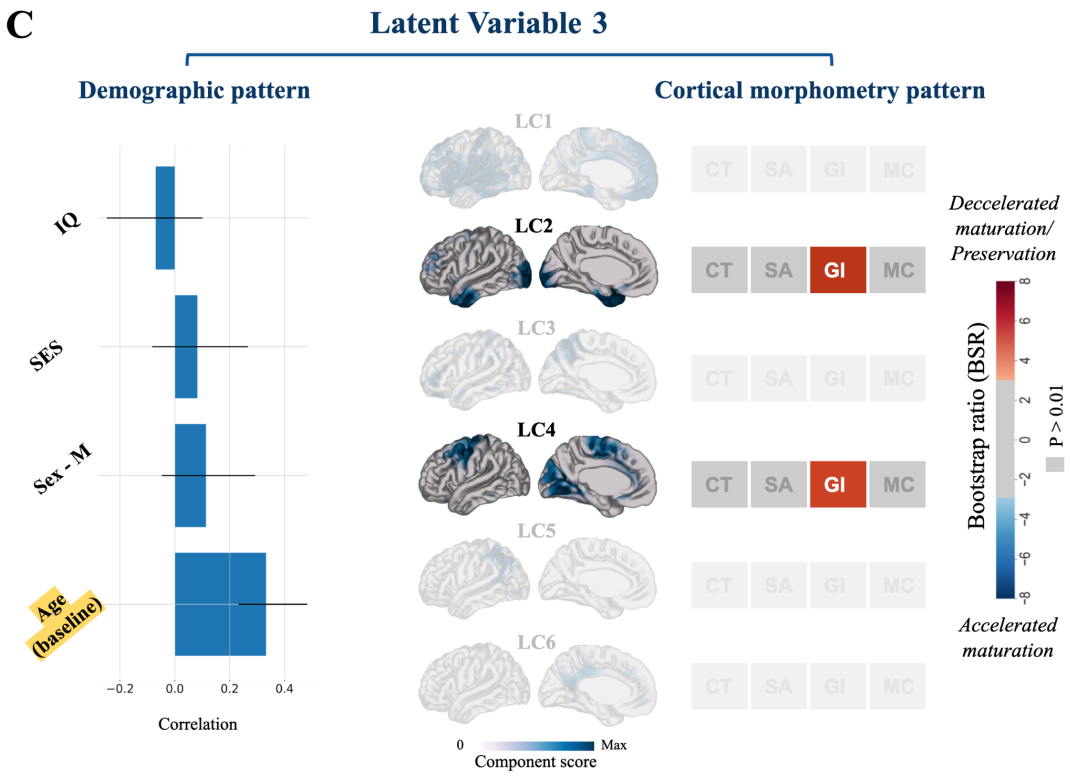

Fig.4.7. BPLS identified three cortical morphometry and demographic latent variables. bPLS analysis identified three (LV1: A; LV2: B; LV3: C) significant latent variables ($p<0.05$), each identifying a pattern of linear correlation between NMF weights and demographics. Bar plots on the left describe the contribution of demographic measures in which the x-axis demonstrates the correlation of each demographic variable within an LV. Error bars indicate the 95% confidence interval; only variables with a BSR> 0.196 ($p <0.05$) are described as contributing to each LV [51] (color-coded in yellow). For each bar plot, cortical components contributing to the LV are shown. The morphometric profile of each component describes to what extent changes across a given metric are identified as being accelerated (blue) or decelerated (red) in the spatial component in relation to the demographic pattern shown in bar plots. Only cortical variables with a BSR > 2.58 ($p <0.01$) are described as contributing to an LV (color-coded according to the BSR plot is shown on the right).

4.5. Morphometric components occupy different positions along gradients of brain function

Fig.4.8 demonstrates parcellation brain maps for NMF components, demonstrating the gradients' value distributions of vertices within each component for the three age groups where more positive values indicate proximity to the transmodal end of the gradients.

In the cross-sectional NMF results (cortical covariance patterns), C2 and C5 are generally associated with a position along the association end of the principal gradients. While components C1, C3, and C4, which are more sensorimotor, lie towards the sensorimotor gradient end, and C6 is prominently distributed over the two ends of gradients. The comparison between how the components situate along the children's second gradients with their situation along the first gradient of adolescents reveals a pattern of shifting in the mean and median values (Fig 4.8) towards the transmodal end of the gradients a seen in C1, C4, and subtly in C6 (which are generally unimodal-centered components).

In the longitudinal NMF (coordinated maturation), in children and adults gradients, components LC2, LC3, and LC4 occupied more sensorimotor spatial locations and lay towards the sensorimotor gradient end. In contrast, the first component, LC1, and to a lesser extent component LC5, is multimodal with especially two peaks at the opposite ends of the gradients. In longitudinal components, this shift from children to adolescents is seen in LC2, LC3, and LC4, components that are generally situated along the unimodal cortical regions.

Interestingly, in both cross-sectional and longitudinal components analyses, from adolescence to adulthood, even though our dataset (5-25 years old) does not fully represent an adult population (22-35 years old), components show a pattern of the shift from an overarching mid-centered situation across the first gradient (i.e., visual system) in adolescents to a more

multimodal-centered organization (i.e., means and medians in adolescents are mid-centered, whereas in adults, are more towards the ends of the gradients more specifically).

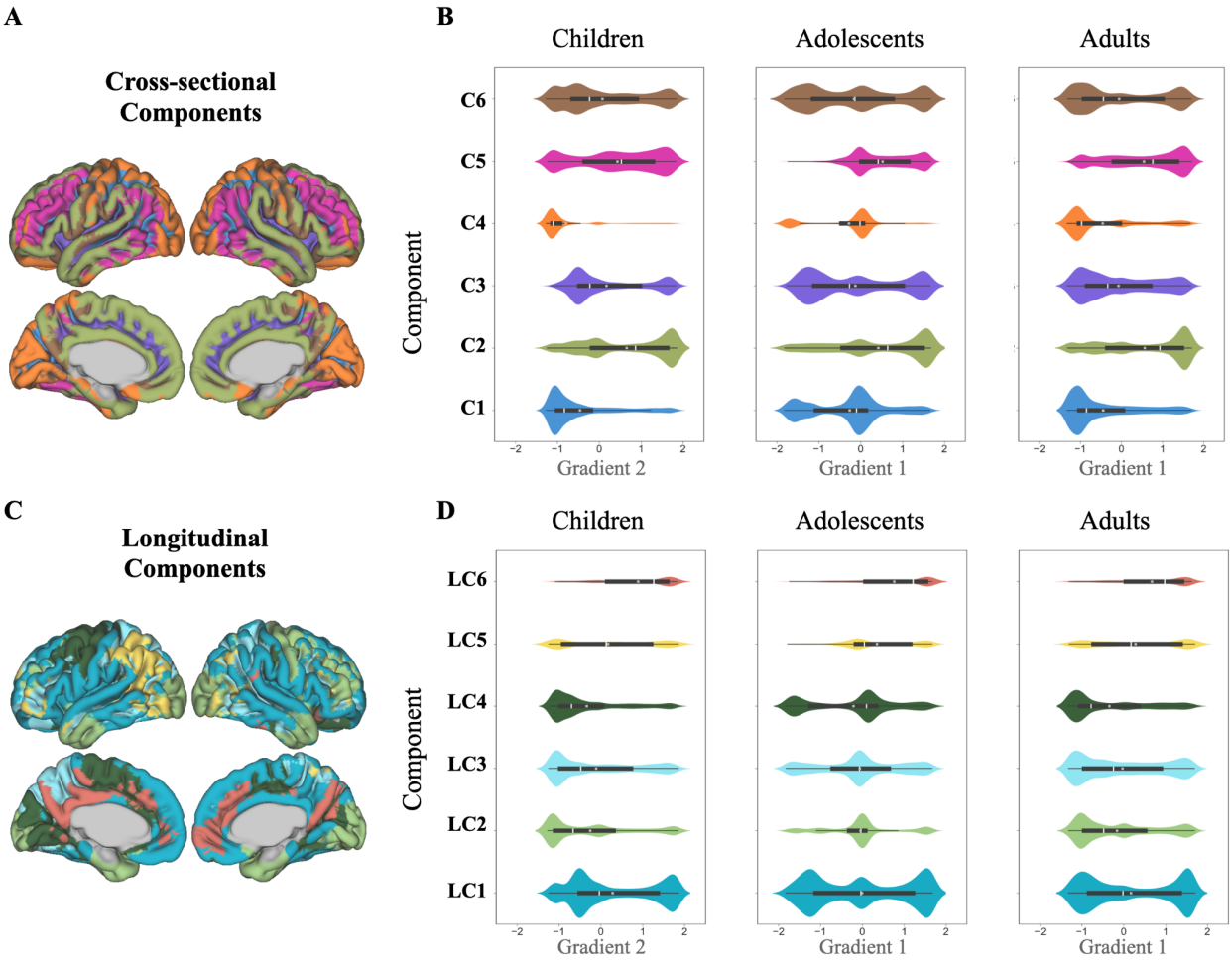

Fig.4.8. A&C) Distribution of cortical components derived from NMF for cross-sectional (A) and longitudinal (C) analyses. B&C) Violin plots demonstrating z-scored gradient value distributions from the three age group maps for each NMF-derived component, where more positive values indicate proximity to the association end of the gradient. The white line in the box plots indicates the mean, and the gray box indicates the median. The Connectome workbench [301] was used to generate the NMF parcellation brain maps (A&C).

Chapter 5. Discussion

5.1. Overview

In the present work, I implemented a multivariate framework, OPNMF, to examine morphological and maturational covariance patterns across measures of CT, SA, GI, and MC. This implementation provided insight into group-level covariation in the morphometric and coordinated maturational aspects of cortical neuroanatomy that are related to inter-individual variations in demographics and cognitive ability. NMF captured covariation patterns across morphometry measures in the cross-sectional implementation, such as higher CT and lower GI covariation in frontotemporal areas and lower CT and higher SA covariation in unimodal areas. Further investigations revealed different contributions of different age, sex, SES, and IQ groups to the found morphometric patterns such that older age dominantly, and lower IQ, and lower SES were related to lower GI, CT, and SA covariance throughout the cortex and local increase in associative cortices sulcal depth in MC. Next, NMF identified patterns within which cortical changes covary coordinatedly through a novel longitudinal implementation of the framework, such as demonstrating preserved SA primarily in unimodal areas through brain development. These patterns were age-related, sex-specific, and varied by different socioeconomic status; as our PLS analysis revealed covariance with female sex, higher SES, higher IQ, and older ages showed a pattern of accelerated maturation of SA mainly, and CT covariance across significant portions of the cortical sheet. Finally, we observed that cortical components occupy spatially different positions along the sensorimotor-association axis of brain function maturational gradients. From childhood to adolescence, the position of morphometric components shifts from a unimodal-centered position to a more transmodal anchored position; whereas from adolescence

to adulthood, the components' situation shifts from an overarching mid-centered distribution in the first gradient (visual system) to a more multimodal-centered organization towards the extreme ends of the gradients.

5.2. Significance

The convoluted anatomy of the cortex and its highly dynamic maturational processes can only be properly mapped through the integration of multiple facets of morphometry. Expanding on multivariate data-driven techniques, we identified spatial patterns of variation across the cortical sheet with respect to multiple brain features within the critical period of brain maturation. The proposed implementation enables describing the heterogeneous contributions of well-defined neuroanatomical features and their relationship within and across cortical components in a single framework. Moreover, using a large, long-running, and well-characterized dataset, we developed a longitudinal implementation of nonnegative matrix factorization which identified patterns of coordinated change across multiple cortical morphometric features. We identified dominant modes of covariance between cortical morphometric features and their coordinated pattern of change, demonstrating sexually differentiated patterns and a strong association with variability in demographics and cognitive ability. This novel characterization of cortical morphometric features provides an important understanding of the interdependencies between morphological measures, their development, and their relationship to critical factors impacting development and will contribute to future studies of neurodevelopmental disorders.

5.3. NMF results

5.3.1. Identifying regions of cortical variability and the choice of parcellation

The NMF technique has been used in voxel- [50,59,269] and vertex-wise [57,274,277] MRI studies to identify structural covariance networks in the context of neurodevelopment [50,57,89,271], and neuropsychiatric disorders [58,59,272–274]. These previous studies have demonstrated that the technique can identify meaningful patterns [49,57,271]. NMF has shown higher specificity, reproducibility, and better statistical power in contrast to other conventional methods such as ICA and PCA [49]. It also leads to purely positive outputs due to its nonnegativity constraint leading to more straightforward representation subsequently, interpretation of the data.

Additionally, with the orthogonality constraints in decomposition, OPNMF prioritizes sparsity in the solution and provides a part-based decomposition with minimally overlapping components where each vertex is assigned to a specific component for a purely additive parts-based representation. Thus, compared to graph theory approaches as in MSNs [43], OPNMF also allows for recovering the contribution of individuals' variations and the neuroanatomical features to the identified patterns. Comparing the NMF-derived components to the MSNs N=4 modular decomposition that approximately corresponds to the lobes of the brain [43], the NMF components provide additional information on the pattern of cortical features covariation in deriving the resultant pattern. For example, the NMF C2 and C3 combination are spatially comparable to the temporal and frontal MSNs' regions; these components indicate a mutual pattern of high CT and low SA in this organization, but high GI and low MC in sulci, whereas low GI and high MC in gyral regions of the modes. NMF framework, providing such

specificity at the morphometric level, could narrow down the further assessments of genetic and cellular associations in the context of normative as well as pathological variations in cortical development.

5.4. Different contributions of demographics and cognitive groups to the morphometric maturational patterns

Existing literature suggests that the hierarchy of cortical organization serves as the foundation for human brain development [302] that integrates differentially with the unique combination of each individual's biological characteristics, exposures, and experiences, resulting in inter-individual cortical variability [302]. Following the identification of group-level morphometric covariation patterns across individuals, bPLS revealed differing contributions of individual participants with different ages, sex, SES, and IQ groups to the found morphometric patterns. Using the weight matrix output from NMFs, corresponding to the weight of each subject-metric pair on the found morphometric pattern, bPLS analysis, and linear regression models revealed unique patterns of associations with different demographic and cognitive ability characteristics. In the following, the findings from both cross-sectional and longitudinal analyses will be discussed.

5.4.1. Inter-individual variability in the context of morphometric networks

Cross-sectional PLS (PLS1) showed associations between inter-individual variations to the group-level variation patterns across individuals and morphometric features, while longitudinal PLS (PLS2) revealed associations between the "tempo" of the change to the

inter-individual variations. In contrast to PLS1, which has revealed one general age-dominant pattern of association with less regional specificity, results from PLS2 showed more specificity in morphometric features and cortical regions.

Older age has shown to be a significant contributing factor to both patterns of morphometric covariation and coordinated change LVs; the relation was such that with the older ages, individuals showed thinner cortical thickness, reduced area, and complexity, and sharpened sulcal curves, keeping with the known literature of pattern of cortical remodeling occurring between the ages 5 to 25 [15,16].

In PLS2, maturational changes of cortical thinning and area reduction have shown to be explicitly accelerated in female individuals with age as expected (LV1, 47% covariance), while the gyrification changes exclusively were shown to be decelerated with age (LV3, 24% covariance). These findings are in line with the previously described sexually differentiated patterns of cortical maturation with females maturing earlier [184,185] and demonstrating statistically significant higher rates of cortical changes [159,187], specifically cortical thinning in the temporal, temporoparietal, and orbitofrontal cortices, interpreted as a faster maturation of regions of the social brain areas in females [159]. The differing tempo of maturation has also been previously reported by Raznahan et al. [15], such that sex differences captured in most cortical regions were mainly reported to be driven by sex differences in SA and, to a lesser extent, CT maturation [15] while GI has been reported to show only subtle sex differences with age in localized frontal regions, suggesting that the mechanisms underlying of age-related changes across these features are quite distinct [159]. These sex-related differing patterns are thought to be genetically determined [187] and could be explained by the different timing and rate of fundamental biological maturation moderated by hormonal processes [189,190].

IQ and SES have shown a similar directionality in associations with both morphometric patterns of covariation (PLS1) and patterns of change (PLS2) and, in fact, in a recent PLS analysis investigating the association between the connectomic organization and childhood SES [303], it has been shown that the structural connectome mediates the relationship between SES and cognitive ability [303]. In our PLS results, while lower SES and IQ were associated with thinner CT, reduced SA, and reduced gyrification/complexity were also associated with accelerated cortical thinning and area reduction (i.e., accelerated maturation) in line with the previous literature [192,199].

Seidlitz et al. [43] have previously demonstrated that inter-individual variation in topography of multiple dimensions of brain organization in the MSN framework is predictive of the inter-individual variation in IQ [43]. Particularly, performing a PLS analysis between the MSNs' nodal degree and IQ measurements, their analysis revealed patterns of association between the left frontal and temporal cortex (left-lateralized temporal and bilateral frontal cortical areas), where a higher degree was reported to be predictive of a higher general IQ, and bilateral primary sensory cortical areas, where a higher degree was specifically predictive of a higher nonverbal IQ [43]. These results are considerably comparable with the pattern of cortical morphometry-cognitive and demographics association captured through bPLS. In components LC1 and LC4, including the bilateral middle temporal, superior, and inferior frontal regions (LC1), and left-lateralized primary sensory cortical areas (somatomotor and visual cortex) (LC4). In these components, LV1 was associated with higher IQ, along with higher SES, and female sex has been linked to covariation of accelerated thinning in cortical thickness in LC1 and surface area reduction in LC1 and LC4. (In cross-sectional analysis, we did not capture regional specificity for IQ associations as the pattern was dominated by age - morphometric relations. In

the multiple linear models on cross-sectional NMF, IQ was not a significant variable in none of the analyses.)

Taken together, the results highlight the complex dynamic changes occurring across this age range and emphasize that inter-individual differences significantly influence the normal variation in cortical patterning. Comparing the results from the two PLS analysis of cross-sectional and longitudinal NMF weights emphasize that inter-individual variations in factors such as age, sex, environmental and cognitive ability are more variably explained by variations in the tempo of anatomical change than morphometric covariations at any one-time point [15]. Overall, these findings support that the integrative NMF-framework approach, simultaneously capturing information about multiple dimensions of brain morphometry, shows a capacity to explain a significant proportion of inter-individual variance in age, sex, IQ, SES, in the identified patterns, but also recovers the contribution of specific cortical features into the patterns of correlation.

5.4.2. Cross-sectional NMF PLS and multiple linear regression results

bPLS analysis identified one LV accounting for 96% of covariance across morphometric variation patterns of cross-sectional NMF-derived components which was dominantly derived by older age, and the subtle impacts of lower socioeconomic status, and lower IQ. The general pattern of negative correlation between age and morphometric measures, keeping with the literature, reflects the expected general pattern of cortical remodeling occurring between the ages 5 to 25: an overall pattern of thinner cortical thickness, reduced area, and complexity (i.e., gyrification), and sharpened sulcal curves in lateral frontal, superior parietal, middle temporal, and occipital regions. Cortical gray matter loss during adolescence [129] is thought to be the

result of synaptic pruning and the encroachment of continued white matter growth [21] which continues well into adulthood [4,304–308]. The harmonious changes of the continuous cortical thinning [18–22], decreasing cortical surface area [11,15,18,19], and the decreasing cortical complexity [14,15,142,155,309] could reflect the known neurodevelopmental underlying cortical maturation linked to the known regressive and progressive processes of increased synaptic pruning [92], myelination [83,310], decreases in neuronal cell numbers [24], reduction in dendrite arborization complexity, length, spines [94], and synaptic densities [311,312].

While fewer studies have investigated cortical MC in the context of development within this period [151,313], it has been hypothesized that increases in the MC could effectively measure the changes attributed to gray matter volume loss [152]. Increasing white matter volume in sulcal regions has also been reported to be linked to the increasing MC, which Could be reflected in a sharpening of the sulci, partly due to the reorganization (or encroachment) of white matter into cortical regions that are normally occupied by gray matter [152]. This hypothesis behind sulcal sharpening is consistent with the negative direction of MC with other metrics found in C1 (sulcal regions in heteromodal association cortices), where increasing MC is associated with decreasing subcomponents of gray matter volumes, CT and SA, and is highly consistent with our understanding of the synaptic pruning versus axonal myelination synchrony.

This cross-sectional LV also indicated a subtle impact of environmental factors, as indexed by Childhood SES, and cognitive performance, indexed by IQ, showing a similar direction in positively associating with morphometric patterns. Individuals with lower SES and IQ showed subtly thinner CT, reduced SA, and reduced gyrification. These findings are consistent with the previously shown positive association between SES and IQ [192], cortical SA

expansion [192,193,216] and thickness [192,212,217–219], and the gyrification that exhibited a pattern of positive correlation to general cognitive ability in mainly parietal and frontal cortical areas [214,215].

Evidence from the extensive previous literature suggests that cortical morphometric changes differ across sexes [119], although the direction of this effect varies as a function of the age and the region being examined [119]. The PLS results, however, did not reveal a significant sex effect in the demographic pattern; it is, therefore, probable that the existing sex-specific differences might be obscured by the overall dominant and strong effect of GI and age (maximal linear association between the two), which has been shown to exhibit little sex-specific differences [159].

Further investigations through multiple linear regression models revealed female sex to be associated with significantly lower weights of SA weights across all components, CT across components C4 and C6, GI across components C2, C5, and 6. In MC weights, conversely, females' weights were significantly higher across all components. Specific age by sex interactions associations with patterns of morphometric variation were also identified specifically in SA weights across C1, C4, C5, and C6 such that females show a faster loss relative to females. Raznahan et al. [15], leveraging over 1250 longitudinally acquired brain scans from typically developing individual youth, have previously shown that differences in CV result from the complex interaction between cortical thickness, surface area, gyrification, and convex hull in a sexually dimorphic and age-dependent manner [15,119]. The differing patterns were such that all measures of morphometry (the mean of each measure across the cortical sheet) were significantly greater in males than females, and sex differences in CV arise mainly due to sex differences in how SA (rather than CT) changes with age [15]. The present age-, sex-, and age by

sex-related findings are consistent with these findings. What is more, we have added a component-level spatial specificity to such previous reports; this enables distinguishing the different effects of age, sex, and their interaction with different cortical regions in a single integrative analytical framework, combining multiple aspects of cortical morphometry, that also recovers the contribution of each feature.

5.4.3. Longitudinal NMF PLS results

PLS identified three LVs (explaining 96% of covariance overall) relating coordinated cortical maturation variability to demographics and cognitive ability variability.

LV1, explaining nearly half of the covariance (47% covariance), revealed an age-related sex-specific pattern influenced by environmental factors and related to the differences in cognitive ability. This LV shows associations between female sex, older ages, higher SES, and higher IQ with a coordinated pattern of accelerated maturation across primarily SA and CT across the majority of the cortex. This differing pattern in the tempo of loss is relatively more demonstrated in SA across components LC1, LC3, LC4, and LC6, which is notably strongly pronounced in LC4, including unimodal areas such as primary somatosensory areas cuneus, and lingual gyrus. To a lesser extent, CT shows a similar pattern across components LC1, and LC2, occupying the majority of the cortex. Socio-environmental factors significantly influencing patterns of brain maturation have been investigated in previous works [192,200–203]. Childhood SES and IQ have also shown a similar direction in associations with morphometric patterns of change, such that Individuals with higher SES and IQ individuals demonstrate patterns of accelerated cortical thinning and area reduction (i.e., accelerated maturation) [192]. In a recent investigation by Rakesh et al. [199], patterns of association between delayed cortical maturation and deprived socio-environmental factors have been observed using SA and CT as a proxy of

brain age [199], along with previous works reporting other types of disadvantages associations with delayed brain development [192,200–203], and higher SES individuals that have shown faster functional brain development, such as increased functional specialization [204] and resting-state connectivity [205–209] in children and adults. Specifically, SA maturation has shown to be vulnerable to the prenatal environmental differences [120] affecting maturation into late adolescence.

The pace of maturation has also been reported to be linked to variations in cognitive ability in previous works. Earlier thinning of CT has been reported to be positively linked to IQ in typically developing individuals in their late childhood, adolescence, and adulthood [212] which becomes more pronounced with increasing age: the higher the IQ, the faster the thinning of cortex over time [212]. Similar to SA, with higher IQ, the surface area has decreased at a higher rate [212], consistent with the present findings.

The sexually differentiated pattern of cortical maturation has been previously described in numerous works, and sexually differing associations seen in this LV were in the expected regions and directionality: maturational changes have shown to be explicitly accelerated in older female individuals compared to males in surface area reduction in the majority of cortex (LC1, LC3, LC4, LC6), and to lesser extents cortical thinning (LC1, LC2), while localized gyrification changes (in unimodal association cortices of occipital lobe, and postcentral areas) were exclusively shown to be decelerated with age across both sexes (LV3). These findings are in line with the previously described sexually differentiated patterns of cortical maturation with females maturing earlier [184,185] and demonstrating significantly higher rates of cortical changes [187], specifically changes of SA [15], and specifically thinning in the temporal, temporoparietal, and

orbitofrontal cortices, interpreted as a “faster maturation of the social brain areas in females” [159].

5.5. Alignment of NMF components with the principal functional gradients

Human brain development follows a pattern of an early maturation of the unimodal visual and sensorimotor areas, followed by the refinements of the multimodal association cortex [2,11,298]. Leveraging the previously described age-dependent patterns of gradual maturation in the macroscale of cortical organization, we investigated how NMF components situate along the gradients of brain function across development.

Consistent with the findings reported in Dong et al. [298], the position of NMF-derived components along the secondary gradient of connectivity in children generally resembles their position along the primary gradient in adolescents (Fig.4.8). From a transition of the gradients point of view, the secondary gradient of children notably demonstrates a shift from a more unimodal-centered organization to a transmodal anchored framework. However, such developmental transitions are not present in all components such as (C2, C3, C5) and (LC1, LC5, LC6) that their positions were spatially consistent across children (second gradient) and adolescents (first gradient); as suggested by Dong et al. [298], this may highlight the presence of stable features of the cortical macroscale organization of the cortex in this overarching pattern of developmental transition.

From adolescence to adulthood, on the other hand, even though our dataset (5-25 years old) does not fully represent an adult population (i.e., 22-35 years old), components show a

pattern of shift from an overarching mid-centered distribution in the first gradient (visual system) to a more multimodal-centered organization towards the extreme ends of the gradients. As suggested in Dong et al. [298], these findings could potentially reflect the continued refinement of the visual system within the global connectivity structure through young adulthood [298].

Taken together, these age-dependent and interconnected patterns of shift across the position of morphometric derived components along functional gradients may reflect the refinements towards the facilitation of multimodal information integration and "segregation of local, specialized processing streams" in the adult-like cortical architecture, as proposed by Dong et al. [298].

5.6. Limitations

The findings of this study should be interpreted while considering its limitations. The primary limitation to the generalization of presented results is that NMF identifies data-driven components; subsequently, the identified spatial patterns are specific to the used data, and the age range studied. Another limitation is the linearity presumption in multivariate approaches. PLS, for example, reduces the complexity of analyses by providing a concise summary of the data; however, it may also mask the potential non-linear relationship between the two. The same is true for the use of slopes as the proxy of change in our longitudinal analysis; our analysis of coordinated maturation is restricted to modeling the effect of age on cortical changes in a linear fashion which conceals nonlinear changes, given that brain development is a nonlinear process [2,186,314]. For example, SA peaks at the age of 8 and decreases gradually afterward; through the linear measure of slope, this cubic trajectory would be interpreted as a slow decline with age

instead. A caveat of the current work could therefore be the large age range studied that might conceal interaction effects that vary by age, such as the cognitive- and demographics-related variability (as shown in previous studies [212]). While NMF is an ideal method to explore large population samples by providing group-level covariation networks, it is limited by the inability to construct individual-level networks; this should be borne in mind for the future clinical implications of this framework. Lastly, manual quality control could potentially be subject to errors and inconsistencies, and the present work is unavoidably no exception to that.

5.7. Future directions

This work would benefit from the integration of white matter indices (such as T1/T2, T2*, Fractional Anisotropy, and Mean Diffusivity) from multi-modal data to delineate networks of coordinate maturation across gray and white matter boundaries, enabling better characterization of the complex and dynamic codependencies between gray and matter tissues. Additional cortical metrics to be investigated using higher resolution MR images could be boundary sharpness coefficient (BSC), which has been proposed as a proxy to capture alterations in microstructure at the cortical gray/white matter boundary [315,316], and measures obtained from different cortical depths, that have been shown specificity in capturing alterations in neuropathological conditions [317–320]. Another direction for future work would be to assess whether the found morphometric components of covariation map onto spatial expression of certain cell types, gene expressions (transcriptional profiling of spatial components), evolutionary hierarchy, and developmental expansion [138] profiles. Moreover, characterizing the normal patterns of cortical maturation across its multiple facets would not only contribute to

better modeling the typical brain development and its underpinning mechanism but also shapes thinking about the mechanisms underlying pathological neurodevelopmental instances. Therefore, an important next step will be to investigate patterns of healthy versus neurodevelopmental and neuropsychiatric populations, such as autism spectrum disorder and psychotic spectrum disorders, to contrast their integrated patterns of maturation, which remains to be determined in future work.

Chapter 6. Conclusion

Characterizing patterns of neurodevelopment across morphological measures is essential for understanding the dynamic processes of typical brain development. Leveraging a data-driven technique, we identified cortical covariation patterns across integrated cortical morphometry measures and their synchronized rate of maturation in typically developing youth. To our knowledge, this is the first implication of NMF that implements integrated longitudinal sMRI data to describe the maturation process. Taken together, we observed a non-uniform relationship between morphometric measures throughout the cortex underlying fundamental neurodevelopmental processes that covary together. The identified patterns were age-related, sexually differentiated, influenced by individual differences in socioeconomic factors, and associated with cognitive ability. This novel characterization of cortical morphometric features maturation provides an important understanding of the interdependencies between morphological measures, their coordinated development, and their relationship to critical factors impacting development.

References

1. Sowell ER, Thompson PM, Holmes CJ, Jernigan TL, Toga AW. In vivo evidence for post-adolescent brain maturation in frontal and striatal regions. Nat Neurosci. 1999;2: 859–861.

2. Giedd JN, Blumenthal J, Jeffries NO, Castellanos FX, Liu H, Zijdenbos A, et al. Brain development during childhood and adolescence: a longitudinal MRI study. Nat Neurosci. 1999;2: 861–863.

3. Dekaban AS. Changes in brain weights during the span of human life: relation of brain weights to body heights and body weights. Ann Neurol. 1978;4: 345–356.

4. Courchesne E, Chisum HJ, Townsend J, Cowles A, Covington J, Egaas B, et al. Normal brain development and aging: quantitative analysis at in vivo MR imaging in healthy volunteers. Radiology. 2000;216: 672–682.

5. Kennedy DN, Makris N, Herbert MR, Takahashi T, Caviness VS Jr. Basic principles of MRI and morphometry studies of human brain development. Dev Sci. 2002;5: 268–278.

6. Lenroot RK, Giedd JN. Brain development in children and adolescents: insights from anatomical magnetic resonance imaging. Neurosci Biobehav Rev. 2006;30: 718–729.

7. Paus T, Collins DL, Evans AC, Leonard G, Pike B, Zijdenbos A. Maturation of white matter in the human brain: a review of magnetic resonance studies. Brain Res Bull. 2001;54: 255–266.

8. Brown TT, Jernigan TL. Brain development during the preschool years. Neuropsychol Rev. 2012;22: 313–333.

9. Jernigan TL, Baaré WFC, Stiles J, Madsen KS. Postnatal brain development: structural imaging of dynamic neurodevelopmental processes. Prog Brain Res. 2011;189: 77–92.

10. Sowell ER, Trauner DA, Gamst A, Jernigan TL. Development of cortical and subcortical brain structures in childhood and adolescence: a structural MRI study. Dev Med Child Neurol. 2002;44: 4–16.

11. Gogtay N, Giedd JN, Lusk L, Hayashi KM, Greenstein D, Vaituzis AC, et al. Dynamic mapping of human cortical development during childhood through early adulthood. Proc Natl Acad Sci U S A. 2004;101: 8174–8179.

12. Shaw P, Kabani NJ, Lerch JP, Eckstrand K, Lenroot R, Gogtay N, et al. Neurodevelopmental trajectories of the human cerebral cortex. J Neurosci. 2008;28: 3586–3594.

13. Giedd JN, Raznahan A, Alexander-Bloch A, Schmitt E, Gogtay N, Rapoport JL. Child psychiatry branch of the National Institute of Mental Health longitudinal structural magnetic resonance imaging study of human brain development. Neuropsychopharmacology. 2015;40: 43–49.

14. White T, Su S, Schmidt M, Kao C-Y, Sapiro G. The development of gyrification in childhood and adolescence. Brain Cogn. 2010;72: 36–45.

15. Raznahan A, Shaw P, Lalonde F, Stockman M, Wallace GL, Greenstein D, et al. How does your cortex grow? J Neurosci. 2011;31: 7174–7177.

16. Bethlehem RAI, Seidlitz J, White SR, Vogel JW, Anderson KM, Adamson C, et al. Brain charts for the human lifespan. bioRxiv. 2021. p. 2021.06.08.447489. doi:10.1101/2021.06.08.447489

17. Zilles K, Palomero-Gallagher N, Amunts K. Development of cortical folding during evolution and ontogeny. Trends Neurosci. 2013;36: 275–284.

18. Ducharme S, Albaugh MD, Nguyen T-V, Hudziak JJ, Mateos-Pérez JM, Labbe A, et al. Trajectories of cortical thickness maturation in normal brain development--The importance of quality control procedures. Neuroimage. 2016;125: 267–279.

19. Tamnes CK, Herting MM, Goddings A-L, Meuwese R, Blakemore S-J, Dahl RE, et al. Development of the Cerebral Cortex across Adolescence: A Multisample Study of Inter-Related Longitudinal Changes in Cortical Volume, Surface Area, and Thickness. J Neurosci. 2017;37: 3402–3412.

20. Fjell AM, Grydeland H, Krogsrud SK, Amlien I, Rohani DA, Ferschmann L, et al. Development and aging of cortical thickness correspond to genetic organization patterns. Proc Natl Acad Sci U S A. 2015;112: 15462–15467.

21. Koolschijn PCMP, Crone EA. Sex differences and structural brain maturation from childhood to early adulthood. Dev Cogn Neurosci. 2013;5: 106–118.

22. van Soelen ILC, Brouwer RM, van Baal GCM, Schnack HG, Peper JS, Collins DL, et al. Genetic influences on thinning of the cerebral cortex during development. Neuroimage. 2012;59: 3871–3880.

23. Geschwind DH, Rakic P. Cortical evolution: judge the brain by its cover. Neuron. 2013;80: 633–647.

24. Pakkenberg B, Gundersen HJ. Neocortical neuron number in humans: effect of sex and age. J Comp Neurol. 1997;384: 312–320.

25. Panizzon MS, Fennema-Notestine C, Eyler LT, Jernigan TL, Prom-Wormley E, Neale M, et al. Distinct genetic influences on cortical surface area and cortical thickness. Cereb Cortex. 2009;19: 2728–2735.

26. Kremen WS, Fennema-Notestine C, Eyler LT, Panizzon MS, Chen C-H, Franz CE, et al. Genetics of brain structure: contributions from the Vietnam Era Twin Study of Aging. Am J Med Genet B Neuropsychiatr Genet. 2013;162B: 751–761.

27. Chen C-H, Fiecas M, Gutierrez ED, Panizzon MS, Eyler LT, Vuoksimaa E, et al. Genetic topography of brain morphology. Proceedings of the National Academy of Sciences. 2013. pp. 17089–17094. doi:10.1073/pnas.1308091110

28. Savalia NK, Agres PF, Chan MY, Feczko EJ, Kennedy KM, Wig GS. Motion-related artifacts in structural brain images revealed with independent estimates of in-scanner head motion. Hum Brain Mapp. 2017;38: 472–492.

29. Sha Z, Schijven D, Carrion-Castillo A, Joliot M, Mazoyer B, Fisher SE, et al. The genetic architecture of structural left-right asymmetry of the human brain. Nat Hum Behav. 2021;5: 1226–1239.

30. Chenn A, Walsh CA. Regulation of cerebral cortical size by control of cell cycle exit in neural precursors. Science. 2002;297: 365–369.

31. Storsve AB, Fjell AM, Tamnes CK, Westlye LT, Overbye K, Aasland HW, et al. Differential

longitudinal changes in cortical thickness, surface area and volume across the adult life span: regions of accelerating and decelerating change. J Neurosci. 2014;34: 8488–8498.

32. Brown TT, Kuperman JM, Chung Y, Erhart M, McCabe C, Hagler DJ Jr, et al. Neuroanatomical assessment of biological maturity. Curr Biol. 2012;22: 1693–1698.

33. Wierenga LM, Langen M, Oranje B, Durston S. Unique developmental trajectories of cortical thickness and surface area. Neuroimage. 2014;87: 120–126.

34. Lyall AE, Shi F, Geng X, Woolson S, Li G, Wang L, et al. Dynamic Development of Regional Cortical Thickness and Surface Area in Early Childhood. Cereb Cortex. 2015;25: 2204–2212.

35. Amlien IK, Fjell AM, Tamnes CK, Grydeland H, Krogsrud SK, Chaplin TA, et al. Organizing Principles of Human Cortical Development--Thickness and Area from 4 to 30 Years: Insights from Comparative Primate Neuroanatomy. Cereb Cortex. 2016;26: 257–267.

36. Dickerson BC, Feczko E, Augustinack JC, Pacheco J, Morris JC, Fischl B, et al. Differential effects of aging and Alzheimer's disease on medial temporal lobe cortical thickness and surface area. Neurobiol Aging. 2009;30: 432–440.

37. Wolosin SM, Richardson ME, Hennessey JG, Denckla MB, Mostofsky SH. Abnormal cerebral cortex structure in children with ADHD. Hum Brain Mapp. 2009;30: 175–184.

38. Frye RE, Liederman J, Malmberg B, McLean J, Strickland D, Beauchamp MS. Surface area accounts for the relation of gray matter volume to reading-related skills and history of dyslexia. Cereb Cortex. 2010;20: 2625–2635.

39. Li W, Yang C, Shi F, Wu S, Wang Q, Nie Y, et al. Construction of Individual Morphological Brain Networks with Multiple Morphometric Features. Front Neuroanat. 2017;11: 34.

40. Hoagey DA, Rieck JR, Rodrigue KM, Kennedy KM. Joint contributions of cortical morphometry and white matter microstructure in healthy brain aging: A partial least squares correlation analysis. Hum Brain Mapp. 2019;40: 5315–5329.

41. Mišić B, Betzel RF, de Reus MA, van den Heuvel MP, Berman MG, McIntosh AR, et al. Network-Level Structure-Function Relationships in Human Neocortex. Cereb Cortex. 2016;26: 3285–3296.

42. Yang J-J, Yoon U, Yun HJ, Im K, Choi YY, Lee KH, et al. Prediction for human intelligence using morphometric characteristics of cortical surface: partial least square analysis. Neuroscience. 2013;246: 351–361.

43. Seidlitz J, Váša F, Shinn M, Romero-Garcia R, Whitaker KJ, Vértes PE, et al. Morphometric Similarity Networks Detect Microscale Cortical Organization and Predict Inter-Individual Cognitive Variation. Neuron. 2018;97: 231–247.e7.

44. Seidlitz J, Nadig A, Liu S, Bethlehem RAI, Vértes PE, Morgan SE, et al. Transcriptomic and Cellular Decoding of Regional Brain Vulnerability to Neurodevelopmental Disorders. bioRxiv. 2019. p. 573279. doi:10.1101/573279

45. Morgan SE, Seidlitz J, Whitaker KJ, Romero-Garcia R, Clifton NE, Scarpazza C, et al. Cortical patterning of abnormal morphometric similarity in psychosis is associated with brain expression of schizophrenia-related genes. Proc Natl Acad Sci U S A. 2019;116: 9604–9609.

46. King DJ, Wood AG. Clinically feasible brain morphometric similarity network construction approaches with restricted magnetic resonance imaging acquisitions. Netw Neurosci. 2020;4: 274–291.

47. Paatero P, Tapper U. Positive matrix factorization: A non-negative factor model with optimal utilization of error estimates of data values. Environmetrics. 1994;5: 111–126.

48. Lee DD, Seung HS. Learning the parts of objects by non-negative matrix factorization. Nature. 1999;401: 788–791.

49. Sotiras A, Resnick SM, Davatzikos C. Finding imaging patterns of structural covariance via Non-Negative Matrix Factorization. Neuroimage. 2015;108: 1–16.

50. Nassar R, Kaczkurkin AN, Xia CH, Sotiras A, Pehlivanova M, Moore TM, et al. Gestational Age is Dimensionally Associated with Structural Brain Network Abnormalities Across Development. Cereb Cortex. 2019;29: 2102–2114.

51. Patel R, Steele CJ, Chen AGX, Patel S, Devenyi GA, Germann J, et al. Investigating microstructural variation in the human hippocampus using non-negative matrix factorization. Neuroimage. 2020;207: 116348.

52. Hyvärinen A, Hoyer PO, Inki M. Topographic independent component analysis. Neural Comput. 2001;13: 1527–1558.

53. Arbabshirani MR, Plis S, Sui J, Calhoun VD. Single subject prediction of brain disorders in neuroimaging: Promises and pitfalls. Neuroimage. 2017;145: 137–165.

54. Beckmann CF, Smith SM. Tensorial extensions of independent component analysis for multisubject FMRI analysis. Neuroimage. 2005;25: 294–311.

55. Beckmann CF, DeLuca M, Devlin JT, Smith SM. Investigations into resting-state connectivity using independent component analysis. Philos Trans R Soc Lond B Biol Sci. 2005;360: 1001–1013.

56. Calhoun VD, Adali T, Pearlson GD, Pekar JJ. A method for making group inferences from functional MRI data using independent component analysis. Human Brain Mapping. 2001. pp. 140–151. doi:10.1002/hbm.1048

57. Sotiras A, Toledo JB, Gur RE, Gur RC, Satterthwaite TD, Davatzikos C. Patterns of coordinated cortical remodeling during adolescence and their associations with functional specialization and evolutionary expansion. Proc Natl Acad Sci U S A. 2017;114: 3527–3532.

58. Kaczkurkin AN, Park SS, Sotiras A, Moore TM, Calkins ME, Cieslak M, et al. Evidence for Dissociable Linkage of Dimensions of Psychopathology to Brain Structure in Youths. Am J Psychiatry. 2019;176: 1000–1009.

59. Pehlivanova M, Wolf DH, Sotiras A, Kaczkurkin AN, Moore TM, Ciric R, et al. Diminished Cortical Thickness Is Associated with Impulsive Choice in Adolescence. J Neurosci. 2018;38: 2471–2481.

60. Robert C, Patel R, Blostein N, Steele CC, Mallar Chakravarty M. Analyses of microstructural variation in the human striatum using non-negative matrix factorization. Neuroimage. 2021; 118744.

61. Huang H, Vasung L. Gaining insight of fetal brain development with diffusion MRI and histology. Int J Dev Neurosci. 2014;32: 11–22.

62. Silbereis JC, Pochareddy S, Zhu Y, Li M, Sestan N. The Cellular and Molecular Landscapes of the Developing Human Central Nervous System. Neuron. 2016;89: 248–268.

63. Heaps-Woodruff JM, Von Nordheim D. Brain development from conception to adulthood. The Wiley Encyclopedia of Health Psychology. Wiley; 2020. pp. 1–4. doi:10.1002/9781119057840.ch1

64. Ouyang M, Dubois J, Yu Q, Mukherjee P, Huang H. Delineation of early brain development from fetuses to infants with diffusion MRI and beyond. Neuroimage. 2019;185: 836–850.

65. Tierney AL, Nelson CA 3rd. Brain Development and the Role of Experience in the Early Years. Zero Three. 2009;30: 9–13.

66. Schlee W, Glöckner F, Kolassa I. Development of neural functional connectivity over the lifespan. Neuroscience Letters. 2011. p. e7. doi:10.1016/j.neulet.2011.05.082

67. Sigelman CK, De George L, Cunial K, Rider EA. Life Span Human Development. Cengage AU; 2018.

68. Jessell TM, Sanes JR. Development. The decade of the developing brain. Curr Opin Neurobiol. 2000;10: 599–611.

69. Rash BG, Grove EA. Area and layer patterning in the developing cerebral cortex. Curr Opin Neurobiol. 2006;16: 25–34.

70. Rhinn M, Picker A, Brand M. Global and local mechanisms of forebrain and midbrain patterning. Curr Opin Neurobiol. 2006;16: 5–12.

71. Tau GZ, Peterson BS. Normal development of brain circuits. Neuropsychopharmacology. 2010;35: 147–168.

72. Rakic P. Mode of cell migration to the superficial layers of fetal monkey neocortex. J Comp Neurol. 1972;145: 61–83.

73. Rakic P. A small step for the cell, a giant leap for mankind: a hypothesis of neocortical expansion during evolution. Trends Neurosci. 1995;18: 383–388.

74. Sidman RL, Rakic P. Neuronal migration, with special reference to developing human brain: a review. Brain Res. 1973;62: 1–35.

75. Barry DS, Pakan JMP, McDermott KW. Radial glial cells: key organisers in CNS development. Int J Biochem Cell Biol. 2014;46: 76–79.

76. Rakic P, Cameron RS, Komuro H. Recognition, adhesion, transmembrane signaling and cell motility in guided neuronal migration. Curr Opin Neurobiol. 1994;4: 63–69.

77. Hatten ME. The role of migration in central nervous system neuronal development. Curr Opin Neurobiol. 1993;3: 38–44.

78. Kornack DR, Rakic P. Radial and horizontal deployment of clonally related cells in the primate neocortex: relationship to distinct mitotic lineages. Neuron. 1995;15: 311–321.

79. Rakic P. Neuronal migration and contact guidance in the primate telencephalon. Postgrad Med J. 1978;54 Suppl 1: 25–40.

80. Monk CS, Webb SJ, Nelson CA. Prenatal neurobiological development: molecular mechanisms and anatomical change. Dev Neuropsychol. 2001;19: 211–236.

81. O'Rourke NA, Dailey ME, Smith SJ, McConnell SK. Diverse migratory pathways in the developing cerebral cortex. Science. 1992;258: 299–302.

82. Bystron I, Blakemore C, Rakic P. Development of the human cerebral cortex: Boulder Committee revisited. Nat Rev Neurosci. 2008;9: 110–122.

83. Stiles J, Jernigan TL. The basics of brain development. Neuropsychol Rev. 2010;20: 327–348.

84. Kersbergen KJ, Makropoulos A, Aljabar P, Groenendaal F, de Vries LS, Counsell SJ, et al. Longitudinal Regional Brain Development and Clinical Risk Factors in Extremely Preterm Infants. J Pediatr. 2016;178: 93–100.e6.

85. Riccobelli D, Bevilacqua G. Surface tension controls the onset of gyrification in brain organoids. J Mech Phys Solids. 2020;134: 103745.

86. Ronan L, Voets N, Rua C, Alexander-Bloch A, Hough M, Mackay C, et al. Differential tangential expansion as a mechanism for cortical gyrification. Cereb Cortex. 2014;24: 2219–2228.

87. White T, Su S, Schmidt M, Kao C-Y, Sapiro G. The development of gyrification in childhood and adolescence. Brain Cogn. 2010;72: 36–45.

88. Collins CE, Airey DC, Young NA, Leitch DB, Kaas JH. Neuron densities vary across and within cortical areas in primates. Proc Natl Acad Sci U S A. 2010;107: 15927–15932.

89. Wang F, Lian C, Wu Z, Zhang H, Li T, Meng Y, et al. Developmental topography of cortical thickness during infancy. Proc Natl Acad Sci U S A. 2019;116: 15855–15860.

90. Giedd J. Brain development, IX: human brain growth. Am J Psychiatry. 1999;156: 4.

91. Neuroscience edited by Dale Purves, George J. Augustine, David Fitzpatrick, William C. Hall, Anthony-Samuel LaMantia, and Leonard E. White. Q Rev Biol. 2012;87: 158–158.

92. Huttenlocher PR, Dabholkar AS. Regional differences in synaptogenesis in human cerebral cortex. J Comp Neurol. 1997;387: 167–178.

93. Kwan KY, Sestan N, Anton ES. Transcriptional co-regulation of neuronal migration and laminar identity in the neocortex. Development. 2012;139: 1535–1546.

94. Petanjek Z, Judaš M, Šimic G, Rasin MR, Uylings HBM, Rakic P, et al. Extraordinary neoteny of synaptic spines in the human prefrontal cortex. Proc Natl Acad Sci U S A. 2011;108: 13281–13286.

95. Innocenti GM, Price DJ. Exuberance in the development of cortical networks. Nat Rev Neurosci. 2005;6: 955–965.

96. Kostović I, Jovanov-Milošević N. The development of cerebral connections during the first 20--45 weeks' gestation. seminars in fetal and neonatal medicine. Elsevier; 2006. pp. 415–422.

97. Sakai J. Core Concept: How synaptic pruning shapes neural wiring during development and, possibly, in disease. Proc Natl Acad Sci U S A. 2020;117: 16096–16099.

98. Miller DJ, Duka T, Stimpson CD, Schapiro SJ, Baze WB, McArthur MJ, et al. Prolonged myelination in human neocortical evolution. Proceedings of the National Academy of Sciences. 2012;109: 16480–16485.

99. Yakovlev PL, Lecours AR (1967) The myelogenetic cycles of regional maturation of the brain. In: *Resional development of the brain in early life* (Minkowski A, eds), pp 3-70. Oxford: Blackwell. [cited 30 Aug 2021]. Available: http://www.sciepub.com/reference/145890

100. Kinney HC, Brody BA, Finkelstein DM, Vawter GF, Mandell F, Gilles FH. Delayed central nervous system myelination in the sudden infant death syndrome. J Neuropathol Exp Neurol. 1991;50: 29–48.

101. Kinney HC, Brody BA, Kloman AS, Gilles FH. Sequence of central nervous system myelination in human infancy. II. Patterns of myelination in autopsied infants. J Neuropathol Exp Neurol. 1988;47: 217–234.

102. Wikipedia contributors. File:Neural crest (Horizontal).svg. In: Wikipedia, The Free Encyclopedia [Internet]. Available: https://en.wikipedia.org/wiki/File:Neural_crest_(Horizontal).svg

103. Poduri A, Evrony GD, Cai X, Walsh CA. Somatic mutation, genomic variation, and neurological disease. Science. 2013;341: 1237758.

104. Poduri A, Volpe JJ. Chapter 6 - Neuronal Migration. In: Volpe JJ, Inder TE, Darras BT, de Vries LS, du Plessis AJ, Neil JJ, et al., editors. Volpe's Neurology of the Newborn (Sixth Edition). Elsevier; 2018. pp. 120–144.e8.

105. Encyclopedia of Infant and Early Childhood Development. Elsevier; 2020.

106. Knickmeyer RC, Gouttard S, Kang C, Evans D, Wilber K, Smith JK, et al. A structural MRI study of human brain development from birth to 2 years. J Neurosci. 2008;28: 12176–12182.

107. Huttenlocher PR. Synaptic density in human frontal cortex - developmental changes and effects of aging. Brain Res. 1979;163: 195–205.

108. Huttenlocher PR, de Courten C. The development of synapses in striate cortex of man. Hum Neurobiol. 1987;6: 1–9.

109. Ball G, Adamson C, Beare R, Seal ML. Modelling neuroanatomical variation during childhood and adolescence with neighbourhood-preserving embedding. Sci Rep. 2017;7: 17796.

110. Reiss AL, Abrams MT, Singer HS, Ross JL, Denckla MB. Brain development, gender and IQ in children. A volumetric imaging study. Brain. 1996;119 (Pt 5): 1763–1774.

111. Gerber AJ, Peterson BS, Giedd JN, Lalonde FM, Celano MJ, White SL, et al. Anatomical brain magnetic resonance imaging of typically developing children and adolescents. J Am Acad Child Adolesc Psychiatry. 2009;48: 465–470.

112. Wilke M, Krägeloh-Mann I, Holland SK. Global and local development of gray and white matter volume in normal children and adolescents. Exp Brain Res. 2007;178: 296–307.

113. Kolb B, Mychasiuk R, Gibb R. Brain development, experience, and behavior. Pediatr Blood Cancer. 2014;61: 1720–1723.

114. Keshavan MS, Giedd J, Lau JYF, Lewis DA, Paus T. Changes in the adolescent brain and the pathophysiology of psychotic disorders. The Lancet Psychiatry. 2014;1: 549–558.

115. Meyer HC, Lee FS. Translating Developmental Neuroscience to Understand Risk for Psychiatric Disorders. Am J Psychiatry. 2019;176: 179–185.

116. Kessler RC, Berglund P, Demler O, Jin R, Merikangas KR, Walters EE. Lifetime prevalence and age-of-onset distributions of DSM-IV disorders in the National Comorbidity Survey Replication. Arch Gen Psychiatry. 2005;62: 593–602.

117. Whiteford HA, Degenhardt L, Rehm J, Baxter AJ, Ferrari AJ, Erskine HE, et al. Global burden of disease attributable to mental and substance use disorders: findings from the Global Burden of Disease Study 2010. Lancet. 2013;382: 1575–1586.

118. Solmi M, Radua J, Olivola M, Croce E, Soardo L, Salazar de Pablo G, et al. Age at onset of mental disorders worldwide: large-scale meta-analysis of 192 epidemiological studies. Mol Psychiatry. 2021. doi:10.1038/s41380-021-01161-7

119. Kaczkurkin AN, Raznahan A, Satterthwaite TD. Sex differences in the developing brain: insights from multimodal neuroimaging. Neuropsychopharmacology. 2019;44: 71–85.

120. Raznahan A, Greenstein D, Lee NR, Clasen LS, Giedd JN. Prenatal growth in humans and postnatal brain maturation into late adolescence. Proc Natl Acad Sci U S A. 2012;109: 11366–11371.

121. Brain Development Cooperative Group. Total and Regional Brain Volumes in a Population-Based Normative Sample from 4 to 18 Years: The NIH MRI Study of Normal Brain Development. Cereb Cortex. 2011;22: 1–12.

122. Giedd JN, White SL, Celano M. Structural Magnetic Resonance Imaging of Typical Pediatric Brain Development. Neurobiology of Mental Illness. 2011. pp. 1209–1217. doi:10.1093/med/9780199798261.003.0074

123. Larsen B, Luna B. Adolescence as a neurobiological critical period for the development of higher-order cognition. Neurosci Biobehav Rev. 2018;94: 179–195.

124. Alexander-Bloch AF, Reiss PT, Rapoport J, McAdams H, Giedd JN, Bullmore ET, et al. Abnormal Cortical Growth in Schizophrenia Targets Normative Modules of Synchronized Development. Biol Psychiatry. 2014;76: 438–446.

125. Gogate N, Giedd J, Janson K, Rapoport JL. Brain imaging in normal and abnormal brain development: new perspectives for child psychiatry. Clinical Neuroscience Research. 2001. pp. 283–290. doi:10.1016/s1566-2772(01)00014-7

126. Lewis DA. Development of the prefrontal cortex during adolescence: insights into vulnerable neural circuits in schizophrenia. Neuropsychopharmacology. 1997;16: 385–398.

127. Rakic P. Specification of cerebral cortical areas. Science. 1988;241: 170–176.

128. Mountcastle VB. The columnar organization of the neocortex. Brain. 1997;120 (Pt 4): 701–722.

129. Sowell ER, Thompson PM, Leonard CM, Welcome SE, Kan E, Toga AW. Longitudinal mapping of cortical thickness and brain growth in normal children. J Neurosci. 2004;24: 8223–8231.

130. Paus T, Keshavan M, Giedd JN. Why do many psychiatric disorders emerge during adolescence? Nat Rev Neurosci. 2008;9: 947–957.

131. Lyttelton OC, Karama S, Ad-Dab'bagh Y, Zatorre RJ, Carbonell F, Worsley K, et al. Positional and surface area asymmetry of the human cerebral cortex. Neuroimage. 2009;46: 895–903.

132. Vidal-Pineiro D, Parker N, Shin J, French L, Grydeland H, Jackowski AP, et al. Cellular correlates of cortical thinning throughout the lifespan. Sci Rep. 2020;10: 21803.

133. Rakic P. Evolution of the neocortex: a perspective from developmental biology. Nat Rev Neurosci. 2009;10: 724–735.

134. Chenn A, Walsh CA. Increased neuronal production, enlarged forebrains and cytoarchitectural distortions in beta-catenin overexpressing transgenic mice. Cereb Cortex. 2003;13: 599–606.

135. Rakic P, Ayoub AE, Breunig JJ, Dominguez MH. Decision by division: making cortical maps. Trends Neurosci. 2009;32: 291–301.

136. Rakic P. Elusive radial glial cells: historical and evolutionary perspective. Glia. 2003;43: 19–32.

137. Cafiero R, Brauer J, Anwander A, Friederici AD. The Concurrence of Cortical Surface Area Expansion and White Matter Myelination in Human Brain Development. Cereb Cortex. 2019;29: 827–837.

138. Hill J, Inder T, Neil J, Dierker D, Harwell J, Van Essen D. Similar patterns of cortical expansion during human development and evolution. Proc Natl Acad Sci U S A. 2010;107: 13135–13140.

139. Mrzljak L, Uylings HB, Van Eden CG, Judás M. Neuronal development in human prefrontal cortex in prenatal and postnatal stages. Prog Brain Res. 1990;85: 185–222.

140. Rakic P, Bourgeois JP, Goldman-Rakic PS. Synaptic development of the cerebral cortex: implications for learning, memory, and mental illness. Prog Brain Res. 1994;102: 227–243.

141. Kennedy H, Van Essen DC, Christen Y. Micro-, Meso- and Macro-Connectomics of the Brain. Springer; 2016.

142. Cao B, Mwangi B, Passos IC, Wu M-J, Keser Z, Zunta-Soares GB, et al. Lifespan Gyrification Trajectories of Human Brain in Healthy Individuals and Patients with Major Psychiatric Disorders. Sci Rep. 2017;7: 511.

143. Raghavan R, Lawton W, Ranjan SR, Viswanathan RR. A Continuum Mechanics-based Model for Cortical Growth. J Theor Biol. 1997;187: 285–296.

144. Richman DP, Stewart RM, Hutchinson JW, Caviness VS Jr. Mechanical model of brain convolutional development. Science. 1975;189: 18–21.

145. Van Essen DC. A tension-based theory of morphogenesis and compact wiring in the central nervous system. Nature. 1997;385: 313–318.

146. Van Essen DC. A 2020 view of tension-based cortical morphogenesis. Proc Natl Acad Sci U S A. 2020. doi:10.1073/pnas.2016830117

147. Xu G, Knutsen AK, Dikranian K, Kroenke CD, Bayly PV, Taber LA. Axons pull on the brain, but

tension does not drive cortical folding. J Biomech Eng. 2010;132: 071013.

148. Bayly PV, Okamoto RJ, Xu G, Shi Y, Taber LA. A cortical folding model incorporating stress-dependent growth explains gyral wavelengths and stress patterns in the developing brain. Phys Biol. 2013;10: 016005.

149. Nie J, Guo L, Li K, Wang Y, Chen G, Li L, et al. Axonal fiber terminations concentrate on gyri. Cereb Cortex. 2012;22: 2831–2839.

150. Ronan L, Pienaar R, Williams G, Bullmore E, Crow TJ, Roberts N, et al. Intrinsic curvature: a marker of millimeter-scale tangential cortico-cortical connectivity? Int J Neural Syst. 2011;21: 351–366.

151. Remer J, Croteau-Chonka E, Dean DC, D'Arpino S, Dirks H, Whiley D, et al. Quantifying cortical development in typically developing toddlers and young children, 1–6 years of age. Neuroimage. 2017;153: 246–261.

152. King JB, Lopez-Larson MP, Yurgelun-Todd DA. Mean cortical curvature reflects cytoarchitecture restructuring in mild traumatic brain injury. Neuroimage Clin. 2016;11: 81–89.

153. Medic N, Kochunov P, Ziauddeen H, Ersche KD, Nathan PJ, Ronan L, et al. BMI-related cortical morphometry changes are associated with altered white matter structure. Int J Obes . 2019;43: 523–532.

154. Eyler CE, Wu Q, Yan K, MacSwords JM, Chandler-Militello D, Misuraca KL, et al. Glioma stem cell proliferation and tumor growth are promoted by nitric oxide synthase-2. Cell. 2011;146: 53–66.

155. Hogstrom LJ, Westlye LT, Walhovd KB, Fjell AM. The structure of the cerebral cortex across adult life: age-related patterns of surface area, thickness, and gyrification. Cereb Cortex. 2013;23: 2521–2530.

156. Ellman LM, Deicken RF, Vinogradov S, Kremen WS, Poole JH, Kern DM, et al. Structural brain alterations in schizophrenia following fetal exposure to the inflammatory cytokine interleukin-8. Schizophr Res. 2010;121: 46–54.

157. Lee NR, Adeyemi EI, Lin A, Clasen LS, Lalonde FM, Condon E, et al. Dissociations in Cortical Morphometry in Youth with Down Syndrome: Evidence for Reduced Surface Area but Increased Thickness. Cereb Cortex. 2016;26: 2982–2990.

158. Raznahan A, Lee Y, Stidd R, Long R, Greenstein D, Clasen L, et al. Longitudinally mapping the influence of sex and androgen signaling on the dynamics of human cortical maturation in adolescence. Proc Natl Acad Sci U S A. 2010;107: 16988–16993.

159. Mutlu AK, Schneider M, Debbané M, Badoud D, Eliez S, Schaer M. Sex differences in thickness, and folding developments throughout the cortex. Neuroimage. 2013;82: 200–207.

160. McCarthy MM. Sex differences in the developing brain as a source of inherent risk. Dialogues Clin Neurosci. 2016;18: 361–372.

161. Loomes R, Hull L, Mandy WPL. What Is the Male-to-Female Ratio in Autism Spectrum Disorder? A Systematic Review and Meta-Analysis. J Am Acad Child Adolesc Psychiatry. 2017;56: 466–474.

162. Raznahan A, Pugliese L, Barker GJ, Daly E, Powell J, Bolton PF, et al. Serotonin transporter genotype and neuroanatomy in autism spectrum disorders. Psychiatric Genetics. 2009. pp. 147–150. doi:10.1097/ypg.0b013e32832a505a

163. Raznahan A, Bolton P. Autism spectrum disorder in childhood. Medicine . 2008;36: 489–492.

164. Polanczyk G, de Lima MS, Horta BL, Biederman J, Rohde LA. The worldwide prevalence of ADHD: a systematic review and metaregression analysis. Am J Psychiatry. 2007;164: 942–948.

165. Remes O, Brayne C, van der Linde R, Lafortune L. A systematic review of reviews on the prevalence of anxiety disorders in adult populations. Brain Behav. 2016;6: e00497.

166. Smink FRE, van Hoeken D, Oldehinkel AJ, Hoek HW. Prevalence and severity of DSM-5 eating disorders in a community cohort of adolescents. Int J Eat Disord. 2014;47: 610–619.

167. Beesdo K, Knappe S, Pine DS. Anxiety and anxiety disorders in children and adolescents: developmental issues and implications for DSM-V. Psychiatr Clin North Am. 2009;32: 483–524.

168. Albert PR. Why is depression more prevalent in women? J Psychiatry Neurosci. 2015;40: 219–221.

169. Froehlich TE, Lanphear BP, Epstein JN, Barbaresi WJ, Katusic SK, Kahn RS. Prevalence, recognition, and treatment of attention-deficit/hyperactivity disorder in a national sample of US children. Arch Pediatr Adolesc Med. 2007;161: 857–864.

170. Avenevoli S, Swendsen J, He J-P, Burstein M, Merikangas KR. Major depression in the national comorbidity survey-adolescent supplement: prevalence, correlates, and treatment. J Am Acad Child Adolesc Psychiatry. 2015;54: 37–44.e2.

171. Willcutt EG. The prevalence of DSM-IV attention-deficit/hyperactivity disorder: a meta-analytic review. Neurotherapeutics. 2012;9: 490–499.

172. Lenroot RK, Giedd JN. Sex differences in the adolescent brain. Brain Cogn. 2010;72: 46–55.

173. De Bellis MD, Keshavan MS, Beers SR, Hall J, Frustaci K, Masalehdan A, et al. Sex differences in brain maturation during childhood and adolescence. Cereb Cortex. 2001;11: 552–557.

174. Sowell ER, Peterson BS, Kan E, Woods RP, Yoshii J, Bansal R, et al. Sex differences in cortical thickness mapped in 176 healthy individuals between 7 and 87 years of age. Cereb Cortex. 2007;17: 1550–1560.

175. Gennatas ED, Avants BB, Wolf DH, Satterthwaite TD, Ruparel K, Ciric R, et al. Age-Related Effects and Sex Differences in Gray Matter Density, Volume, Mass, and Cortical Thickness from Childhood to Young Adulthood. J Neurosci. 2017;37: 5065–5073.

176. Bramen JE, Hranilovich JA, Dahl RE, Forbes EE, Chen J, Toga AW, et al. Puberty influences medial temporal lobe and cortical gray matter maturation differently in boys than girls matched for sexual maturity. Cereb Cortex. 2011;21: 636–646.

177. Luders E, Narr KL, Thompson PM, Woods RP, Rex DE, Jancke L, et al. Mapping cortical gray matter in the young adult brain: effects of gender. Neuroimage. 2005;26: 493–501.

178. Ruigrok ANV, Salimi-Khorshidi G, Lai M-C, Baron-Cohen S, Lombardo MV, Tait RJ, et al. A

meta-analysis of sex differences in human brain structure. Neurosci Biobehav Rev. 2014;39: 34–50.

179. Ritchie SJ, Cox SR, Shen X, Lombardo MV, Reus LM, Alloza C, et al. Sex Differences in the Adult Human Brain: Evidence from 5216 UK Biobank Participants. Cereb Cortex. 2018;28: 2959–2975.

180. Bramen JE, Hranilovich JA, Dahl RE, Chen J, Rosso C, Forbes EE, et al. Sex matters during adolescence: testosterone-related cortical thickness maturation differs between boys and girls. PLoS One. 2012;7: e33850.

181. Nguyen T-V, McCracken JT, Albaugh MD, Botteron KN, Hudziak JJ, Ducharme S. A testosterone-related structural brain phenotype predicts aggressive behavior from childhood to adulthood. Psychoneuroendocrinology. 2016;63: 109–118.

182. Fish AM, Cachia A, Fischer C, Mankiw C, Reardon PK, Clasen LS, et al. Influences of Brain Size, Sex, and Sex Chromosome Complement on the Architecture of Human Cortical Folding. Cereb Cortex. 2017;27: 5557–5567.

183. Gautam P, Anstey KJ, Wen W, Sachdev PS, Cherbuin N. Cortical gyrification and its relationships with cortical volume, cortical thickness, and cognitive performance in healthy mid-life adults. Behav Brain Res. 2015;287: 331–339.

184. Giedd JN. Structural magnetic resonance imaging of the adolescent brain. Ann N Y Acad Sci. 2004;1021: 77–85.

185. Malina RM, Bouchard C, Bar-Or O. Growth, Maturation, and Physical Activity. Human Kinetics; 2004.

186. Lenroot RK, Gogtay N, Greenstein DK, Wells EM, Wallace GL, Clasen LS, et al. Sexual dimorphism of brain developmental trajectories during childhood and adolescence. Neuroimage. 2007;36: 1065–1073.

187. Brouwer RM, Schutte J, Janssen R, Boomsma DI, Hulshoff Pol HE, Schnack HG. The Speed of Development of Adolescent Brain Age Depends on Sex and Is Genetically Determined. Cereb Cortex. 2021;31: 1296–1306.

188. Raznahan A, Lerch JP, Lee N, Greenstein D, Wallace GL, Stockman M, et al. Patterns of coordinated anatomical change in human cortical development: a longitudinal neuroimaging study of maturational coupling. Neuron. 2011;72: 873–884.

189. Neufang S, Specht K, Hausmann M, Güntürkün O, Herpertz-Dahlmann B, Fink GR, et al. Sex differences and the impact of steroid hormones on the developing human brain. Cereb Cortex. 2009;19: 464–473.

190. Nguyen T-V. Sex Differences in Testosterone-related Patterns of Cortical Maturation Across Childhood and Adolescence. McGill University Libraries; 2011.

191. Hollingshead AB. Two factor index of social position (privately printed). New Haven. 1957.

192. McDermott CL, Seidlitz J, Nadig A, Liu S, Clasen LS, Blumenthal JD, et al. Longitudinally Mapping Childhood Socioeconomic Status Associations with Cortical and Subcortical Morphology. J Neurosci. 2019;39: 1365–1373.

193. Noble KG, Houston SM, Brito NH, Bartsch H, Kan E, Kuperman JM, et al. Family income, parental education and brain structure in children and adolescents. Nat Neurosci. 2015;18: 773–778.

194. Kostović I, Judaš M, Sedmak G. Developmental history of the subplate zone, subplate neurons and interstitial white matter neurons: relevance for schizophrenia. Int J Dev Neurosci. 2011;29: 193–205.

195. Kostovic I, Rakic P. Developmental history of the transient subplate zone in the visual and somatosensory cortex of the macaque monkey and human brain. J Comp Neurol. 1990;297: 441–470.

196. Piccolo LR, Merz EC, He X, Sowell ER, Noble KG, Pediatric Imaging, Neurocognition, Genetics Study. Age-Related Differences in Cortical Thickness Vary by Socioeconomic Status. PLoS One. 2016;11: e0162511.

197. Makinodan M, Rosen KM, Ito S, Corfas G. A critical period for social experience-dependent oligodendrocyte maturation and myelination. Science. 2012;337: 1357–1360.

198. Konrad K, Firk C, Uhlhaas PJ. Brain development during adolescence: neuroscientific insights into this developmental period. Dtsch Arztebl Int. 2013;110: 425–431.

199. Rakesh D, Cropley V, Zalesky A, Vijayakumar N, Allen NB, Whittle S. Neighborhood disadvantage and longitudinal brain-predicted-age trajectory during adolescence. Dev Cogn Neurosci. 2021;51: 101002.

200. Hair NL, Hanson JL, Wolfe BL, Pollak SD. Association of Child Poverty, Brain Development, and Academic Achievement. JAMA Pediatr. 2015;169: 822–829.

201. Hanson JL, Hair N, Shen DG, Shi F, Gilmore JH, Wolfe BL, et al. Family poverty affects the rate of human infant brain growth. PLoS One. 2013;8: e80954.

202. Whittle S, Vijayakumar N, Simmons JG, Dennison M, Schwartz O, Pantelis C, et al. Role of Positive Parenting in the Association Between Neighborhood Social Disadvantage and Brain Development Across Adolescence. JAMA Psychiatry. 2017;74: 824–832.

203. JednorÃ³g K, Altarelli I, Monzalvo K, Fluss J, Dubois J, Billard C, et al. Correction: The Influence of Socioeconomic Status on Children's Brain Structure. PLoS ONE. 2012. doi:10.1371/annotation/47661de2-2c53-4396-9f88-06b5ad233566

204. Raizada RDS, Richards TL, Meltzoff A, Kuhl PK. Socioeconomic status predicts hemispheric specialisation of the left inferior frontal gyrus in young children. Neuroimage. 2008;40: 1392–1401.

205. Sripada RK, Swain JE, Evans GW, Welsh RC, Liberzon I. Childhood poverty and stress reactivity are associated with aberrant functional connectivity in default mode network. Neuropsychopharmacology. 2014;39: 2244–2251.

206. Smith SM, Nichols TE, Vidaurre D, Winkler AM, Behrens TEJ, Glasser MF, et al. A positive-negative mode of population covariation links brain connectivity, demographics and behavior. Nat Neurosci. 2015;18: 1565–1567.

207. Barch D, Pagliaccio D, Belden A, Harms MP, Gaffrey M, Sylvester CM, et al. Effect of Hippocampal and Amygdala Connectivity on the Relationship Between Preschool Poverty and School-Age Depression. Am J Psychiatry. 2016;173: 625–634.

208. Marshall NA, Marusak HA, Sala-Hamrick KJ, Crespo LM, Rabinak CA, Thomason ME. Socioeconomic disadvantage and altered corticostriatal circuitry in urban youth. Hum Brain Mapp. 2018;39: 1982–1994.

209. Tooley UA, Mackey AP, Ciric R, Ruparel K, Moore TM, Gur RC, et al. Associations between Neighborhood SES and Functional Brain Network Development. Cereb Cortex. 2020;30: 1–19.

210. Bajaj S, Raikes A, Smith R, Dailey NS, Alkozei A, Vanuk JR, et al. The Relationship Between General Intelligence and Cortical Structure in Healthy Individuals. Neuroscience. 2018;388: 36–44.

211. Shaw P, Greenstein D, Lerch J, Clasen L, Lenroot R, Gogtay N, et al. Intellectual ability and cortical development in children and adolescents. Nature. 2006;440: 676–679.

212. Schnack HG, van Haren NEM, Brouwer RM, Evans A, Durston S, Boomsma DI, et al. Changes in thickness and surface area of the human cortex and their relationship with intelligence. Cereb Cortex. 2015;25: 1608–1617.

213. Vuoksimaa E, Panizzon MS, Chen C-H, Fiecas M, Eyler LT, Fennema-Notestine C, et al. Is bigger always better? The importance of cortical configuration with respect to cognitive ability. Neuroimage. 2016;129: 356–366.

214. Tadayon E, Pascual-Leone A, Santarnecchi E. Differential Contribution of Cortical Thickness, Surface Area, and Gyrification to Fluid and Crystallized Intelligence. Cereb Cortex. 2020;30: 215–225.

215. Gregory MD, Kippenhan JS, Dickinson D, Carrasco J, Mattay VS, Weinberger DR, et al. Regional Variations in Brain Gyrification Are Associated with General Cognitive Ability in Humans. Curr Biol. 2016;26: 1301–1305.

216. Judd N, Sauce B, Wiedenhoeft J, Tromp J, Chaarani B, Schliep A, et al. Cognitive and brain development is independently influenced by socioeconomic status and polygenic scores for educational attainment. Proc Natl Acad Sci U S A. 2020;117: 12411–12418.

217. Mackey AP, Finn AS, Leonard JA, Jacoby-Senghor DS, West MR, Gabrieli CFO, et al. Neuroanatomical correlates of the income-achievement gap. Psychol Sci. 2015;26: 925–933.

218. Lawson GM, Duda JT, Avants BB, Wu J, Farah MJ. Associations between children's socioeconomic status and prefrontal cortical thickness. Dev Sci. 2013;16: 641–652.

219. Alnæs D, Kaufmann T, Marquand AF, Smith SM, Westlye LT. Patterns of sociocognitive stratification and perinatal risk in the child brain. Proc Natl Acad Sci U S A. 2020;117: 12419–12427.

220. Lerch JP, van der Kouwe AJW, Raznahan A, Paus T, Johansen-Berg H, Miller KL, et al. Studying neuroanatomy using MRI. Nat Neurosci. 2017;20: 314–326.

221. Currie S, Hoggard N, Craven IJ, Hadjivassiliou M, Wilkinson ID. Understanding MRI: basic MR physics for physicians. Postgrad Med J. 2013;89: 209–223.

222. Elmaoğlu M, Çelik A. MRI Handbook: MR Physics, Patient Positioning, and Protocols. Springer Science & Business Media; 2011.

223. Pykett IL, Newhouse JH, Buonanno FS, Brady TJ, Goldman MR, Kistler JP, et al. Principles of

nuclear magnetic resonance imaging. Radiology. 1982;143: 157–168.

224. Nishimura DG. Principles of Magnetic Resonance Imaging. Stanford University; 1996.

225. Bansal R, Hao X, Liu F, Xu D, Liu J, Peterson BS. The effects of changing water content, relaxation times, and tissue contrast on tissue segmentation and measures of cortical anatomy in MR images. Magn Reson Imaging. 2013;31: 1709–1730.

226. van Geuns RJ, de Bruin HG, Rensing BJ, Wielopolski PA, Hulshoff MD, van Ooijen PM, et al. Magnetic resonance imaging of the coronary arteries: clinical results from three dimensional evaluation of a respiratory gated technique. Heart. 1999;82: 515–519.

227. Despotović I, Goossens B, Philips W. MRI segmentation of the human brain: challenges, methods, and applications. Comput Math Methods Med. 2015;2015: 450341.

228. Vovk U, Pernus F, Likar B. A Review of Methods for Correction of Intensity Inhomogeneity in MRI. IEEE Trans Med Imaging. 2007;26: 405–421.

229. Sled JG, Zijdenbos AP, Evans AC. A nonparametric method for automatic correction of intensity nonuniformity in MRI data. IEEE Trans Med Imaging. 1998;17: 87–97.

230. de Boor C. On calculating with B-splines. J Approx Theory. 1972;6: 50–62.

231. Tustison NJ, Avants BB, Cook PA, Zheng Y, Egan A, Yushkevich PA, et al. N4ITK: improved N3 bias correction. IEEE Trans Med Imaging. 2010;29: 1310–1320.

232. Tustison NJ, Gee J. N4ITK: Nick's N3 ITK implementation for MRI bias field correction. Insight J. 2010. doi:10.54294/jculxw

233. Eskildsen SF, Coupé P, Fonov V, Manjón JV, Leung KK, Guizard N, et al. BEaST: brain extraction based on nonlocal segmentation technique. Neuroimage. 2012;59: 2362–2373.

234. Avants BB, Epstein CL, Grossman M, Gee JC. Symmetric diffeomorphic image registration with cross-correlation: evaluating automated labeling of elderly and neurodegenerative brain. Med Image Anal. 2008;12: 26–41.

235. Blakemore S-J. Imaging brain development: the adolescent brain. Neuroimage. 2012;61: 397–406.

236. Mason C. The Development of Developmental Neuroscience. Journal of Neuroscience. 2009. pp. 12735–12747. doi:10.1523/jneurosci.4648-09.2009

237. de Graaf-Peters VB, Hadders-Algra M. Ontogeny of the human central nervous system: what is happening when? Early Hum Dev. 2006;82: 257–266.

238. Good CD, Johnsrude IS, Ashburner J, Henson RN, Friston KJ, Frackowiak RS. A voxel-based morphometric study of ageing in 465 normal adult human brains. Neuroimage. 2001;14: 21–36.

239. Hutton C, Draganski B, Ashburner J, Weiskopf N. A comparison between voxel-based cortical thickness and voxel-based morphometry in normal aging. Neuroimage. 2009;48: 371–380.

240. Riccelli R, Toschi N, Nigro S, Terracciano A, Passamonti L. Surface-based morphometry reveals the neuroanatomical basis of the five-factor model of personality. Soc Cogn Affect Neurosci.

2017;12: 671–684.

241. MacDonald D, Crabtree JR, Wiesinger G, Dax T, Stamou N, Fleury P, et al. Agricultural abandonment in mountain areas of Europe: Environmental consequences and policy response. J Environ Manage. 2000;59: 47–69.

242. Fischl B, Dale AM. Measuring the thickness of the human cerebral cortex from magnetic resonance images. Proc Natl Acad Sci U S A. 2000;97: 11050–11055.

243. Kim JS, Singh V, Lee JK, Lerch J, Ad-Dab'bagh Y, MacDonald D, et al. Automated 3-D extraction and evaluation of the inner and outer cortical surfaces using a Laplacian map and partial volume effect classification. Neuroimage. 2005;27: 210–221.

244. Lepage C, Wagstyl K, Jung B, Seidlitz J, Sponheim C, Ungerleider L, et al. CIVET-Macaque: An automated pipeline for MRI-based cortical surface generation and cortical thickness in macaques. Neuroimage. 2021;227: 117622.

245. Lerch JP, Evans AC. Cortical thickness analysis examined through power analysis and a population simulation. Neuroimage. 2005;24: 163–173.

246. Jeon S, Lepage C, Lewis L, Khalili-Mahani N, Bermudez P, Vincent R, et al. Reproducibility of Cortical Thickness Measurement: CIVET (v2. 1) vs. Freesurfer (v6. 0-beta & v5. 3). On Human Brain Mapping Symposium. 2017. Available: https://archive.aievolution.com/2017/hbm1701/index.cfm?do=abs.viewAbs&abs=3137

247. Lepage C, Lewis L, Jeun S, Bermudez P, Khalili-Mahani N, Omidyegaheh M, et al. Human MR evaluation of cortical thickness using CIVET v2. 1. Organization for Human Brain Mapping. 2017. Available: https://archive.aievolution.com/2017/hbm1701/index.cfm?do=abs.viewAbs&abs=3292

248. Bedford S. Large-Scale Analysis of Heterogeneity and Cortical Thickness in Autism Spectrum Disorder. 2018. Available: https://search.proquest.com/openview/cc617b927926a579165d798ad82e756c/1?pq-origsite=gscholar&cbl=18750&diss=y

249. Bailey DH, Barrio R, Borwein JM. High-precision computation: Mathematical physics and dynamics. Appl Math Comput. 2012;218: 10106–10121.

250. CIVET. [cited 8 Apr 2022]. Available: https://mcin.ca/technology/civet/

251. McConnell Brain Imaging Centre. BIC - the McConnell brain imaging centre: CIVET-2-1-0-introduction. [cited 10 Mar 2022]. Available: https://www.bic.mni.mcgill.ca/ServicesSoftware/CIVET-2-1-0-Introduction

252. Collins DL, Neelin P, Peters TM, Evans AC. Automatic 3D intersubject registration of MR volumetric data in standardized Talairach space. J Comput Assist Tomogr. 1994;18: 192–205.

253. Zijdenbos AP, Jimenez A, Evans AC. Pipelines: Large Scale Automatic Analysis of 3D Brain Data Sets. Neuroimage. 1998;7: S783.

254. Lyttelton O, Boucher M, Robbins S, Evans A. An unbiased iterative group registration template for cortical surface analysis. Neuroimage. 2007;34: 1535–1544.

255. Redolfi A, Manset D, Barkhof F, Wahlund L-O, Glatard T, Mangin J-F, et al. Head-to-head

comparison of two popular cortical thickness extraction algorithms: a cross-sectional and longitudinal study. PLoS One. 2015;10: e0117692.

256. MacDonald D, Kabani N, Avis D, Evans AC. Automated 3-D extraction of inner and outer surfaces of cerebral cortex from MRI. Neuroimage. 2000;12: 340–356.

257. Jubault T, Gagnon J-F, Karama S, Ptito A, Lafontaine A-L, Evans AC, et al. Patterns of cortical thickness and surface area in early Parkinson's disease. Neuroimage. 2011;55: 462–467.

258. Toro R, Perron M, Pike B, Richer L, Veillette S, Pausova Z, et al. Brain size and folding of the human cerebral cortex. Cereb Cortex. 2008;18: 2352–2357.

259. Gonzalez-Escamilla G, Groppa S. 7 Tesla MRI will soon be helpful to guide clinical practice in multiple sclerosis centres - No. Mult Scler. 2021;27: 362–363.

260. Matsuda Y, Ohi K. Cortical gyrification in schizophrenia: current perspectives. Neuropsychiatr Dis Treat. 2018;14: 1861–1869.

261. Ronan L, Voets NL, Hough M, Mackay C, Roberts N, Suckling J, et al. Consistency and interpretation of changes in millimeter-scale cortical intrinsic curvature across three independent datasets in schizophrenia. Neuroimage. 2012;63: 611–621.

262. Gilmore AD, Buser NJ, Hanson JL. Variations in structural MRI quality significantly impact commonly used measures of brain anatomy. Brain Inform. 2021;8: 7.

263. Blumenthal JD, Zijdenbos A, Molloy E, Giedd JN. Motion artifact in magnetic resonance imaging: implications for automated analysis. Neuroimage. 2002;16: 89–92.

264. Reuter M, Tisdall MD, Qureshi A, Buckner RL, van der Kouwe AJW, Fischl B. Head motion during MRI acquisition reduces gray matter volume and thickness estimates. Neuroimage. 2015;107: 107–115.

265. Alexander-Bloch A, Clasen L, Stockman M, Ronan L, Lalonde F, Giedd J, et al. Subtle in-scanner motion biases automated measurement of brain anatomy from in vivo MRI. Hum Brain Mapp. 2016;37: 2385–2397.

266. Satterthwaite TD, Wolf DH, Loughead J, Ruparel K, Elliott MA, Hakonarson H, et al. Impact of in-scanner head motion on multiple measures of functional connectivity: relevance for studies of neurodevelopment in youth. Neuroimage. 2012;60: 623–632.

267. Bedford SA, Park MTM, Devenyi GA, Tullo S, Germann J, Patel R, et al. Large-scale analyses of the relationship between sex, age and intelligence quotient heterogeneity and cortical morphometry in autism spectrum disorder. Mol Psychiatry. 2020;25: 614–628.

268. Jolliffe IT, editor. Principal Component Analysis for Special Types of Data. Principal Component Analysis. New York, NY: Springer New York; 2002. pp. 338–372.

269. Varikuti DP, Genon S, Sotiras A, Schwender H, Hoffstaedter F, Patil KR, et al. Evaluation of non-negative matrix factorization of grey matter in age prediction. Neuroimage. 2018;173: 394–410.

270. Devarajan K. Nonnegative matrix factorization: an analytical and interpretive tool in computational biology. PLoS Comput Biol. 2008;4: e1000029.

271. Nazeri A, Krsnik Ž, Kostović I, Ha SM, Kopić J, Alexopoulos D, et al. Neurodevelopmental Patterns of Early Postnatal White Matter Maturation Represent Distinct Underlying Microstructure and Histology. bioRxiv. 2022. p. 2022.02.11.480169. doi:10.1101/2022.02.11.480169

272. Jirsaraie RJ, Kaczkurkin AN, Rush S, Piiwia K, Adebimpe A, Bassett DS, et al. Accelerated cortical thinning within structural brain networks is associated with irritability in youth. Neuropsychopharmacology. 2019;44: 2254–2262.

273. Kaczkurkin AN, Sotiras A, Baller EB, Barzilay R, Calkins ME, Chand GB, et al. Neurostructural Heterogeneity in Youths With Internalizing Symptoms. Biol Psychiatry. 2020;87: 473–482.

274. Sanfelici R, Ruef A, Antonucci LA, Penzel N, Sotiras A, Dong MS, et al. Novel Gyrification Networks Reveal Links with Psychiatric Risk Factors in Early Illness. Cereb Cortex. 2021. Available: https://academic.oup.com/cercor/advance-article-abstract/doi/10.1093/cercor/bhab288/6369971

275. Cui Z, Li H, Xia CH, Larsen B, Adebimpe A, Baum GL, et al. Individual Variation in Functional Topography of Association Networks in Youth. Neuron. 2020;106: 340–353.e8.

276. Neufeld NH, Mulsant BH, Dickie EW, Meyers BS, Alexopoulos GS, Rothschild AJ, et al. Resting state functional connectivity in patients with remitted psychotic depression: A multi-centre STOP-PD study. EBioMedicine. 2018. pp. 446–453. doi:10.1016/j.ebiom.2018.09.025

277. Neufeld NH, Kaczkurkin AN, Sotiras A, Mulsant BH, Dickie EW, Flint AJ, et al. Structural brain networks in remitted psychotic depression. Neuropsychopharmacology. 2020;45: 1223–1231.

278. Yang Z, Oja E. Linear and nonlinear projective nonnegative matrix factorization. IEEE Trans Neural Netw. 2010;21: 734–749.

279. Robert C, Patel R, Blostein N, Steele CC, Mallar Chakravarty M. Microstructural variation in the human striatum using non-negative matrix factorization. bioRxiv. 2021. p. 2021.06.10.447764. doi:10.1101/2021.06.10.447764

280. Patel R, Mackay CE, Jansen MG, Devenyi GA, Clare O'Donoghue M, Kivimäki M, et al. Individual variation in brain microstructural-cognition relationships in aging. bioRxiv. 2021. p. 2021.02.19.431732. doi:10.1101/2021.02.19.431732

281. He Y, Chen ZJ, Evans AC. Small-world anatomical networks in the human brain revealed by cortical thickness from MRI. Cereb Cortex. 2007;17: 2407–2419.

282. Bassett DS, Bullmore E, Verchinski BA, Mattay VS, Weinberger DR, Meyer-Lindenberg A. Hierarchical organization of human cortical networks in health and schizophrenia. J Neurosci. 2008;28: 9239–9248.

283. Wechsler D. Wechsler abbreviated scale of intelligence--second edition. PsycTESTS Dataset. American Psychological Association (APA); 2018. doi:10.1037/t15171-000

284. Watt NF. Two-factor index of social position: Amherst modification. Unpublished manuscript, Department of Psychology, University of Denver. 1976;9: 15.

285. Dadar M, Fonov VS, Collins DL, Alzheimer's Disease Neuroimaging Initiative. A comparison of publicly available linear MRI stereotaxic registration techniques. Neuroimage. 2018;174: 191–200.

286. Bussy A, Patel R, Plitman E, Tullo S, Salaciak A, Bedford SA, et al. Hippocampal shape across the healthy lifespan and its relationship with cognition. Neurobiol Aging. 2021;106: 153–168.

287. Attendee Interactive. OHBM. [cited 30 Aug 2021]. Available: https://archive.aievolution.com/2017/hbm1701/index.cfm?do=abs.viewAbs&abs=3292

288. Collins DL, Louis Collins D, Neelin P, Peters TM, Evans AC. Automatic 3D Intersubject Registration of MR Volumetric Data in Standardized Talairach Space. Journal of Computer Assisted Tomography. 1994. pp. 192–205. doi:10.1097/00004728-199403000-00005

289. Barr DJ, Levy R, Scheepers C, Tily HJ. Random effects structure for confirmatory hypothesis testing: Keep it maximal. J Mem Lang. 2013;68. doi:10.1016/j.jml.2012.11.001

290. Boutsidis C, Gallopoulos E. SVD based initialization: A head start for nonnegative matrix factorization. Pattern Recognit. 2008;41: 1350–1362.

291. Halko N, Martinsson PG, Tropp JA. Finding Structure with Randomness: Probabilistic Algorithms for Constructing Approximate Matrix Decompositions. SIAM Rev. 2011;53: 217–288.

292. Hochberg Y, Benjamini Y. More powerful procedures for multiple significance testing. Stat Med. 1990;9: 811–818.

293. Krishnan A, Williams LJ, McIntosh AR, Abdi H. Partial Least Squares (PLS) methods for neuroimaging: a tutorial and review. Neuroimage. 2011;56: 455–475.

294. McIntosh AR, Lobaugh NJ. Partial least squares analysis of neuroimaging data: applications and advances. Neuroimage. 2004;23 Suppl 1: S250–63.

295. McIntosh AR, Mišić B. Multivariate statistical analyses for neuroimaging data. Annu Rev Psychol. 2013;64: 499–525.

296. Zeighami Y, Fereshtehnejad S-M, Dadar M, Collins DL, Postuma RB, Mišić B, et al. A clinical-anatomical signature of Parkinson's disease identified with partial least squares and magnetic resonance imaging. Neuroimage. 2019;190: 69–78.

297. Chen ZJ, He Y, Rosa-Neto P, Gong G, Evans AC. Age-related alterations in the modular organization of structural cortical network by using cortical thickness from MRI. Neuroimage. 2011;56: 235–245.

298. Dong H-M, Margulies DS, Zuo X-N, Holmes AJ. Shifting gradients of macroscale cortical organization mark the transition from childhood to adolescence. doi:10.1101/2020.11.17.385260

299. Margulies DS, Ghosh SS, Goulas A, Falkiewicz M, Huntenburg JM, Langs G, et al. Situating the default-mode network along a principal gradient of macroscale cortical organization. Proc Natl Acad Sci U S A. 2016;113: 12574–12579.

300. Markello R. neuromaps: A toolbox for comparing brain maps. Github; Available: https://github.com/rmarkello/neuromaps

301. workbench: Connectome Workbench. Github; Available: https://github.com/Washington-University/workbench

302. Sydnor VJ, Larsen B, Bassett DS, Alexander-Bloch A, Fair DA, Liston C, et al.

Neurodevelopment of the association cortices: Patterns, mechanisms, and implications for psychopathology. Neuron. 2021;109: 2820–2846.

303. Johnson A, Bathelt J, Akarca D, Crickmore G, Astle DE, RED Team. Far and wide: Associations between childhood socio-economic status and brain connectomics. Dev Cogn Neurosci. 2021;48: 100888.

304. YAKOVLEV, P. The myelogenetic cycles of regional maturation of the brain. Regional development of the brain in early life. 1967; 3–70.

305. Raz N, Lindenberger U, Rodrigue KM, Kennedy KM, Head D, Williamson A, et al. Regional brain changes in aging healthy adults: general trends, individual differences and modifiers. Cereb Cortex. 2005;15: 1676–1689.

306. Gogtay N, Lu A, Leow AD, Klunder AD, Lee AD, Chavez A, et al. Three-dimensional brain growth abnormalities in childhood-onset schizophrenia visualized by using tensor-based morphometry. Proc Natl Acad Sci U S A. 2008;105: 15979–15984.

307. Gogtay N, Thompson PM. Mapping gray matter development: Implications for typical development and vulnerability to psychopathology. Brain Cogn. 2010;72: 6–15.

308. Westlye LT, Walhovd KB, Dale AM, Bjørnerud A, Due-Tønnessen P, Engvig A, et al. Life-span changes of the human brain white matter: diffusion tensor imaging (DTI) and volumetry. Cereb Cortex. 2010;20: 2055–2068.

309. Madan CR. Age-related decrements in cortical gyrification: Evidence from an accelerated longitudinal dataset. Eur J Neurosci. 2021;53: 1661–1671.

310. Natu VS, Gomez J, Barnett M, Jeska B, Kirilina E, Jaeger C, et al. Apparent thinning of human visual cortex during childhood is associated with myelination. Proc Natl Acad Sci U S A. 2019;116: 20750–20759.

311. Dickstein DL, Kabaso D, Rocher AB, Luebke JI, Wearne SL, Hof PR. Changes in the structural complexity of the aged brain. Aging Cell. 2007;6: 275–284.

312. Brans RGH, Kahn RS, Schnack HG, van Baal GCM, Posthuma D, van Haren NEM, et al. Brain plasticity and intellectual ability are influenced by shared genes. J Neurosci. 2010;30: 5519–5524.

313. Operto G, Auzias G, Le Troter A, Perrot M, Rivière D, Dubois J, et al. Structural group analysis of cortical curvature and depth patterns in the developing brain. 2012 9th IEEE International Symposium on Biomedical Imaging (ISBI). 2012. pp. 422–425.

314. Satterthwaite TD, Shinohara RT, Wolf DH, Hopson RD, Elliott MA, Vandekar SN, et al. Impact of puberty on the evolution of cerebral perfusion during adolescence. Proc Natl Acad Sci U S A. 2014;111: 8643–8648.

315. Drakulich S, Thiffault A-C, Olafson E, Parent O, Labbe A, Albaugh MD, et al. Maturational trajectories of pericortical contrast in typical brain development. Neuroimage. 2021;235: 117974.

316. Olafson E, Bedford SA, Devenyi GA, Patel R, Tullo S, Park MTM, et al. Examining the Boundary Sharpness Coefficient as an Index of Cortical Microstructure in Autism Spectrum Disorder. Cereb Cortex. 2021;31: 3338–3352.

317. Rowley CD, Bazin P-L, Tardif CL, Sehmbi M, Hashim E, Zaharieva N, et al. Assessing intracortical myelin in the living human brain using myelinated cortical thickness. Front Neurosci. 2015;9: 396.

318. Rowley C. Mapping intracortical myelin in humans using magnetic resonance imaging. 2018. Available: https://macsphere.mcmaster.ca/handle/11375/23655

319. Rowley CD, Sehmbi M, Bazin P-L, Tardif CL, Minuzzi L, Frey BN, et al. Age-related mapping of intracortical myelin from late adolescence to middle adulthood using T1 -weighted MRI. Hum Brain Mapp. 2017;38: 3691–3703.

320. Sehmbi M, Rowley CD, Minuzzi L, Kapczinski F, Kwiecien JM, Bock NA, et al. Age-related deficits in intracortical myelination in young adults with bipolar disorder type I. J Psychiatry Neurosci. 2019;44: 79–88.